DEVELOPMENTAL DYNAMICS 244:1485–1518, 2015
DOI: 10.1002/DVDY.24340

RESEARCH ARTICLE

Postembryonic Staging of Wild-Type Goldfish, with Brief Reference to Skeletal Systems

Ing-Jia Li, Chun-Ju Chang, Shi-Chieh Liu, Gembu Abe, and Kinya G. Ota*

Laboratory of Aquatic Zoology, Marine Research Station, Institute of Cellular and Organismic Biology, Academia Sinica, Yilan, Taiwan

Background: **Artificial selection of postembryonic features is known to have established morphological variation in goldfish (*Carassius auratus*). Although previous studies have suggested that goldfish and zebrafish are almost directly comparable at the embryonic level, little is known at the postembryonic level. Results: Here, we categorized the postembryonic developmental process in the wild-type goldfish into 11 different stages. We also report certain differences between the postembryonic developmental processes of goldfish and zebrafish, especially in the skeletal systems (scales and median fin skeletons), suggesting that postembryonic development underwent evolutionary divergence in these two teleost species. Conclusions: Our postembryonic staging system of wild-type goldfish paves the way for careful and appropriate comparison with other teleost species. The staging system will also facilitate comparative ontogenic analyses between wild-type and mutant goldfish strains, allowing us to closely study the relationship between artificial selection and molecular developmental mechanisms in vertebrates. *Developmental Dynamics 244:1485–1518, 2015*. © 2015 The Authors. Developmental Dynamics published by Wiley Periodicals, Inc. on behalf of American Association of Anatomists**

Key words: artificial selection; domestication; ontogeny; morphology; phylogeny

Submitted 16 February 2015; First Decision 10 July 2015; Accepted 23 August 2015; Published online 28 August 2015

Introduction

Goldfish (*Carassius auratus*) is a popular domesticated ornamental fish (Hervey and Hems, 1948; Matsui et al., 1981; Smartt, 2001). According to analyses of Chinese archives, the goldfish was originally bred for food, and subsequently for ornamental purposes (Hervey and Billardon-Sauvigny, 1950; Chen, 1956; Smartt, 2001). Moreover, records indicate that intensive goldfish breeding for ornamental purposes began during the Song dynasty; this suggests that the diversification of goldfish strains may have occurred from the 10th century CE onward (Chen, 1956). Through this breeding process, several morphologically divergent goldfish strains were established. Although there is no consensus, these strains were categorized into sixteen groups, based on trunk shape, eye morphology, and the number and length of the fins, in a recent book by Smartt (2001). These morphological variations provided insights to 19th century biologists into how animal body shapes diverge in nature (Darwin, 1868; Bateson, 1894). Later researchers were also intrigued by the morphological variations of goldfish and wrote descriptions of goldfish varieties at the levels of anatomy, embryology, and genetics (Berndt, 1925; Chen, 1925; Koh, 1931, 1932; Matsui, 1933, 1934, 1972; Li et al., 1959; Asano and Kubo, 1972; Komiyama et al., 2009; Wang et al., 2013, 2014).

The close phylogenetic relationship between goldfish and zebrafish (Saitoh et al., 2003, 2006) suggest that the well-established molecular techniques, as well as mutant, morphant, and gene expression patterns, catalogued in The Zebrafish Model Organism Database (Bradford et al., 2011), can be directly applied to goldfish research (Mabee et al., 2007; Schlling and Webb, 2007; Tsai et al., 2013). Moreover, it was recently confirmed that these two teleost species are similar in terms of embryological development (Tsai et al., 2013). Such similarities with zebrafish provide us with an opportunity to investigate at a molecular level how the highly divergent morphological features of goldfish were established during artificial selection. In fact, we recently succeeded in identifying the gene responsible for the bifurcated axial skeleton of the twin-tail goldfish (Abe et al., 2014). In this earlier study, we reported that a mutation in one of the two *chordin* genes was selected for during domestication, and this mutation altered dorsal–ventral patterning during early development (Abe et al., 2014). This success raises the prospect that further detailed comparative embryological studies between goldfish and zebrafish (and its mutants) will enhance our understanding of how artificial selection and developmental processes are related (Tsai et al., 2013; Abe et al., 2014).

Grant sponsor: The National Science Council of Taiwan; Grant number: 102-2313-B-001-005-MY3.
*Correspondence to: Kinya G. Ota, Marine Research Station, Institute of Cellular and Organismic Biology, Academia Sinica, No.23-10, Dawen Road, Jiaoxi, Yilan, 26242, Taiwan. E-mail: otakinya@gate.sinica.edu.tw

Article is online at: http://onlinelibrary.wiley.com/doi/10.1002/dvdy.24340/abstract

TABLE 1. Comparison of Postembryonic Staging Tables

Ballae 1940 (24°C-28°C), English[a]				Li et al., 1959 (25°C), Chinese[a]				Kajishima 1960 (21 ± 1°C), Japanese[a]			
stages	sl (mm)	dpf	figures	stages[b]	sl	dpf[c]	Figure	stages	sl	dpf	Figure
Newly hatched larvae	4.5		Fig.17	Hatchout stage	NA	2.6	Plate II Fig. 33	Hatching	NA	4.1[c]	Fig. 25
5.8-mm stage	5.8	1–2	Fig.18	Gill circulation stage	NA	2.9	NA				
				Swim bladder formation stage	NA	3.4	NA	Air bladder develops	NA	6	Fig. 26
				Lower jaw formation	NA	3.8	NA				
				Swimming stage	NA	4.3	NA				
				Liver formation stage	NA	4.9	NA				
				Branchiostegal membrane formation stage	NA	5.7	NA				
6.8-mm stage	6.8	7–8	Fig.19	Caudal fin ray formation stage	NA	7.7	NA	Tail fin rays develop	NA	11	Fig. 27
				Swim bladder divided stage	NA	11.7	NA				
				Dorsal fin ray formation stage	NA	12.7	NA				
				Anal fin ray formation stage	NA	13.7	NA	Dorsal and anal fin rays develop	NA	25	Fig. 28
				Pectral fin ray formation stage	NA	14.7	NA				
				Pelvic fin ray formation stage	NA	15.4	NA				
7.9-mm stage	7.9	15–18	Fig.20	Body shape differentiation stage	NA	17.2	NA				
				Scale formation stage	NA	19.5	NA				
9.4-mm stage	9.4	22–23	Fig.21								
11.6-mm stage	11.6	37	NA								
15.7-mm stage	15.7	63	NA								

[a]Languages used in these papers.
[b]The stage names are direct translations from the Chinese (Li 1959) into English.
[c]These dpf's were originally represented as hours post-fertilization.
NA, not available.

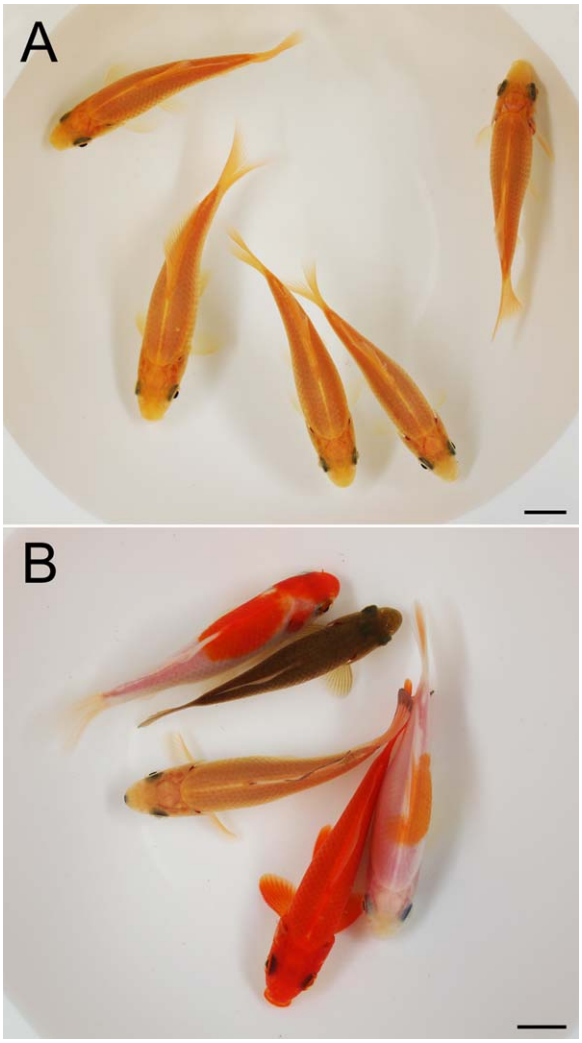

Fig. 1. Dorsal view of two goldfish strains. **A:** Japanese single tail Wakin. **B:** The common goldfish strain of Taiwan. These two goldfish strains exhibit similar morphology. Scale bars = 1 cm.

This possibility is also supported by recent progress of genomic studies on domesticated mammals and birds (for example, dog, cat, cow, chicken, and pigeon) (Lindblad-Toh et al., 2005; Wayne and Ostrander, 2007; Akey et al., 2010; Vonholdt et al., 2010; Shapiro et al., 2013). These studies explain the processes underlying fixation of genetic mutations through selective pressure on favorable morphological and/or physiological features, providing a more specific and promising framework for combined genomic and developmental biological approaches to investigate how fixed mutations altered ontogenetic processes to form the favorable morphological features in domestic animals in the context of evolutionary developmental biology (Cresko et al., 2007). Although the above-mentioned mammals and birds may also be suitable for combination approaches, domesticated teleost species which produce a large number of offspring (larval and juvenile materials) are more suitable (Tsai et al., 2013). In this respect, goldfish seems to be well-suited for comparative ontogeny.

Comparative studies of ontogenetic process require not only embryonic, but also postembryonic staging tables, as several important morphogenetic processes which form characteristic features of each species (for example, internal and external skeletal structures and scale patterns) are known to proceed during postembryonic stages (Arratia et al., 1990, 1991; Cubbage and Mabee, 1996; Schilling and Kimmel, 1997; Van der Heyden and Huyssune, 2000; Van der Heyden et al., 2000; Witten et al., 2001; Yelick and Schilling, 2002; Mabee et al., 2002; Bird and Mabee, 2003; Sire and Huysseune, 2003; Webb and Shirey, 2003; Elizondo et al., 2005; Sire and Akimenko, 2004; Thorsen and Hale, 2005; Patricia et al., 2007; Patterson et al., 2008; Parichy et al., 2009; Kimmel et al., 2010; Budi et al., 2011; Bensimon-Brito et al., 2012). However, at present there is no widely available postembryonic developmental staging table for goldfish, in practice. Although several early researchers described the postembryonic developmental process of goldfish (Watase, 1887; Khan, 1929; Battle, 1940; Hervey and Hems, 1948; Li et al., 1959; Kajishima, 1960), these anatomical and postembryonic observations are difficult to compare with the zebrafish postembryonic staging table, due to the paucity of detailed descriptions of the representative characteristics for each stage (akin to the "developmental milestones" in the zebrafish postembryonic staging table produced by Parichy et al., 2009).

While three embryological papers provided relatively detailed postembryonic staging tables for goldfish (Ballard, 1940; Li et al., 1959; Kajishima, 1960), their reports lack several crucial descriptions (Table 1). For example, Kajishima (1960) categorized postembryonic goldfish larvae into four stages based on morphological characteristics and date postfertilization; however, no descriptions of ontogenetic order of morphological characteristics were provided (Table 1). Battle (1940) described goldfish larvae at seven different times postfertilization, but the staging index was not explicitly defined (Table 1). Moreover, the strains or morphologies of the parental goldfish were not specified in these two studies (Battle, 1940; Kajishima, 1960). The lack of resolution makes it difficult to apply these staging tables to recent studies of developmental biology (Battle, 1940; Kajishima, 1960).

Of particular interest, Li et al. (1959) provided a relatively comprehensive postembryonic staging table; this study contains the fifteen postembryonic stages (including hatchout and posthatchout stages). However, to our knowledge, Li et al. (1959) seems to be cited by only four papers (Wang et al., 2010; Li et al., 2012; Tsai et al., 2013; Ma et al., 2015). This small citation number may be due to the following reasons.

First, Li et al. (1959) was completely written (with the exception of its abstract) in Chinese (a mixture of traditional and simplified Chinese [Hanzi or Kanji] characters). The lack of annotations on embryological and anatomical terminologies in any other language (for example, Latin, English, or German) mean that a certain reading skill of Chinese characters is required to understand the enclosed descriptions (Li et al., 1959). Moreover, no figures and photographs of posthatchout stages were provided in their staging table (Table 1) (Li et al., 1959). The absence of visual information precludes us from evaluating the accuracy, adequacy, and suitability of the provided information for each research field (Table 1).

More critically, no standard lengths were contained in this postembryonic staging table (Table 1). Although the goldfish larvae in Li et al. (1959) were reared at constant temperature (25°C), their growth rate is uncertain. The observation that the growth rate of postembryonic and free-feeding teleost larvae is influenced by environmental factors (Kilambi and Robinson, 1979; Shelton et al., 1981; Schram et al., 2006; Merino et al., 2007; Parichy et al., 2009) indicates that the chronological developmental time table of Li et al. (1959) is insufficient for estimation of

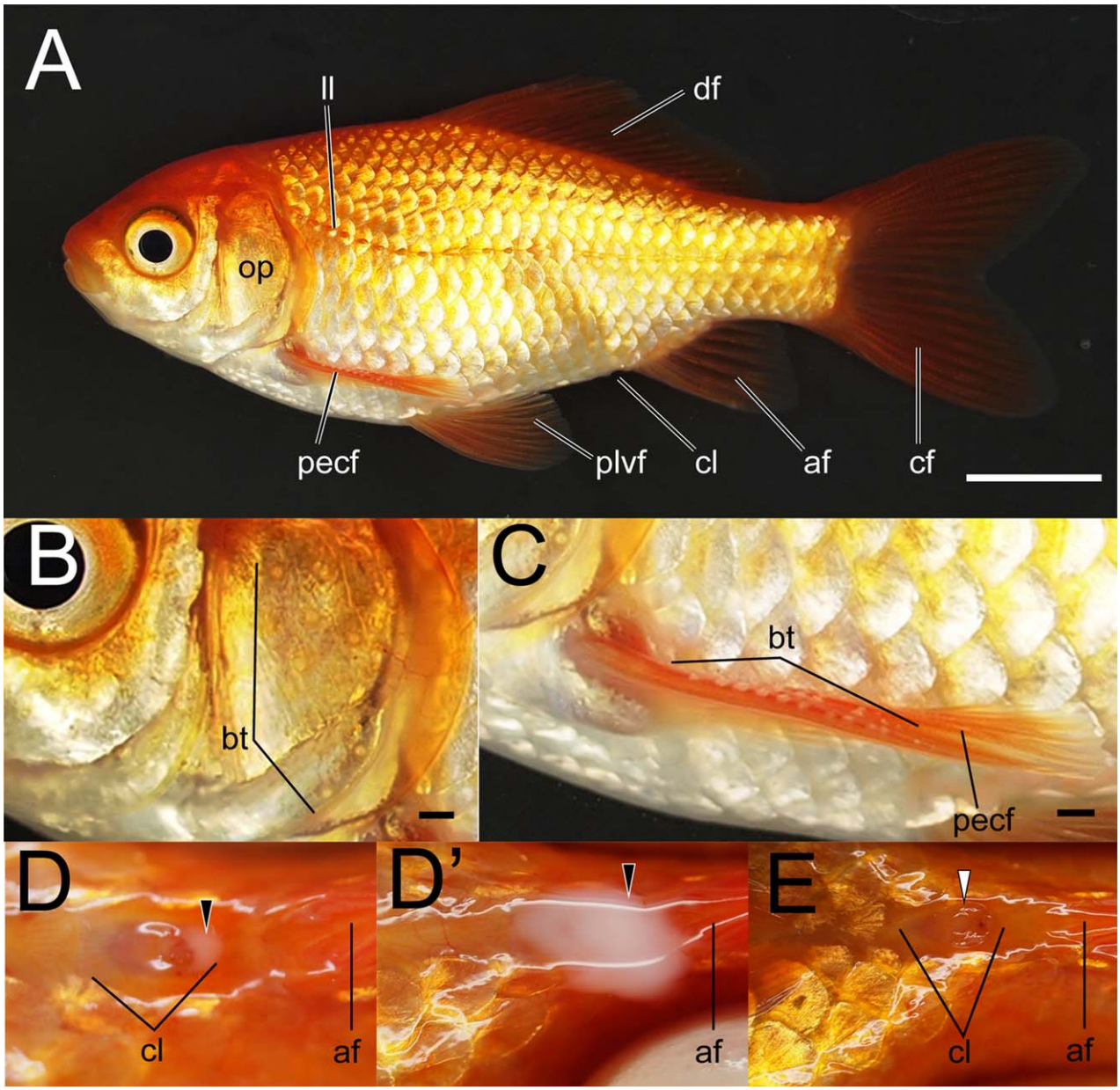

Fig. 2. Adult stage. **A–E**: Lateral views of the whole body (A), operculum (B), and pectoral fin (C); and ventral views of the male (D,D′), and female (E) cloaca regions were captured using a light-field camera. Squeezed sperm from male goldfish are visible in (D,D′). On the opercular and anterior side of the pectoral fins, breeding tubercles (bt) can be observed (B,C). Black arrowheads indicate sperm (D,D′). The white arrowhead indicates a prominent cloaca in squeezed female (E). The specimens in D and E are approximately 7 cm in total length. af, anal fin; bt, breeding tubercles; cf, caudal fin; cl, cloaca; df, dorsal fin; ll, lateral line; op, operculum; pecf, pectoral fin; plvf, pelvic fin. Scale bars = 1 cm in A; 1 mm in B,C.

developmental timing during late ontogenesis. The lack of a reliable and widely available normal goldfish postembryonic staging table impedes identification of commonly conserved (and divergent) morphological features between goldfish, zebrafish, and other teleost species.

To remedy this situation, we comprehensively examined goldfish postembryonic development. We measured the development rate of postembryonic goldfish, and examined the appearance of several traits in fresh goldfish larvae, juvenile, and adult specimens. Moreover, we analyzed skeletal development through alizarin red and fluorescent dye staining, and conventional histology. Our goldfish postembryonic staging system should facilitate comparative analysis with late-stage specimens in other teleost species at the levels of anatomy and developmental biology (Swarup, 1958; Armstrong and Child, 1965; Morrison et al., 2001; Martinez and Bolker, 2003; Iwamatsu, 2004; Fujimura and Okada, 2007; Parichy et al., 2009), facilitating further progress in the field of evolutionary developmental biology.

Results

Variation in Common Goldfish Strains

In this study, we used common goldfish individuals of two different strains: Japanese single tail *Wakin* strain and the common goldfish strain of Taiwan. Individuals from both common

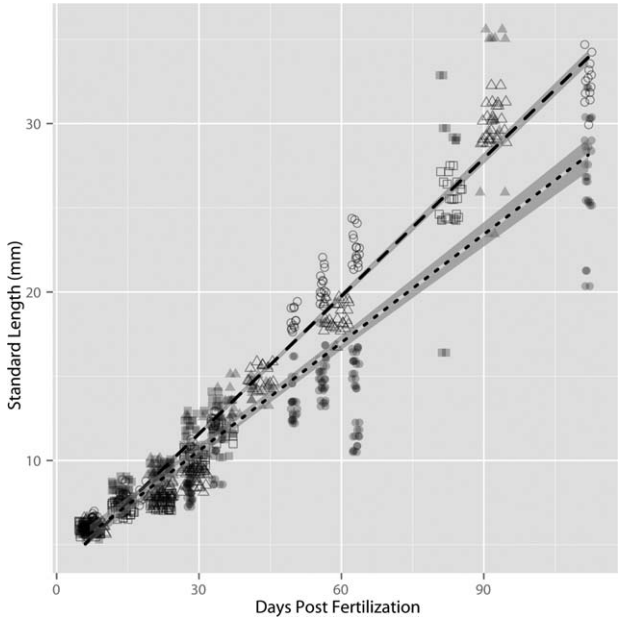

Fig. 3. Relationship between total length and days postfertilization. The growth rates of individually and collectively maintained goldfish specimens are shown as scatter plots with blank and filled points, respectively. Points derived from different clutches are indicated by different shapes; circular, triangular and square points indicate #20140313, #20140331, and #20140409, respectively. Regression lines of individually and collectively maintained goldfish specimens are shown as dashed ($y = 0.272x + 3.40$, $r^2 = 0.97$) and dotted lines ($y = 0.214x + 4.151$, $r^2 = 0.83$). The 95% confidence intervals are indicated as grey areas (see Experimental procedures). A total of 422 and 407 values were derived from 76 individually and 66 collectively maintained specimens, respectively.

goldfish strains are quite similar in their morphology (both possess typical common goldfish morphology: slender body and short tail) (Fig. 1). However, there are differences in their coloration: all of the Japanese goldfish individuals exhibit identical coloration (the entire body is orange; Fig. 1A), while the common goldfish strain of Taiwan exhibits diverse coloration (red and white, dark brown, and orange; Fig. 1B). These differences in coloration seem to be derived from the varying intents of Japanese and Taiwanese breeders. Japanese breeders may have intended to maintain homogenous coloration in their goldfish population for ornamental purposes, while Taiwanese breeders may have intend to maintain heterogeneous populations for ease of breeding, because their goldfish juveniles are used as feed for predatory aquarium organisms.

With the exception of coloration, no other ornamental features were identified in these two goldfish strains; for example, long-tail (such as the "*Comet*" strain) or broadly round-tail (like as "*Bristol Shubunkin*") individuals were not present (Figs. 1, 2A). Moreover, to avoid the use of twin-tail goldfish specimens, all specimens homozygous or heterozygous for the wild-type *chdA* allele were used (see details in Abe et al., 2014). These goldfish strains were sexed and used for artificial fertilization (Tsai et al., 2013; see the Experimental Procedures section) (Fig. 2). All larvae and juveniles used in this study possessed wild-type phenotypes. Both goldfish strains were used for the following experiments (see the Growth Rate and Anatomical Traits and Their Order of Appearance sections); clutch number #20140313 is derived from the Japanese *Wakin* goldfish strain and clutch numbers #20140331 and #20140409 from the common goldfish strain of Taiwan.

Life History Stage Definitions

We defined the goldfish larval stages based on the embryonic and postembryonic staging tables of zebrafish (Kimmel et al., 1995; Parichy et al., 2009). In brief, hatching and the presence of the protruding mouth was defined as the end of the embryonic period, and the intermediate stages between the end of the embryonic period and juvenile period were defined as the larval period. The complete loss of the median fin fold defines the juvenile stages (see below, Juvenile period). The production of viable gametes defines the adult period (Fig. 2).

Growth Rate

Population density is known to affect growth rate in several teleosts (Kilambi and Robinson, 1979; Shelton et al., 1981; Schram et al., 2006; Merino et al., 2007; Parichy et al., 2009), including goldfish (Feldlite and Milstein, 2000). To investigate how population density affects the growth rate of goldfish, specimens were divided into two groups. Specimens of the first group were maintained alone (the "individually maintained" group), while specimens of the second group were kept with other goldfish (the "collectively maintained" group) (see details in the Experimental Procedures section). For all of these goldfish lines, standard length was measured at various days post fertilization (dpf) (Fig. 3). The collectively maintained individuals exhibited dispersed standard lengths at later dpf (Fig. 3), while individually maintained goldfish specimens possessed relatively similar standard lengths (the dashed line in Fig. 3). In other words, collectively maintained individuals could be extremely small or extremely large at later dpf. As larger individuals have a competitive advantage, it is presumed that larger individuals would tend to get larger, while the growth of smaller individuals would be impeded, by collective maintenance. Thus, to avoid confusion derived from variation in growth rates, individually maintained specimens were used to examine the order in which morphological traits appear (Figs. 4, 5).

Anatomical Traits and Their Order of Appearance

To generate widely applicable indices for goldfish larval and juvenile stage identification, we examined the zebrafish postembryonic staging table (Parichy et al., 2009) and selected the following 10 traits: (1) inflation of the posterior lobe of the swim bladder; (2) appearance of caudal fin rays; (3) appearance of the forked caudal fin; (4) inflation of the anterior lobe of the swim bladder; (5) appearance of the dorsal fin ray; (6) appearance of the anal fin ray; (7) appearance of the pelvic fin bud; (8) appearance of the pelvic fin ray; (9) disappearance of the fin fold; and (10) appearance of scales.

These traits are easily visible under stereomicroscopy in lateral views of live samples. Because caudal, dorsal, and anal fin rays in the lateral view can be easily counted, these anatomical features could be quantified and used as representative stage indices (Fig. 6). Moreover, our observations indicate their appearance order seems to be correlated with development (standard length and days post fertilization) in the Japanese single tail *Wakin* strains and the common goldfish strain of Taiwan (Fig. 4).

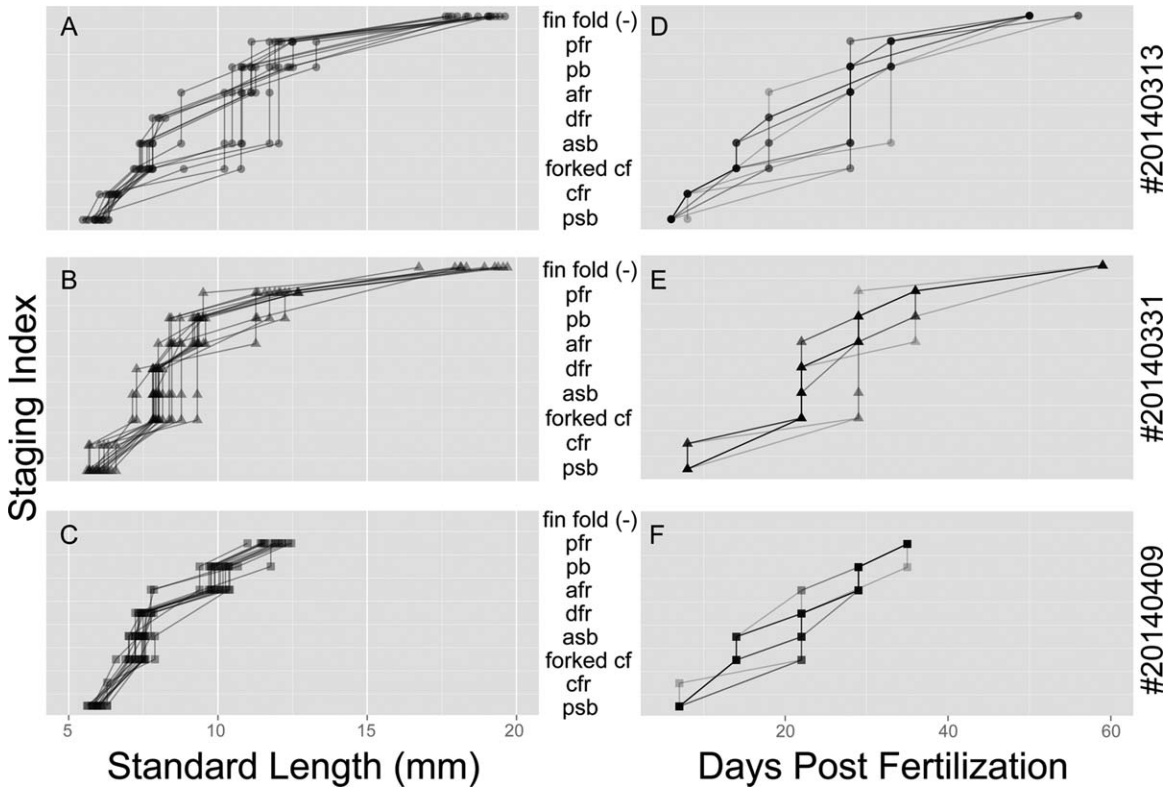

Fig. 4. Representative appearance sequences of developmental indices in three different clutches. **A–C**: Relationship between standard length and observed staging index. **D–F**: Relationship between days post fertilization and observed staging index. Identical individuals are connected by lines. A total of 334 data points derived from 45 individuals were examined.

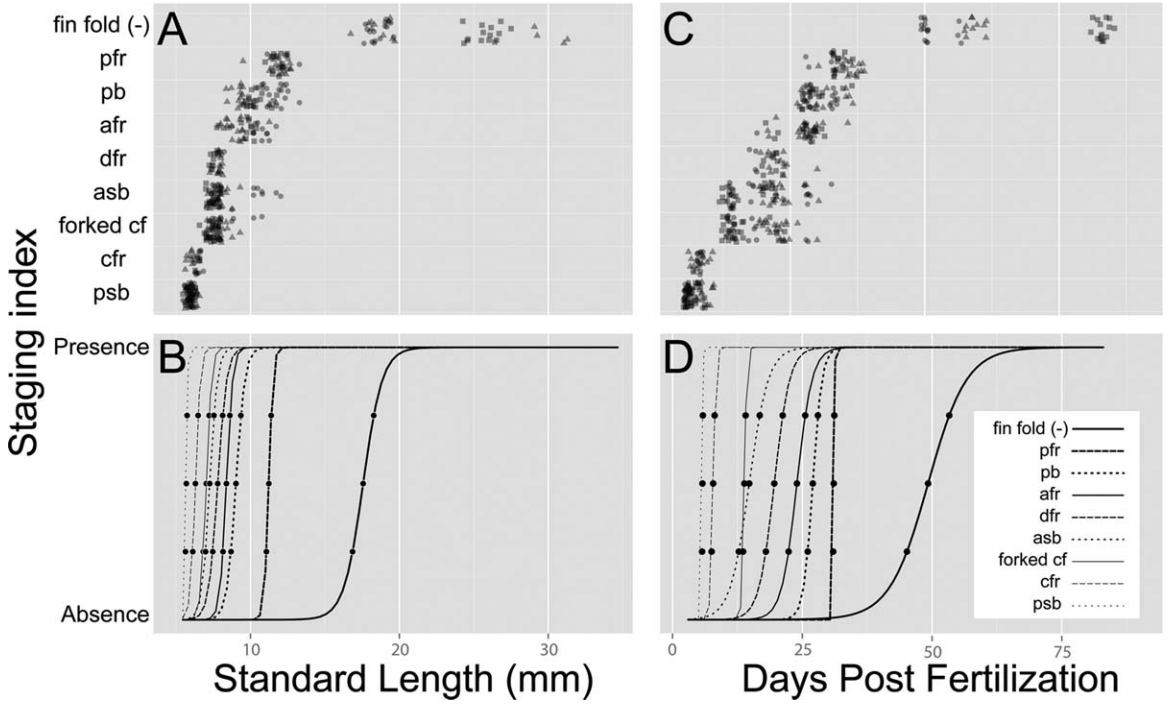

Fig. 5. Appearance sequence of the staging indices in individually maintained specimens. **A,B**: Relationship between standard length and observed staging index. **C,D**: Relationship between days post fertilization and observed standing index. The juveniles derived from different clutches are indicated by differently shaped points (circular, triangular, and square points indicate #20140313, #20140331, and #20140409, respectively). B,D: Prediction line from logistic regression with generalized linearized model. Black circles indicate 25, 50, and 75% probability. A total of 442 points derived from 76 individuals are plotted. All points are jittered to prevent obscuration of overlapping data. asb, anterior swim bladder; afr, anal fin ray; cfr, caudal fin fold; dfr, dorsal fin ray; fin fold (-), disappearance of fin fold; forked cf, forked caudal fin; pb, pelvic fin bud; pfr, pelvic fin ray; psb, posterior swim bladder.

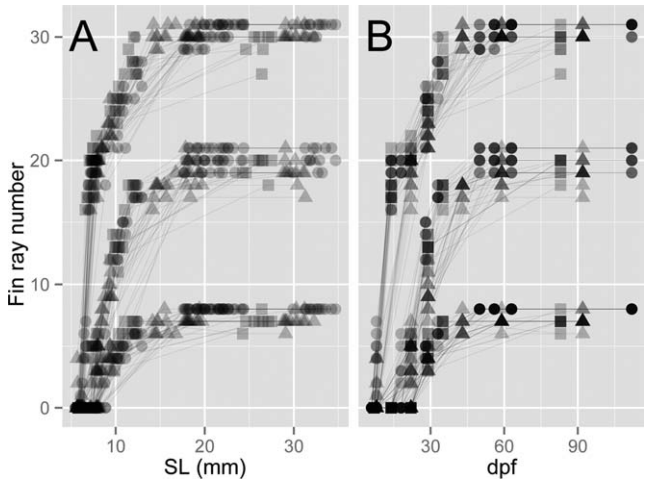

Fig. 6. A,B: Relationships between median fin ray numbers and standard length (SL). The relationships between caudal (top), dorsal (middle), and anal (bottom) fin ray number and standard length in individually maintained juveniles are plotted. The juveniles derived from different clutches are indicated by differently shaped points (circular, triangular, and square points indicate #20140313, #20140331, and #20140409, respectively). In total, 251 points were derived from 40 individuals. dpf, days postfertilization.

Related to the above, it should be noted that pigmentation patterns were not used as an index for the goldfish strains, because our goldfish strains, especially the common goldfish strain of Taiwan, varied in their coloration (Fig. 1); importantly, it has also been reported that the pigmentation process of the juvenile reflects the coloration patterns of the adult (Goodrich and Hansen, 1931). Moreover, some other quantitative developmental traits which were measured in the zebrafish were not applied to the goldfish, because the opacity of the goldfish larvae makes it difficult to measure these indices from early to late stages; for example, the angle of the anterior/posterior swim bladder lobes and flexion of the notochord are difficult to accurately measure, especially in late stage larvae (Parichy et al., 2009). Furthermore, traits closely related to behavior and physiology were not used in our study (although swimming behavior and blood circulation patterns were examined by Li et al., 1959; Table 1), because these traits are difficult to examine in anesthetized specimens.

To determine whether the aforementioned anatomical traits are suitable for staging goldfish, we examined the order of their appearance in individually maintained specimens (Experimental Procedures) (Fig. 5). Although standard length at the time of appearance of each anatomical trait varied (Fig. 5), the order in which the anatomical traits appeared was consistent in all examined individuals (Fig. 4). Moreover, we predicted the order and probability of appearance based on all of the data from individually maintained organisms (Fig. 5). The relationship between standard length and the appearance order of the staging indices was consistent. On the other hand, the order of appearance based on the estimated curves of appearance probability for the forked caudal fin fold and anterior swim bladder were inverted (Fig. 5D). This inconsistency seems to be derived from the wide and largely overlapping distribution patterns of the appearance timing of these two staging indices (Fig. 5C,D), suggesting that these two events tend to occur with closely related timing (Fig. 5).

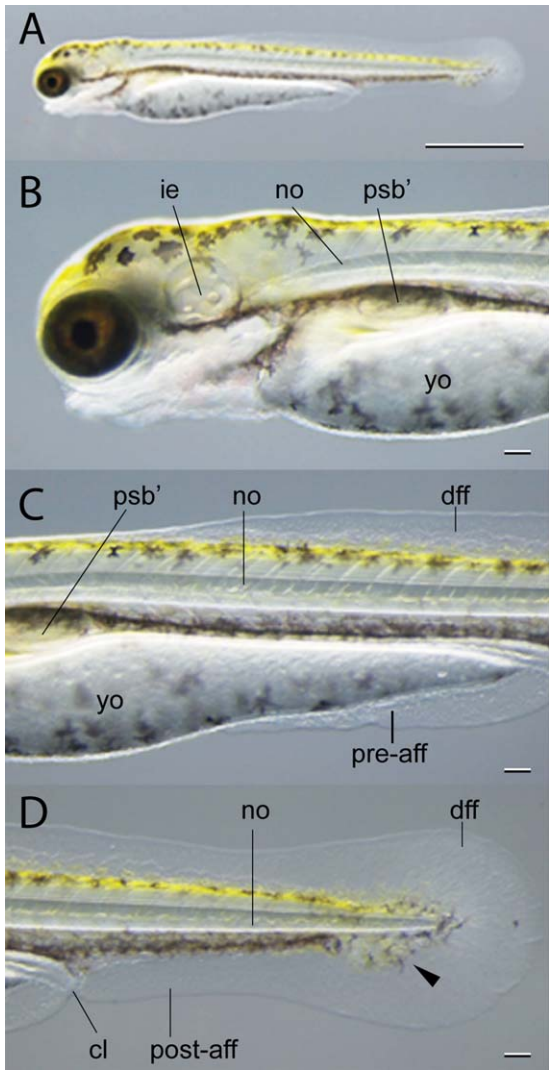

Fig. 7. Larvae at the prot stage. **A–D**: Lateral views of the whole body (A), and anterior (B), mid-trunk (C), and caudal (D) regions, were photographed under oblique light. The posterior swim bladder primordia are visible (psb′) (B). The arrowhead indicates caudal fin condensation (D). cl, cloaca; dff, dorsal fin fold; ie, inner ear; no, notochord; postaff, postanal fin fold; preaff, preanal fin fold; psb′, primordia of posterior swim bladder; yo, yolk. Scale bars = 1 mm in A; 0.1 mm in B–D.

Developmental Stages

Based on the order in which anatomical traits appeared, we categorized postembryonic goldfish development into the following eleven stages: protruding mouth (prot), Posterior swim bladder lobe (Psb), Caudal fin ray (Cr), Forked caudal fin (Fcf), Anterior swim bladder (Asb), Dorsal fin ray (Dr), Anal fin ray (Ar), Pelvic fin bud (Pb), Pelvic fin ray (Pr), Juvenile, and Adult (Figs. 2, 7–19; Table 2). Here, we describe the characteristics of each stage in representative individuals. Moreover, we report the standard length of onset at each larval stage, predicted from 76 individuals (Table 2; Fig. 5; see the Experimental Procedures section).

Prot Stage

All goldfish individuals hatch in the prot stage; as such, we defined this stage as the initial postembryonic stage (Fig. 7A–D).

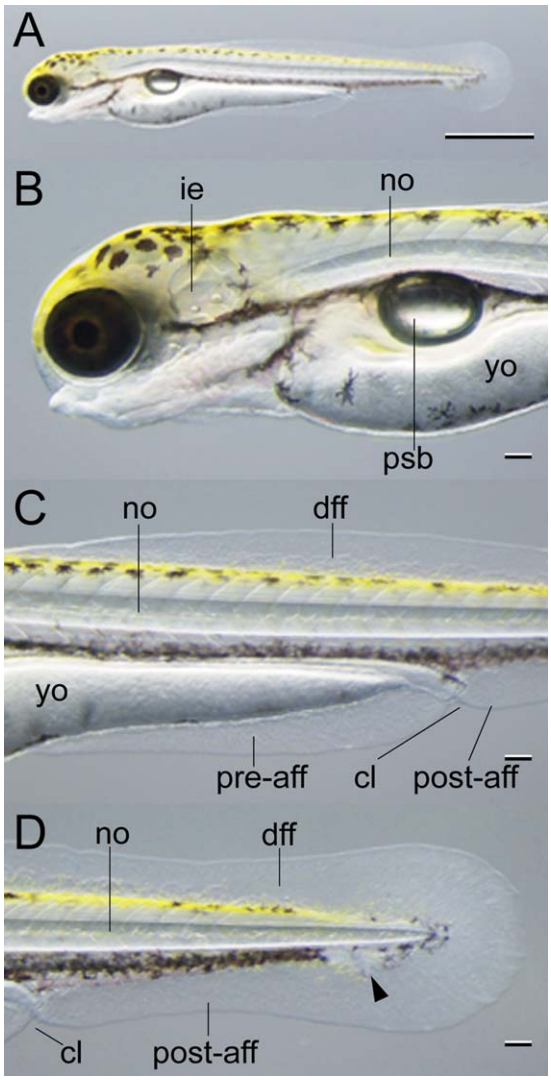

Fig. 8. Psb stage larvae. **A–D**: Lateral views of the whole body (A), and anterior (B), mid-trunk (C), and caudal (D) regions, were photographed under oblique light. The arrowhead indicates caudal fin condensation (D). The posterior swim bladder is visible (psb). cl, cloaca; dff, dorsal fin fold; ie, inner ear; no, notochord; postaff, postanal fin fold; preaff, preanal fin fold; psb, posterior swim bladder; yo, yolk. Scale bars = 1 mm in A; 0.1 mm in B–D.

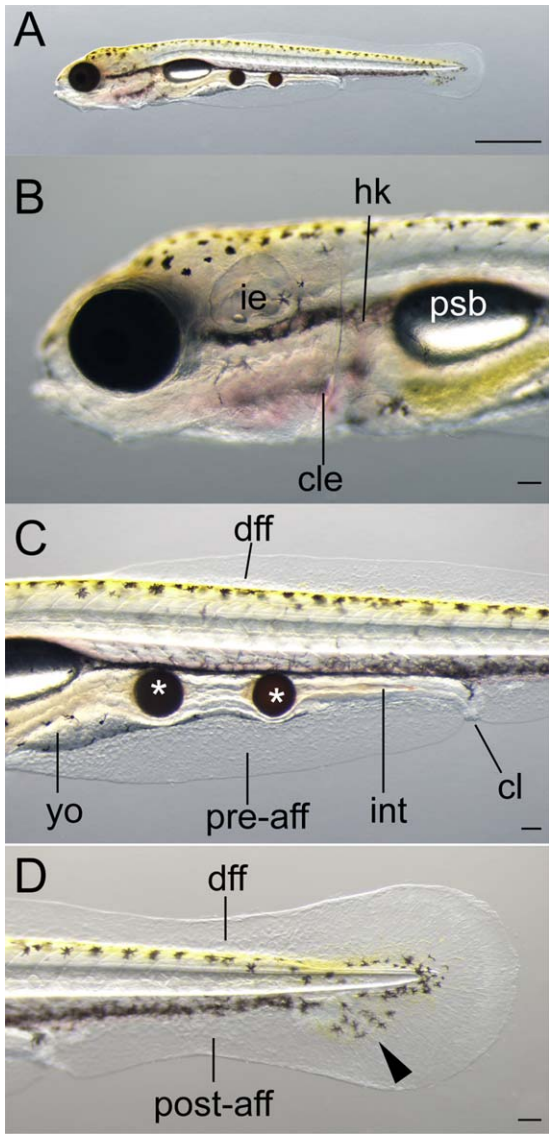

Fig. 9. Late Psb stage larvae. **A–D**: Lateral views of the whole body (A), anterior (B), mid-trunk (C), and caudal (D) regions, were photographed under oblique light. The arrowhead indicates the caudal fin condensation area (D). White asterisks indicate undigested brine shrimp eggs. cl, cloaca; cle, cleithrum; dff, dorsal fin fold; hk, head kidney; ie, inner ear; int, intestine; postaff, postanal fin fold; preaff, preanal fin fold; psb, posterior swim bladder; yo, yolk. Scale bars = 1 mm in A and 0.1 mm in B–D.

At this stage, the swim bladder has not yet developed; however, its primordia can be recognized in some individuals (Fig. 7B). Furthermore, most of the yolk remains (Fig. 7C). Presumably because individuals at this stage are dependent on the yolk for their nutrition, prot stage larvae exhibit little variation in growth rate as compared with later postembryonic stages (Figs. 8–19). Although gaps in the melanophore are known to be present in zebrafish embryos and larvae, such gaps cannot be defined in goldfish individuals at the equivalent stage due to highly divergent polymorphisms in the pigmentation patterns which were established by domestication (Berndt, 1925; Goodrich and Anderson, 1939; Kajishima, 1977; Smartt, 2001). Dorsal, preanal, and postanal fin folds are also recognizable at this stage. Furthermore, the notochord of the caudal region is straight (Fig. 7D). Larvae of this stage exhibit swimming behavior, but they tend to stay near the bottom of the aquarium tank. This stage is quite similar with the zebrafish prot stage (Tsai et al., 2013).

Psb Stage

Larvae of this stage tend to show active swimming at the surface or middle of the tank, consistent with Li et al. (1959) (Table 1). The developing posterior swim bladder is silver in color and round in shape (Fig. 8A,B). This stage is equivalent to the stage of inflation of the swim bladder posterior lobe (pSB) in zebrafish (Parichy et al., 2009). Moreover, it is worth noting that the appearance order of the protruding mouth and swim bladder is conserved among zebrafish, medaka, and cichlid species (Fujimura and Okada, 2007).

As compared with the previous stage, the lower jaws and mouth opening at the Psb stage extend more toward the anterior (Fig. 8B). Yolk, as well as dorsal, preanal, and postanal fin folds, are still present (Fig. 8B–D), and the notochord remains straight at this stage (Fig. 8D). Moreover, condensation of the caudal fin and

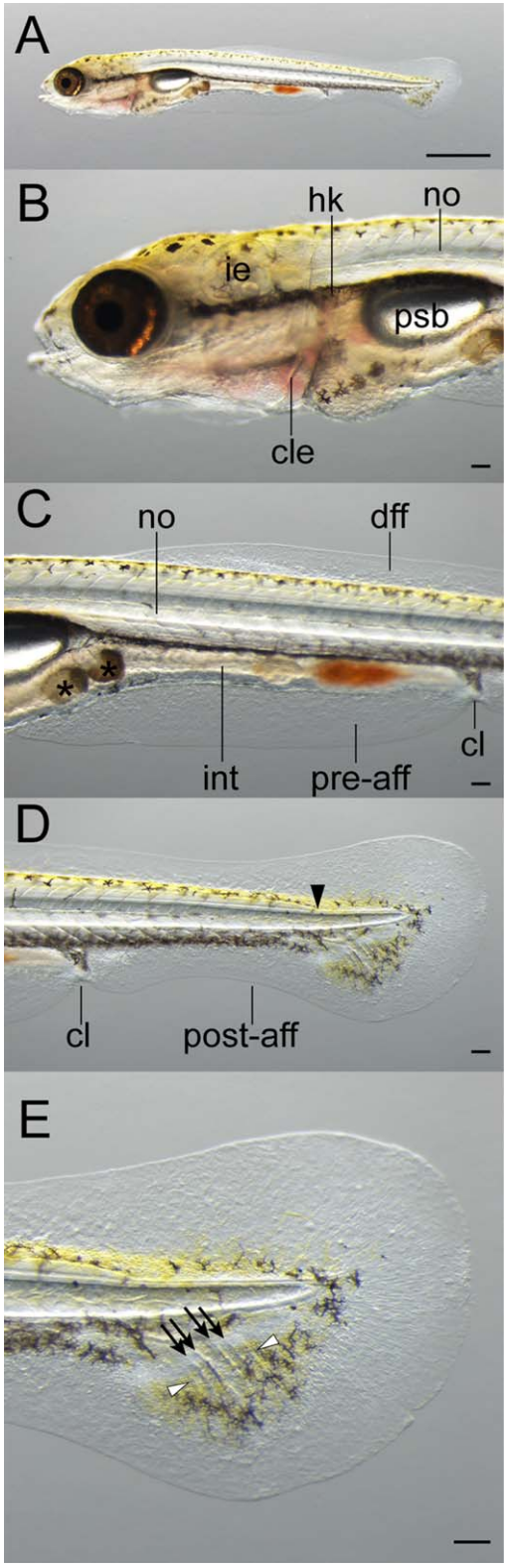

Fig. 10. Cr4 sub-stage larvae. **A–E**: Lateral views of the whole body (A), anterior (B), mid-trunk (C), and caudal (D,E) regions, were photographed under a light field. The black arrowhead indicates flection of the notochord. Four caudal fin rays are visible (black arrows in E). Developing fin rays are indicated by white arrowheads. cl, cloaca; cle, cleithrum; dff, dorsal fin fold; hk, head kidney; ie, inner ear; int, intestine; no, notochord; postaff, postanal fin fold; preaff, preanal fin fold; psb, posterior swim bladder. Scale bars = 1 mm in A; 0.1 mm in B–E.

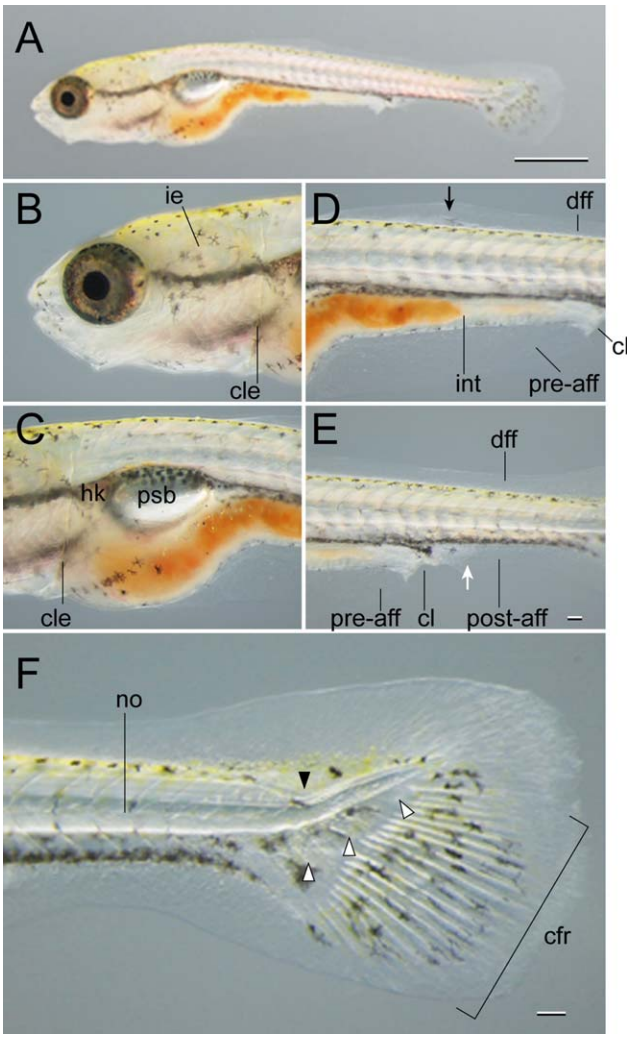

Fig. 11. Cr17 sub-stage larvae. **A–F**: Lateral views of the whole body (A), and head (B), swim bladder (C), dorsal fin (D), cloaca (E), and caudal fin (F) regions, were photographed under a light field (A) and oblique light (B–F). Seventeen caudal fin rays are visible (cfr in F). Black and white arrows indicate condensation of cells in the dorsal and anal fins, respectively. Black and white arrowheads indicate the bending point of the notochord and caudal fin skeletons, respectively. cl, cloaca; cle, cleithrum; cfr, caudal fin ray; dff, dorsal fin fold; hk, head kidney; ie, inner ear; int, intestine; no, notochord; postaff, postanal fin fold; preaff, preanal fin fold; psb, posterior swim bladder. Scale bars = 1 mm in A; 0.1 mm in E,F. B–E are at the same magnification.

fin ray primordial cell population can be seen as a whitish region at the ventral side of the notochord (black arrowhead in Fig. 8D).

At the late Psb stage, the yolk tends to be absorbed, and simultaneously, the larva exhibits a slightly elongated snout and contains digested materials in its intestine (Fig. 9A–C). Head kidney is also visible from this stage onward (Fig. 9B). Residual yolk tend to be located at the anterior–ventral side of the trunk region (Fig. 9C). Dorsal fin fold and postanal fin fold are slightly reduced at this stage as compared with the previous stage (Figs. 8, 9D). Yolk cannot be observed at subsequent stages (Fig. 10).

Cr Stage

The transparency of the entire body fades during this stage, as apparent when compared with the two previous stages (Figs.

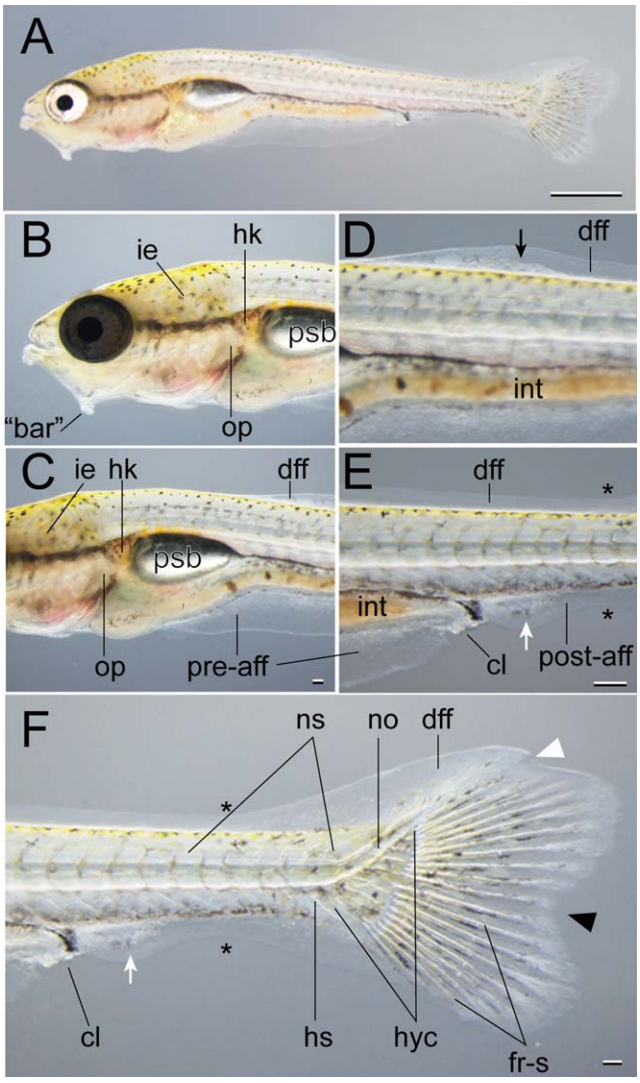

Fig. 12. Fcf stage larvae. **A–F**: Lateral views of the whole body (A), and head (B), swim bladder (C), dorsal fin (D), cloaca, (E), and caudal fin (F) regions, were photographed under a light field (A,F) and oblique light (B–E). The white arrowhead indicates the concave region of the fin fold (F). The black arrowhead indicates a large concave point that divides the upper and lower caudal fin lobes (F). Black and white arrows indicate dorsal and anal fin condensation, respectively (D,E). Asterisks indicate the narrowest area of the fin fold at the caudal region (E,F). Twenty caudal fin rays can be recognized (F). A single segment is recognizable on each caudal fin ray (F). **"bar", "larval barbel"**; cl, cloaca; dff, dorsal fin fold; fr-s, segment of fin ray; hk, head kidney; hs, hemal spine; hyc, hypural complex; ie, inner ear; int, intestine; no, notochord; ns, neural spine; op, opercular; postaff, postanal fin fold; preaff, preanal fin fold; psb, posterior swim bladder. Scale bars = 1 mm in A; 0.1 mm in C,E. Panels B and C are at the same magnification, as are D and E.

7–19, 10, 11). In larvae with a standard length of 5.6 to 6.1mm, over four caudal fin rays can be observed (Fig. 10D). Although caudal fin rays are also present during earlier stages, these fin rays cannot be easily detected by light field stereomicroscopy. Based on the ease of observing caudal fin rays in lateral views of fresh live larvae, we categorized larvae with 4 to 20 caudal fin rays into Cr stage (Figs. 10, 11). Moreover, we subdivided this stage into four sub-stages based on the total number of caudal fin rays; for example, larvae with four caudal fin rays would be considered to be at sub-stage Cr4. The representative characteristics of the early and late Cr stages are described here using Cr4 and Cr17 sub-stage larval specimens, respectively (Figs. 10, 11).

By the early Cr stage, the residual yolk has disappeared (Fig. 10A–C). Slight flection of the notochord is observed (arrowhead in Fig. 10D). Caudal fin rays are present at the posterior side of the site at which flection of the notochord occurs (Fig. 10D,E); these caudal fin rays are first visible in larvae with standard lengths of 6.4 to 6.6 mm, and their number increases dramatically in larvae from 6.5 mm to 7.5 mm (Fig. 6).

In late Cr stage larvae, the body maintains a similar appearance and shape to the early Cr stage (Figs. 10, 11), but there are differences in the dorsal fin fold, postanal fin fold, and shape of the notochord at the caudal level (Fig. 11B–F). Transparency fades further from the entire body with the development of the cranial and trunk muscles (Fig. 11B–E). Slightly whitish areas, which may be a mesenchymal cell population, can be recognized at the mid-trunk level in the dorsal fin fold (black arrow in Fig. 11D) and the anal fin fold at the posterior side of the cloaca (Fig. 11E).

Flection of the notochord is evident by this stage (black arrowhead in Fig. 11F), and caudal fin skeletons are visible under oblique light (Fig. 11F). At this stage, the caudal fin is not homocercal (Fig. 11F). The caudal fin ray number of zebrafish seems to be saturated at a relatively early larval stage (6.0 mm larva, equivalent to aSB stage in zebrafish) (Parichy et al., 2009), while it occurs in goldfish at a later stage (15-mm larvae, equivalent with Pr stage) (Fig. 6). These differences seem to be derived from the difference in the maximum number of caudal fin rays at the adult stage (Fujita, 1990; Parichy et al., 2009). In some other investigated teleost species (rainbow trout, Ballard, 1973; medaka, Iwamatsu, 2004; Nile tilapia, Fujimura and Okada, 2007), caudal fin rays also appear before the other median fins rays (dorsal and anal fin rays), suggesting that this is a highly conserved feature.

Fcf Stage

In larvae with 20 or more caudal fin rays, the caudal fin rays start to exhibit a homocercal shape (Fig. 12A). Although it is possible to apply a caudal fin ray number index at this stage, counting the total fin ray number is quite time-consuming and involves an elevated risk of error. For these reasons, we applied the shape of the fin lobe as an index for staging of the larva; the initial larval stage, Fcf, exhibits a largely concaved point in the caudal fin (Fig. 12A–F). Presumably due to the square shape of the caudal fin of medaka, flounder, and Nile tilapia, this index was not used for staging of these species (Martinez and Bolker, 2003; Iwamatsu, 2004; Fujimura and Okada, 2007). Moreover, this staging index was not previously included in the zebrafish postembryonic staging table (Parichy et al., 2009). However, the appearance timing of the largely concave point seems consistent between goldfish and zebrafish; this feature is present in both teleosts before anterior swim bladder appearance.

By this stage, well-developed lower jaw skeletons can be observed (Fig. 12B); in other words, larvae possess angulated lower jaws. At the ventral side of the lower jaw, a "larval barbel" can be observed in some individuals (Fig. 12B). Moreover, this larval barbel tends to appear only on the left or right ventrolateral side. It is not clear why the larval barbel shows such asymmetry in location. Moreover, it remains unknown whether this larval barbel is homologous with the barbel of zebrafish (Parichy et al., 2009). The goldfish larval barbel tends to fade around the

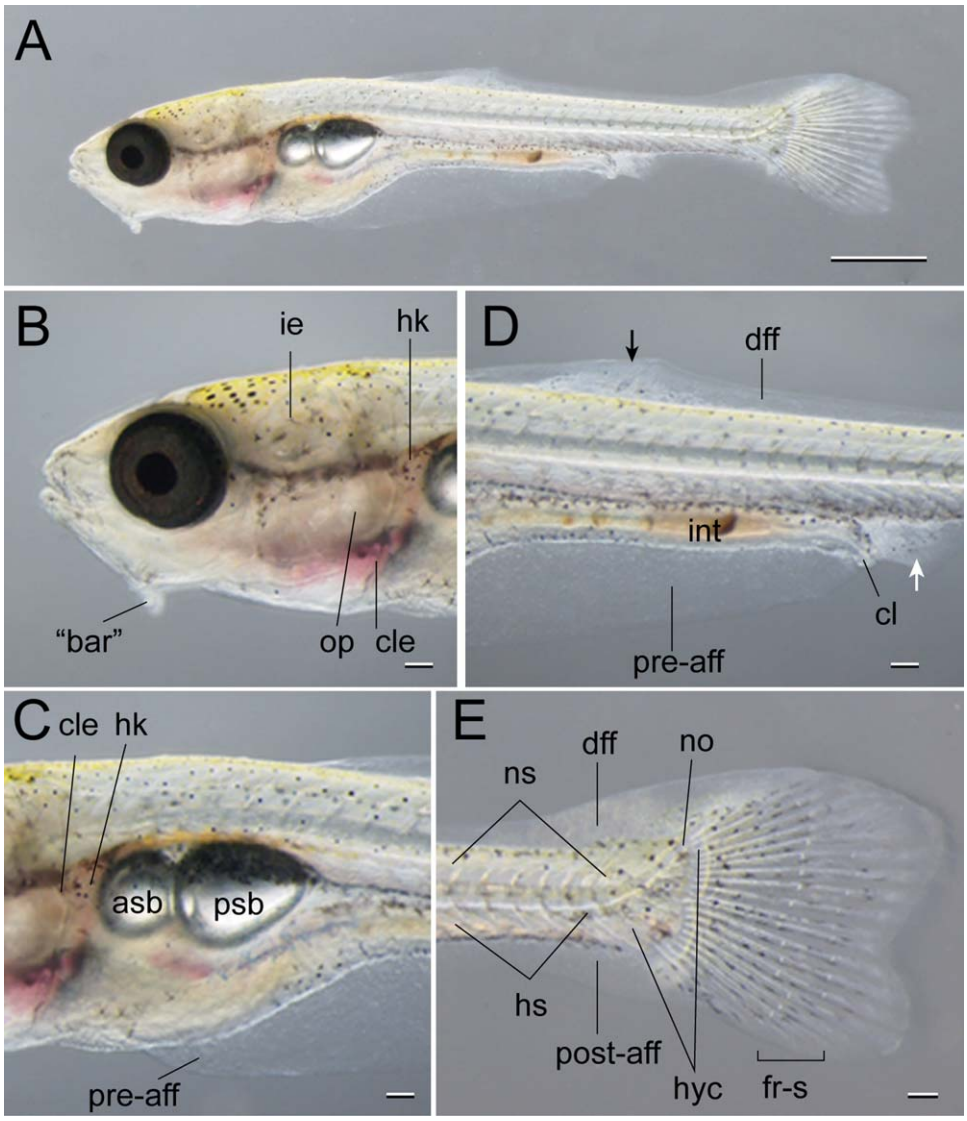

Fig. 13. Asb stage larvae. **A–E**: Lateral views of the whole body (A), and head (B), swim bladder (C), dorsal fin (D), and caudal fin (E) regions, were photographed under oblique light. Black and white arrows indicate condensation of the dorsal and anal fins, respectively (D). asb, anterior swim bladder; **"bar"**, **"larval barbel"**; cl, cloaca; cle, cleithrum; dff, dorsal fin fold; fr-s, segment of fin ray; hk, head kidney; hs, hemal spine; hyc, hypural complex; ie, inner ear; int, intestine; no, notochord; ns, neural spine; op, opercular; postaff, postanal fin fold; preaff, preanal fin fold; psb, posterior swim bladder. Scale bars = 1 mm in A; 0.1 mm in B–E.

Pr stage and cannot be observed in any juvenile individuals of later stages (Figs. 12B, 17C). Migratory mesenchymal cells can be observed in the dorsal fin fold and postanal fin fold (the black arrow in Fig. 12D and the white arrow in Fig. 12E). The primordia of the anal fin are also visible at the prominent postanal fin fold, where mesenchymal cells show condensation (Fig. 12E,F). The posterior side of the caudal fin possesses two concave points, one large and one small. The small concave point is located on the dorsal side of the caudal fin, and disappears at later stages (white arrowhead in Fig. 12F, compare with Fig. 13). The large concave point is enhanced at later stages; this point divides the upper and lower caudal fin lobes (black arrowheads in Figs. 12F, 13). Reduction of the dorsal and postanal fin folds is also evident at this stage (Figs. 11F, 12F). From this stage, segments of fin rays become easily visible under the stereomicroscope (Fig. 12F).

Asb Stage

At this stage, the anterior lobe of the swim bladder is visible from the lateral view (Fig. 13A). Surface cranial morphology is similar with that of the previous stage (Figs. 12B, 13B). The anterior swim bladder lobe is smaller than the posterior one, and is round in shape (Fig. 13C). On the other hand, the posterior swim bladder is oval in shape (Fig. 13C). All three fin folds can still be observed (Fig. 13A,D,E). The primordial cells of the dorsal and anal fins in the fin folds are still visible as a condensed region when viewed from the outside (Fig. 13D). In our observations of live specimens, it was difficult to determine whether dorsal or anal fin condensation started first (Figs. 11–13). More than two segments can be observed on several caudal fin rays (Fig. 13E). Caudal internal skeletons can also be observed (Fig. 13E). From this stage, the anterior swim bladder lobe increases in size, becoming larger than the posterior swim bladder lobe (Figs. 12–14).

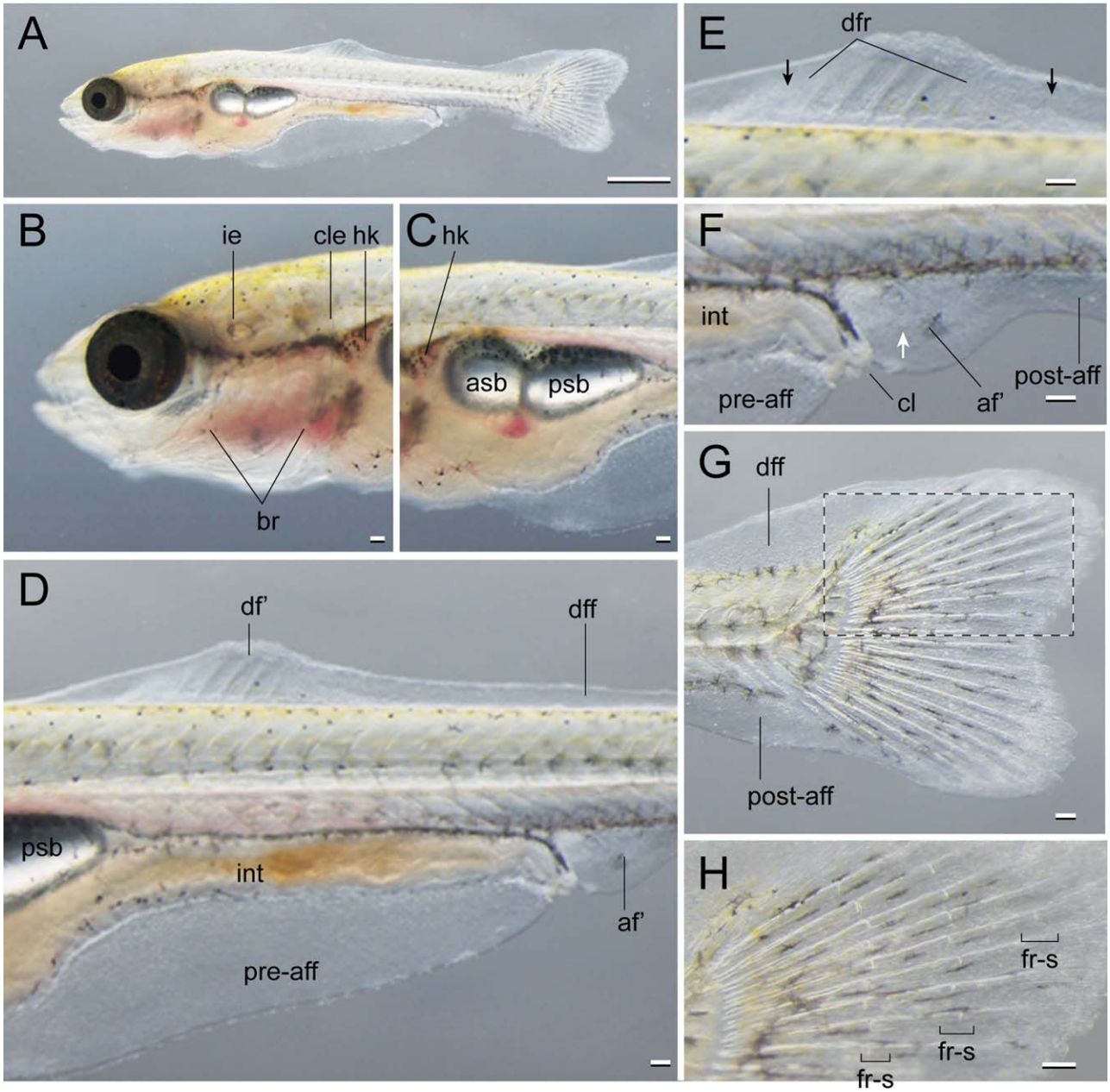

Fig. 14. Dr stage larvae. **A–H**: Lateral views of the whole body (A), and head (B), swim bladder (C), mid-trunk (D), dorsal fin (E), anal fin (F), caudal fin (G), and dorsal side of the caudal fin (H) regions, were photographed under oblique light (A–G) and a light field (H). Panel H is a magnified view of the boxed area (hatched lines) in G. The dorsal fin ray can be observed (D,E). Black and white arrows indicate condensation of the dorsal and anal fins, respectively (E,F). Several caudal fin rays have three segments (H). af′, anal fin primordia; asb, anterior swim bladder; br, branchial arch; cl, cloaca; cle, cleithrum; dff, dorsal fin fold; df′, dorsal fin primordia; fr-s, segment of fin ray; hk, head kidney; ie, inner ear; int, intestine; postaff, postanal fin fold; preaff, preanal fin fold; psb, posterior swim bladder. Scale bars = 1 cm in A; 0.1 cm in B–H.

Dr Stage

At the Dr stage, the anterior swim bladder is larger as compared with that of the previous stage (Figs. 13, 14). Surface cranial morphology remains similar to that of the previous stage (Figs. 13B, 14B). The anterior and posterior swim bladders exhibit oval and elongated oval shapes, respectively (Fig. 14C). All of the fin folds remain (Fig. 14D); however, dorsal and post anal fin folds are evidently reduced in comparison with previous stages, at the level of the most posterior end of the anal fin condensation region (Fig. 14F). The dorsal fin fold at the mid trunk level is prominent, and several fin rays can be observed (Fig. 14D). Condensation of the mesenchymal cell populations can be observed at the anterior and posterior ends of the dorsal fin ray area (black arrows in Fig. 14E). Dorsal fin rays appear earlier than anal fin rays (Fig. 14E,F), and a large part of the preanal fin fold remains (Fig. 14D). At the level of the notochord flection, the dorsal and postanal fin folds largely remain (Fig. 14G). The caudal fins of specimens at this stage exhibit almost symmetrical homocercal shapes (Fig. 14G). Three segments can be observed in the caudal fin fold (Fig. 14H).

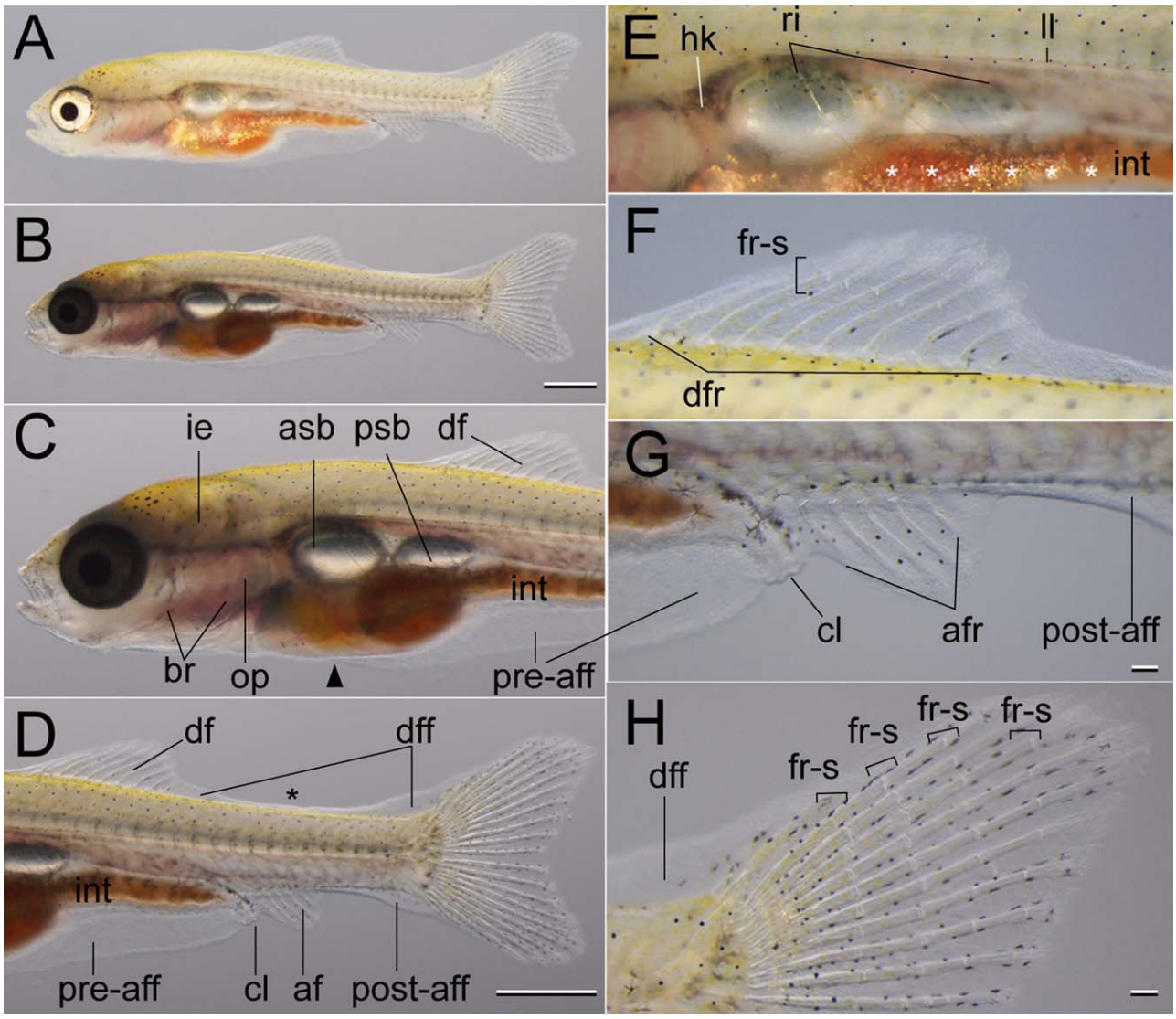

Fig. 15. Ar stage larvae. **A–H**: Lateral views of the whole body (A,B), anterior (C), posterior (D), swim bladder (E), dorsal fin (F), anal fin (G), and dorsal part of the caudal fin (H) were photographed under a light field (A,E,F,H) and oblique light (B,C,D,G). The black arrowheads indicate the anterior end of the preanal fin fold and the anal fin fold. The black asterisk indicates the narrowest region of the dorsal fin fold (D). White asterisks indicate iridophores in the intestine area (E). af, anal fin; afr, anal fin ray; asb, anterior swim bladder; br, branchial arch; cl, cloaca; df, dorsal fin; dff, dorsal fin fold; dfr, dorsal fin ray; fr-s, segment of fin ray; hk, head kidney; ie, inner ear; int, intestine; ll, lateral line; op, opercular; postaff, postanal fin fold; preaff, preanal fin fold; psb, posterior swim bladder; ri, rib. Scale bars = 1 mm in B,D; 0.1 mm in G,H. Panels A and B, C and D, and E, F, and G are at the same magnification.

Ar Stage

The dorsal and anal fin folds are largely reduced at this stage, and the outline of the dorsal and caudal fins are clear (Fig. 15A–D), forming a curved triangular shape (Fig. 15F,G). At this stage, both the dorsal and anal fin fold possess fin rays (Fig. 15D,F,G). The anterior lobe of the swim bladder is larger than the posterior lobe of the swim bladder (Fig. 15C,E). At around the cloacal level, the dorsal fin fold is almost completely reduced (the black asterisk in Fig. 15D). Nine dorsal fin rays and five anal fin rays can be seen in the individual shown here (Fig. 14F,G). Several dorsal fins contain one segment (Fig. 15F), while the anal fin rays do not (Fig. 15G). At the posterior side of the anal fin, part of the anal fin fold remains (the white arrowhead in Fig. 15G). A maximum of four segments are observed in the caudal fin rays (Fig. 15H). Although anal fin rays appear first, followed by dorsal fin rays, in zebrafish (Parichy et al., 2009), this ontogenetic sequence is reversed in goldfish; this ontogenetic sequence is consistent with Li et al. (1959).

Pb Stage

Increased body thickness, well-developed muscle tissues, and pigmentation collectively result in a further reduction of transparency in Pb stage larvae as compared with larvae at earlier stages (Fig. 16A,B). When viewed from the surface, substantial changes in the cranial region or swim bladder cannot be observed (Fig. 16C,D). Pelvic fin buds appear on the ventral side of the trunk region,

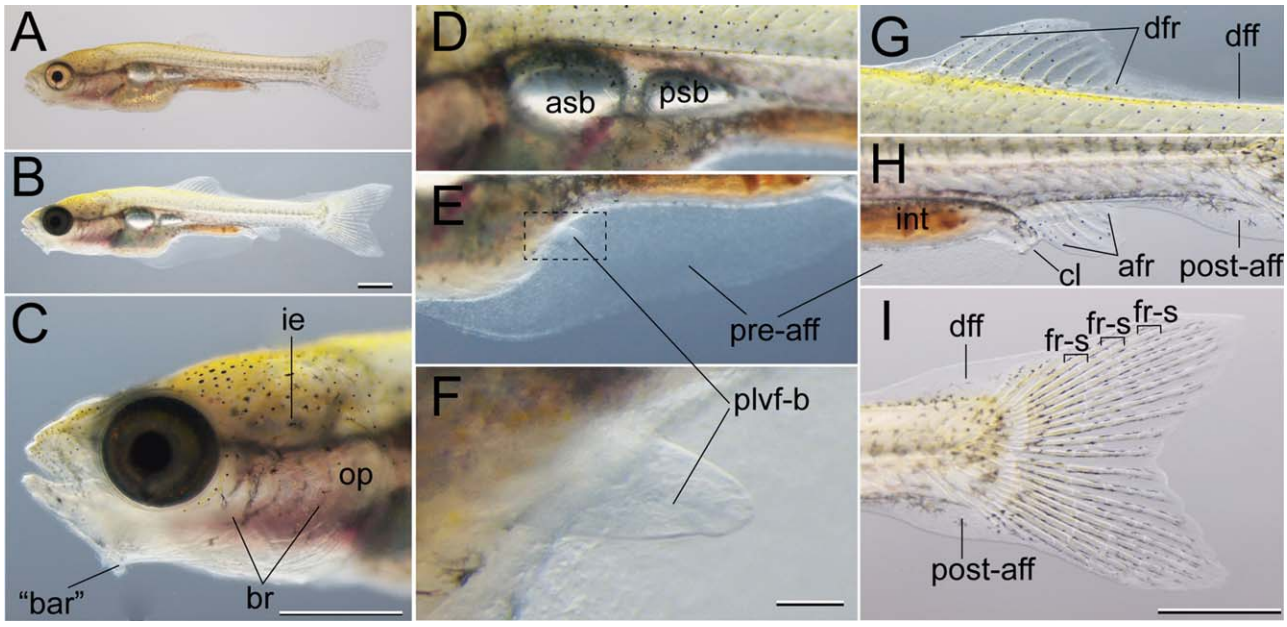

Fig. 16. Pb stage larvae. **A–I**: Lateral views of the whole body (A,B), head (C), swim bladder (D), ventral side of the mid-trunk (E), pelvic fin bud (F), dorsal fin (G), anal fin (H), and caudal fin (I) were photographed under a light field (A,I) and oblique light (B–H). Panel F is a magnified view of the boxed area (hatched lines) in E. Dorsal and post anal fin folds are still readily visible at the caudal region (G–I). afr, anal fin ray; asb, anterior swim bladder; "bar", "larval barbel"; br, branchial arch; cl, cloaca; dff, dorsal fin fold; dfr, dorsal fin ray; fr-s, segment of fin ray; ie, inner ear; int, intestine; op, opercular; plvf-b, pelvic fin bud; postaff, postanal fin fold; preaff, preanal fin fold; psb, posterior swim bladder. Scale bars = 1 mm in B,C,I; 0.1 mm in F. Panels A and B, and C–E, G, and H, are at the same magnification.

where they are attached to the stem of the preanal fin fold at the end of the posterior swim bladder (Fig. 16B,E). The buds possess apical folds, akin to those of the pelvic fins (Fig. 16F). Dorsal and anal fin folds are retained but are reduced in size (Fig. 16G–I).

Pr Stage

By this stage, body parts containing muscles and/or intestine are semitransparent or almost completely opaque (Fig. 17A,B). While the anterior lobe of the swim bladder is visible, the posterior lobe of the swim bladder is difficult to see from the body surface, because of the well-developed intestine and kidney (Fig. 17A–D). Dorsal and postanal fin folds cannot be observed at low magnification (Fig. 17A,B), and the preanal fin fold is reduced in comparison with that at the Pb stage (Fig. 17D). Although the pelvic fin rays are not easily recognized under low magnification (Fig. 17D), they are visible under higher magnification (Fig. 17D,E). The dorsal and anal fin rays possess four and three segments, respectively (Fig. 17F,G). At higher magnifications, dorsal and postanal fin folds can be observed in the caudal region (Fig. 17H). The dorsal and anal fin rays at posterior regions are elongated (Fig. 17FG), and these fins exhibit a trapezium shape (Fig. 17D). At this stage, almost all of the fin rays at the dorsal, anal, and caudal fins have appeared (Figs. 6, 17F–H). In addition, over seven caudal fin segments can be observed (Fig. 17I), and squamation and mineralized scale tissues are also visible (Fig. 20A–C). The sequence in which pelvic fin bud and pelvic fin ray appear in goldfish is almost consistent with that of zebrafish (Parichy et al., 2009). In both teleost species, the pelvic fin bud appears after the anal and dorsal fin rays appear (Figs. 14–16), and this is followed by the appearance of the pelvic fin rays (Fig. 17). This ontogenetic sequence seems to be conserved among teleost species (Fujimura and Okada, 2007).

Juvenile Stage

The juvenile stage of zebrafish is defined by the completion of scale patterning (squamation) and the complete loss of the fin fold (Parichy et al., 2009). However, this definition cannot be directly applied to goldfish, because the developmental processes of squamation and fold reduction are different between these two teleost species. It seems that these two developmental events occur almost simultaneously in zebrafish, but not in goldfish. In the latter, squamation seems to finish after the complete reduction of the fin fold. In fact, we observed two types of "fin fold-less" postembryonic goldfish specimens: one is completely scaled, while the other is not. Thus, to describe the developmental process and characteristics of the goldfish juvenile, we used the squamation patterns to divide fish into the following early and late juvenile sub-stages: "Incompletely scaled juvenile (IsJ)" and "Completely scaled juvenile (CsJ)" (Figs. 18, 19).

IsJ Sub-stage

At this stage, almost the entire body is covered by scales (Fig. 18A); however, the anterior–dorsal trunk region lacks scales (asterisks in Fig. 18B). Although the transparency of fresh scales (Fig. 18B) makes scaled and unscaled regions difficult to distinguish in lateral views of live juveniles, squamation patterns were confirmed by alizarin red staining of fixed samples (Fig. 18D–I). At the IsJ sub-stage, pigmented scales reduce the visibility of the swim bladder (Fig. 18A,B). Dorsal, pelvic, and anal fins are well developed, and all of the fin folds have completely disappeared

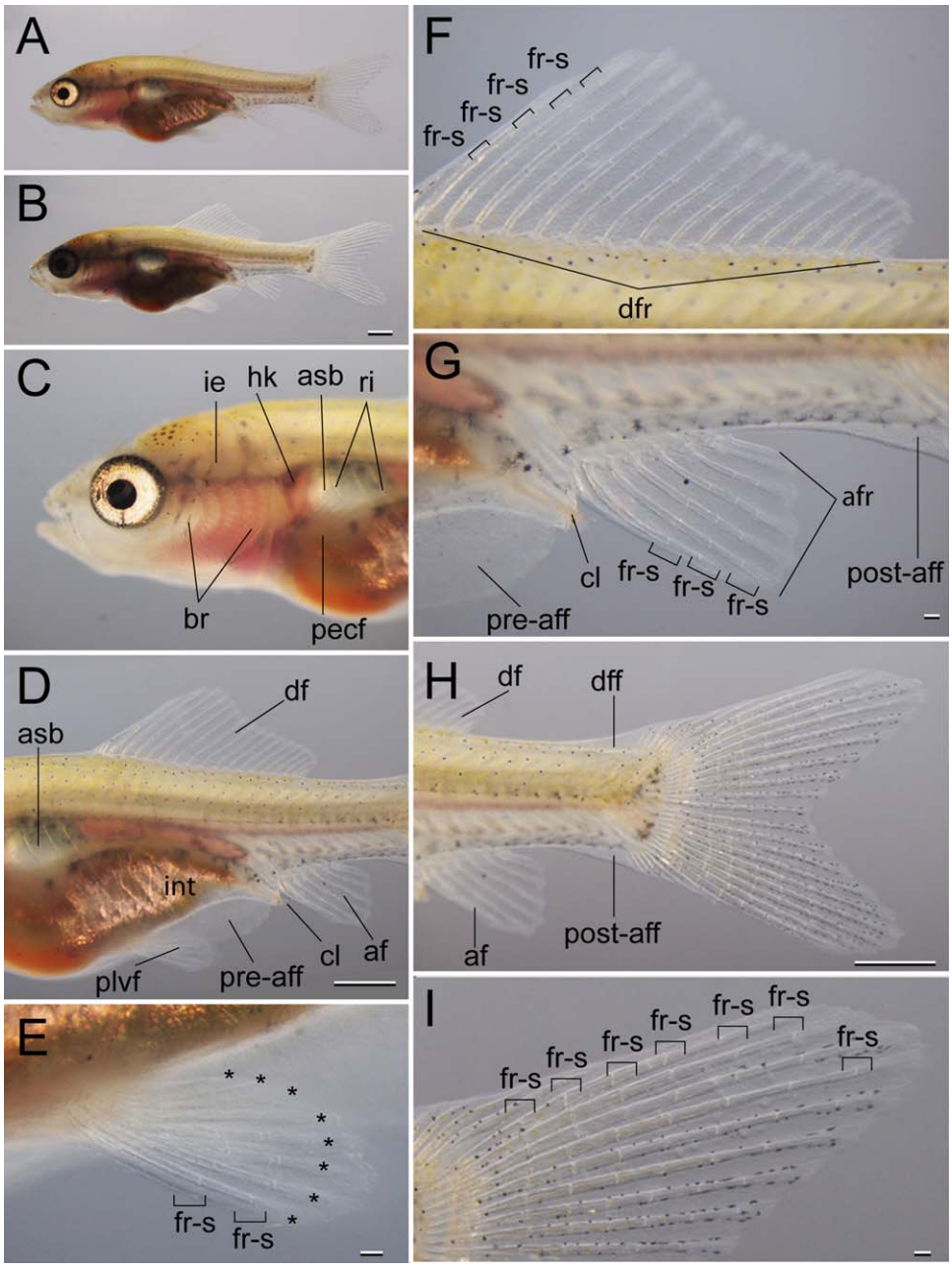

Fig. 17. Pr stage larvae. **A–I**: Lateral views of the whole body (A,B), and anterior (C), trunk (D), pelvic fin (E), dorsal fin (F), anal fin (G), posterior (H), and caudal (I) regions, were photographed under a light field (A,C–I) and oblique light (B). The examined individual exhibits a total length of 12 mm, and has nine fin rays in the pelvic fin. Black asterisks indicate fin rays. Two segments are visible in the pelvic fin ray (fr-s in E). af, anal fin; afr, anal fin ray; asb, anterior swim bladder; br, branchial arch; cl, cloaca; df, dorsal fin; dff, dorsal fin fold; dfr, dorsal fin ray; fr-s, segment of fin ray; hk, head kidney; ie, inner ear; int, intestine; pecf, pectoral fin; plvf, pelvic fin; postaff, postanal fin fold; preaff, preanal fin fold; ri, rib. Scale bars = 1 mm in B,D,H; 0.1 mm in E,G,I. Panels A and B, C and D, F, and G, are at the same magnification.

by this stage (Fig. 18A, C). Nineteen caudal fin rays are exposed on the outside of the body (Fig. 18F). The second externally visible caudal fin ray is evidently thicker than the others, and this fin ray has segmental posterior serrations (Fig. 18D). The anal fin ray is also well developed, and one of its fin rays is thicker than the others, and exhibits posterior serration (Fig. 18E). With regard to the nomenclature problem of the "spine," as indicated by Mabee et al. (2002), these serrated and segmented "spine-like" fin rays in goldfish differ from the true bone spines observed in *Acanthopterygii* (spiny finned) species; true spines are not segmented, in contrast to goldfish "spines". Thus, to avoid confusion, we have designated these goldfish spine-like fin rays as "segmented fin spines" (sfs in Fig. 18E).

CsJ Sub-stage

Juveniles of this stage are very similar to the adult in terms of external skeletal morphology (Figs. 2, 19). Squamation patterning is complete by this stage (Figs. 19, 20J,K). The dermal cranium and scales (Fig. 21) are strongly pigmented (through the presence

TABLE 2. Postembryonic Stages of the Goldfish

Stage name (Abb)	Descriptions (SL and dpf onset)	Corresponding figures and panels
Protruding mouth (prot)	Extended mouth, yolk, all fin folds remain; straight notochord at the caudal fin level (5mm and 3dpf) (Tsai et al., 2013)	Fig. 7; Fig. 25AA′
Posterior swim bladder (Psb)	Inflation of the posterior swim bladder; lower jaw extension (5.6-5.7mm and 5.7-5.8dpf)	Fig. 8; Fig. 9; Fig. 22; Fig. 25BB′; Fig. 28A; Fig. 36A-C
Caudal fin ray (Cr)	More than four visible caudal fin rays, snout length longer than at Psb, slightly bent caudal fin; this stage can be divided into sub-stages based on the number of fin rays (6.1-6.3mm and 7.5-7.8dpf)	Fig. 10; Fig. 11; Fig. 22BC; Fig. 25CC'DD′; Fig. 33BCD; Fig. 36D
Forked caudal fin (Fcf)	Appearance of a largely concaved point in the caudal fin, evident anal and dorsal fin condensation; slightly reduced dorsal and post-anal fin rays (6.8-7.0mm and 13.6 −13.8dpf)	Fig. 12A; Fig. 27A; Fig. 33E
Anterior swim bladder (Asb)	Inflation of anterior swim bladder; enhanced anal and dorsal fin condensation (7.0-7.3mm and 12.8-14.8dpf)	Fig. 13; Fig. 33F; Fig. 34A
Dorsal fin ray (Dr)	Dorsal fin ray appearance; anterior swim bladder lobe is larger than that of Asb stage (7.5-7.8mm and 18.0-20.0dpf)	Fig. 14
Anal fin ray (Ar)	Anal fin ray appearance; lack of the dorsal fin fold at the anal fin level, anterior swim bladder is larger than posterior swim bladder; curved triangle shape-like dorsal fin (8.2–8.4mm and 22.3–24.0dpf)	Fig. 15
Pelvic fin bud (Pb)	Pelvic fin bud appearance (8.7-9.0mm and 26.0–27.0dpf)	Fig. 16; Fig. 28A; Fig. 29A; Fig. 31A; Fig. 34B; Fig. 35AB;
Pelvic fin ray (Pr)	Pelvic fin ray appearance; elongated most posterior dorsal and anal fin rays; trapezium shaped dorsal and anal fins (11.0–11.2mm and 31.0–31.1dpf)	Fig. 17; Fig. 20; Fig. 23AA'; Fig. 24AB; Fig. 26AB; Fig. 29B; Fig 30AB; Fig. 31B; Fig. 32B
Juvenile	Complete loss of the fin fold; incomplete squamation; posterior serrations at the anterior dorsal and anal fin ray; this stage can be divided into two sub-stages based on squamation patterns (17.0-17.6mm and 45.2–49.2dpf)	Fig. 18; Fig. 19; Fig. 21; Fig. 23BB'; Fig. 24CD; Fig. 26CD; Fig. 27C; Fig. 28C; Fig. 29CD; Fig. 30CD; Fig. 31CD; Fig. 32CD; Fig. 34CD; Fig. 35CD
Adult	Produce mature eggs and sperm; SL onset, 5cm-	Fig. 2

of melanophores and iridophores) in most specimens, but variations in pigmentation patterns are observed between individuals and strains (Matsui et al., 1981; Smartt, 2001). The thickness of the dorsal and anal segmented fin spines distinguishes them from other fin rays (sfs in Fig. 19C,E).

Adult Stage

Goldfish individuals of over 5 cm in standard length tend to show external sexual traits (Fig. 2). Most of the male individuals possess breeding tubercles on the opercular and pectoral fins (Fig. 2B) and produce mature sperm in the breeding season (Fig. 2D,D′). Mature female goldfish have a prominent cloaca, as is also observed in zebrafish (Fig. 2E) (Dranow et al., 2013). It is known that goldfish must experience seasonal changes of temperature and light condition before egg spawning (Razani and Hanyu, 1986). This suggests that constant water temperature and light cycle may inhibit the development and spawning of mature eggs, even when female individuals are greater than 5 cm in total length and possess external sexual traits. Moreover, our empirical observations indicate that adult females of more than 10 cm in standard length are able to stably spawn mature eggs.

Skeletal System

Goldfish skeletons are of particular interest on account of their highly divergent skeletal morphologies, and they have been extensively studied using classical anatomical techniques (Watase, 1887; Berndt, 1925; Koh, 1931, 1932; Asano and Kubo, 1972). However, little is known about the underlying developmental process of even wild-type strains; this in stark contrast with zebrafish, the skeletal systems of which have been intensively investigated using several different techniques (including the use of alizarin red staining, fluorescence microscopy techniques, and histological techniques) (Du et al., 2001; Kimmel et al., 2007; Parichy et al., 2009; Bensimon-Brito et al., 2012). Thus, here we applied both fluorescence microscopy and classic techniques (alizarin red staining) to study goldfish skeletal morphogenesis (Figs. 22–35). Moreover, to reveal the relationship between skeletal tissues and nonskeletal tissues, we prepared two different

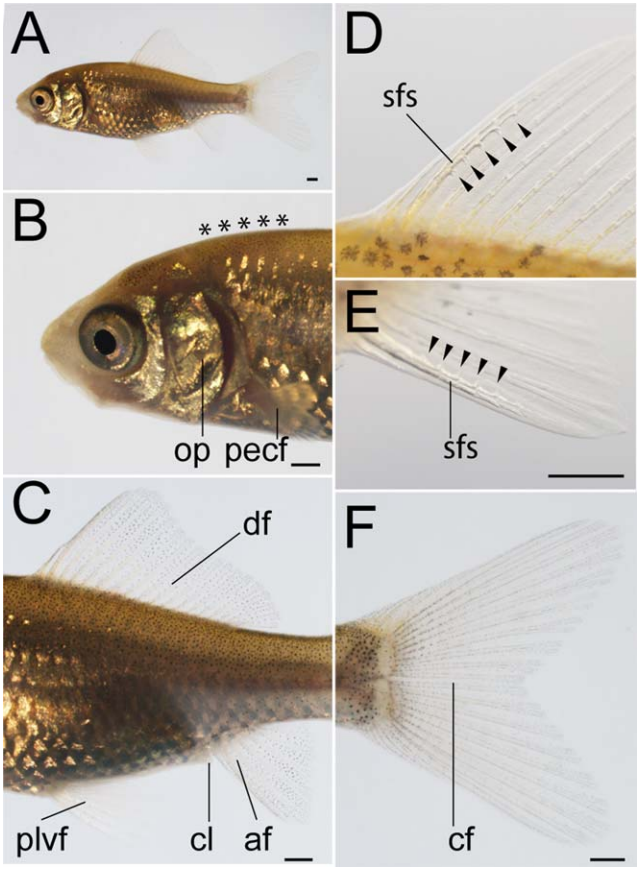

Fig. 18. IsJ sub-stage specimen. **A–F**: Lateral views of the whole body (**A**), and anterior (**B**), mid-trunk (**C**), dorsal (**D**), anal fin (**E**), and caudal fin (**F**) regions, were photographed under a light field. Black asterisks indicate scales missing from the anterior dorsal trunk region. Black arrowheads indicate posterior serrations in the dorsal and anal fin rays (D, E). af, anal fin, cf, caudal fin; cl, cloaca; df, dorsal fin; op, opercular; pecf, pectoral fin; plvf, pelvic fin; sfs, segmented fin spine. Scale bars = 1 mm. Panels D and E are at the same magnification.

types of alizarin red-stained samples; transparent and opaque samples (see the Experimental Procedures section).

The morphological similarities of the goldfish and zebrafish skeletal systems allowed relatively easy comparison of skeletons (Figs. 22, 23); we describe here the developmental process of goldfish skeletal system formation based on earlier descriptions of the zebrafish skeletal system (Cubbage and Mabee, 1996; Du et al., 2001; Bird and Mabee, 2003; Parichy et al., 2009). Skeletal features which are not well-described in zebrafish are also depicted based on early studies of adult goldfish and other related teleost species (Koh, 1931; Gregory, 1933; Fink and Fink, 1981; Fujita, 1990). To systematically describe goldfish skeletons, we explain mid-trunk and cranial skeletons, and pectoral-, pelvic-, dorsal-, anal-, and caudal fin regions, separately (Figs. 22–35).

Mid-trunk Skeletons

A segmentally arranged vertebral body can be observed in Psb stage larvae under fluorescence microscopy; at this stage, around fifteen calcified vertebral structures can be seen in the lateral view (Fig. 22A). The number of calcified vertebral structures increases during development, to a maximum of 20 vertebrae in goldfish with three caudal fin rays (Fig. 22B). In Cr10 sub-stage individuals with more than 27 calcified vertebrae, neural spines can be recognized on the fourth to eighth vertebrae (Fig. 22C). At the Cr16 sub-stage, there are around 28 calcified vertebrae (Fig. 22D), with eight vertebrae at the anterior trunk region possessing attached neural spines (Fig. 22D). Furthermore, although calcification can be observed at the dorsal side of the notochord at the caudal region (Fig. 22D) (Bensimon-Brito et al., 2012), certain vertebrae are yet to be calcified (Fig. 22D).

At the Pr stage, all of the vertebral bodies and their attaching skeletal elements are well calcified (Figs. 23A, 24A,B); in fact, neural and hemal spines can be observed throughout the trunk region (Fig. 23A). Moreover, some of the supraneuralis elements are also visible at the dorsal aspect of the fourth vertebral body (Figs. 23A, 24AB). Calcification of the vertebral elements which contribute to the Weberian apparatus can be observed at this stage (Fig. 24A); this is consistent with previous reports (Watson, 1939; Coburn and Futey, 1996; Grande and Yong, 2004), which also reported that the first to fourth vertebral elements from the most anterior vertebra form the Weberian apparatus. Furthermore, the os suspensorium, tripus, and the fourth rib were observed at this stage, and the third supraneuralis is also visible as small ossified skeletal elements at the first to fourth vertebral levels (Fig. 24A,B). At the CsJ sub-stage, these skeletal elements closely approach each other, and the third supraneuralis connects with the fourth vertebrae (Fig. 24CD), which is also consistent with earlier reports (Watson, 1939; Coburn and Futey, 1996; Grande and Yong, 2004).

Cranial Skeletons

From the lateral surface view, changes in cranial morphology can be observed, especially, in the mouth region (length of snout and lower jaw) (Fig. 25A–D). Moreover, the order of appearance of cranial skeletal structures can be traced using a calcein-stained florescent view (Fig. 25A′,B′,C′,D′). At prot stage, calcification of the cleithrum, fifth ceratobranchial, opercular, and dentary can be observed (Fig. 25A,A′). At Psb stage, calcification of the cranial skeletons (hyoid, maxilla, branchiostegal, and quadrate) can also be observed (Fig. 25B,B′). At the Cr4 sub-stage, the anguloarticular, retroarticular, and interopercle rays show strong calcification (Fig. 25C′), and by the Cr16 sub-stage, the subopercle, premaxilla, and first to fourth ceratobranchials are easily identified (Fig. 25D′).

At the late larval stages (from Fcf stage), the complexity of the cranial skeleton increases, and its complexity impedes the observation and identification of each cranial skeletal structure. Thus, to examine the surface and deep region of the cranial skeletal system, we separately observed opaque and transparent skeletal samples (Figs. 26–28). Most of the branchial and facial bones which are visible on the surface appear at the Fcf stage; however, larvae at this stage lack the skeletal elements of the cranium (parietal, frontal, posttemporal, pterotic) (Fig. 27A). These skeletal elements seem to appear at later stages (Fig. 27B,C). From the ventral view, skeletal elements of hyoid and branchial arches (basihyal, branchiostegal rays, ceratohyal, ventral hyophyal, urohyal) and facial bones (anguloarticular, retroarticular, dentally, quadrate, inter opercular, sub-opercular) are visible (Fig. 28). Most of these hyoid and branchial arches can be easily seen in the pectoral fin to IsJ sub-stages (Fig. 28); however, basihyal, ceratohyal, hyophyal ventral, and urohyal tend to be difficult to see through

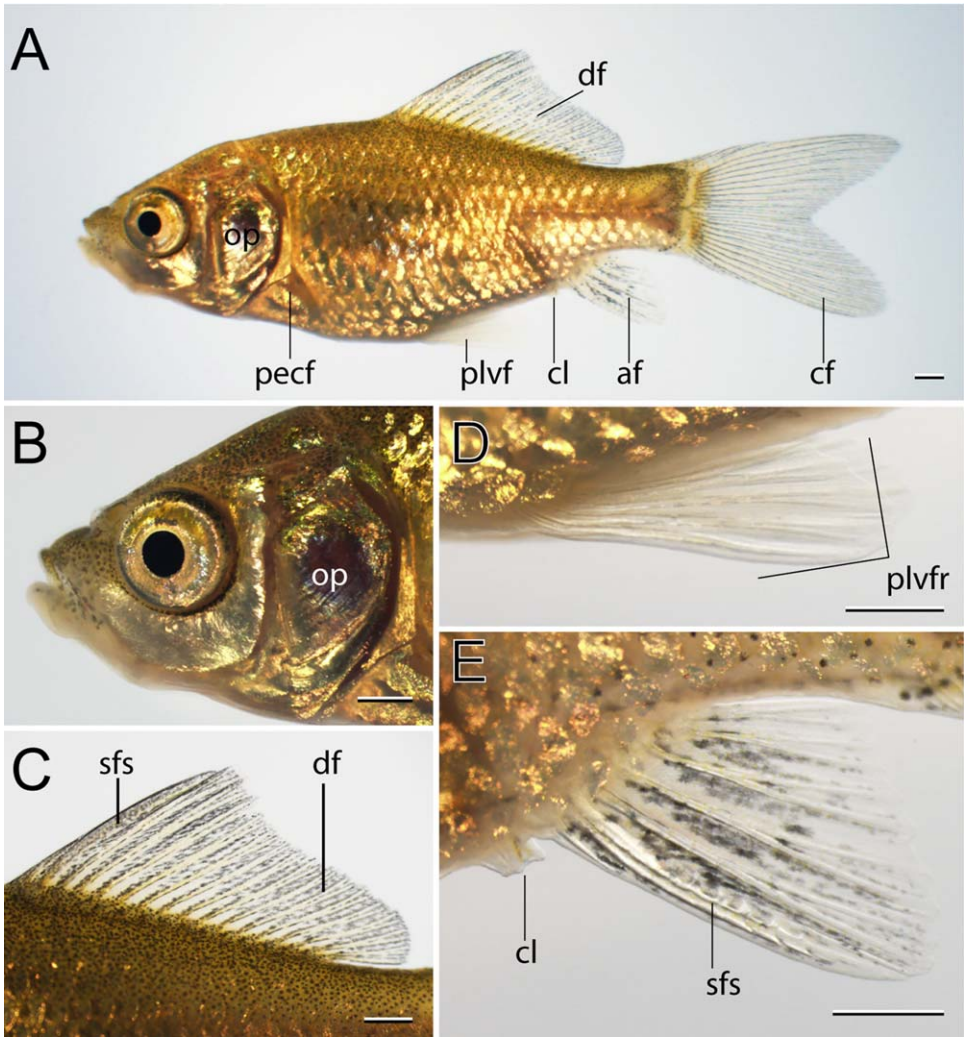

Fig. 19. CsJ sub-stage specimen. **A–E**: Lateral views of the whole body (A), head (B), dorsal fin (C), pelvic fin (D), and anal fin (E) were photographed under a light field. af, anal fin; cf, caudal fin; cl, cloacal; df, dorsal fin; pecf, pectoral fin; plvf, pelvic fin; plvfr, pelvic fin ray; sfs, segmented fin spine. Scale bars = 1 mm.

the surface, due to the development of nonskeletal connective tissues at Pr stage and IsJ sub-stage (compare Figs. 28A and 28B,C). Moreover, the cleithrum is obscure, because this bone is covered by muscle tissues at the Pr stage (Fig. 28C). In early Pr stage larvae, the palatine and kinethmoid, which are related to suction feeding, can be observed; moreover, calcification of the palatine is also observed (Fig. 26A,B). At the IsJ stage, the frontal and parietal bones are well calcified (Fig. 27B), and can be observed in transparent skeletal samples at CsJ sub-stage (Fig. 26C,D). The ectopterygoid and metapterygoid are also visible at the juvenile stages (Fig. 26). In addition, the kinethmoid and its attached palatine are observed at the cranial region in Pr stage and CsJ sub-stage specimens (Fig. 26). The elongated postcleithrum is also clearly visible in specimens of this stage (Fig. 26).

Pectoral Fin Skeletons

Pectoral fin skeletons consist of fin rays and radials, and the radial basements are supported by the pectoral girdle (Figs. 24, 29) (Grandel and Schulte-Merker, 1998; Liem et al., 2001; Kardong, 2012). Although the fin rays are relatively easily recognized in fixed and stained specimens (Figs. 27B,C, 29), the transparency of fin rays and fin lobe make them hard to observe in live fish from the lateral view (Figs. 7–19). Calcified fin rays are readily visible in goldfish larvae and juvenile specimens stained with alizarin red (Fig. 29). Four to five mineralized fin rays are visible at the Pb stage (Fig. 29A), and they increase to around nine fin rays by the pelvic fin ray stage (Fig. 29B). At the juvenile stage, around 14 pectoral fin rays are visible from the lateral view in alizarin red-stained samples (Fig. 29C,D). At the CsJ sub-stage, these fin rays are bifurcated at the distal side (Fig. 29C,D,D′).

Of the internal skeletal structures of the pectoral girdle, the cleithrum can be observed at early stages (Kimmel et al., 1995; Grandel and Schulte-Merker, 1998; Du et al., 2001; Mabee et al., 2002). By the prot stage at the latest, this skeleton can be observed as calcified tissues (Fig. 25A′). Because this skeleton is located at a relatively shallow part of the fish body, it can be observed in its entirety in live early larval stage specimens and

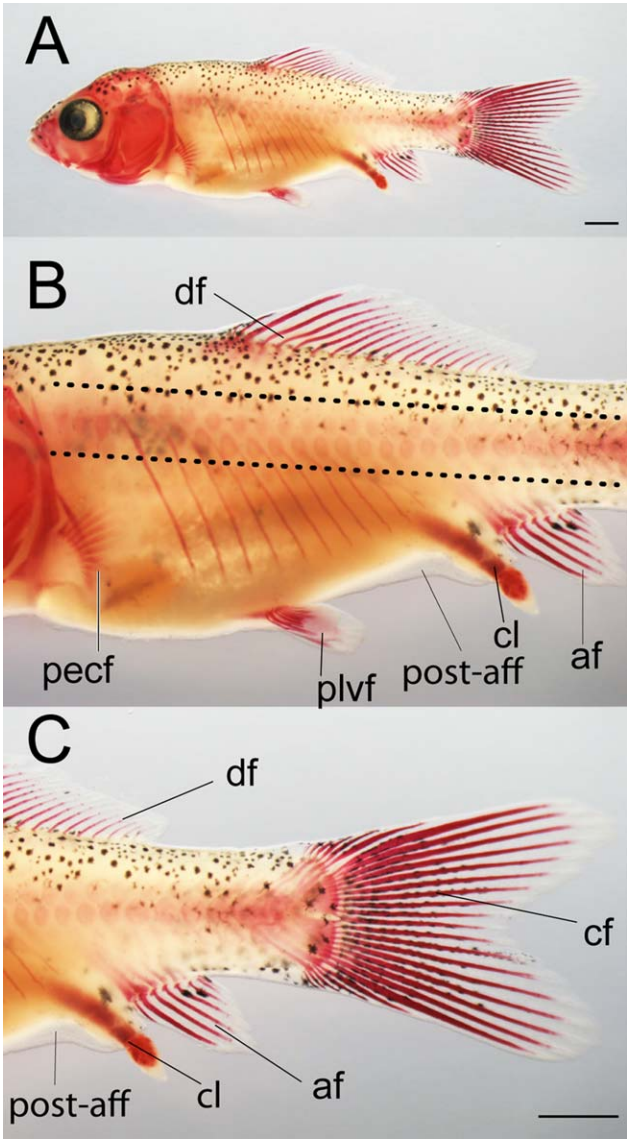

Fig. 20. Scale distribution patterns of Pr stage larvae (13.75 mm). **A–C**: Lateral view of the whole body (A), and magnified views of the trunk (B) and caudal (C) region. Dotted lines indicate the approximate boundary between scaled and scale-less areas on the left side of the body (B). af, anal fin, cf, caudal fin; cl, cloaca; df, dorsal fin; pecf, pectoral fin; plvf, pelvic fin. postaff, post anal fin fold. Scale bars = 1 mm.

alizarin red-stained late stage specimens under light field stereomicroscopy (Figs. 10B, 26). Moreover, the closely related postcleithrum can be observed at the level of the pectoral fin in lateral views of Pr stage larvae and juveniles (Fig. 26).

Pelvic Fin Skeleton

Of goldfish fins, the pelvic fin is the last to appear and calcify, similar to development in zebrafish (Grandel and Schulte-Merker, 1998) (Fig. 30). At the Pr stage, the preanal fin fold is still present (Fig. 30A). During development of Pr stage juveniles, the preanal fin fold gradually degenerates, while the pelvic fin and its fin rays develop (Fig. 30B). At the IsJ sub-stage, the morphology of the each fin ray is homogenous (Fig. 30C), but at the CsJ stage, several pelvic fin rays are bifurcated (Fig. 30D).

Dorsal Fin Skeleton

In Pb stage larvae, eight mineralized fin rays can be observed in the dorsal fin (Fig. 31A). Among them, the most anterior fin rays tend to show strong calcification (Fig. 31A); fin ray primordia also can be observed at this stage (Fig. 31A). In a Pr stage specimen in which 19 mineralized dorsal fin rays are visible, the third visible fin ray appears to be relatively strongly calcified (Fig. 31B). At the IsJ sub-stage, the third fin ray exhibits segmented fin spine-specific characteristics (posterior serrations) (sfs in Fig. 31C), and the posterior serrations are more evident at CsJ substage (sfs in Fig. 31D). Moreover, some fin rays were bifurcated at their distal part (Fig. 31D). Although posterior serrations are not visible in the paired fins of goldfish (Figs. 29, 30), they can be observed in the dorsal and anal fins (Figs. 31, 32).

At the Pr stage, approximately nine dorsal radials can be detected (Fig. 24A). These radials have attached fin rays and show metameric patterns (Lindsey, 1955) (Figs. 23, 24), although there are exceptional radials at the most anterior part of the dorsal fin (Patterson, 1992). Of these, the first and second radials show relatively strong calcification patterns at the Pr and juvenile stages (Figs. 23, 24A,C). During juvenile development, the distance between dorsal radials and neural spines decreases (Fig. 24C). The outline of the proximal tip of the proximal radials tends to be cuneiform, as observed in some other teleost species (Eaton, 1945) (Fig. 24A,C). The observed topographic relationship between these radials, fin rays, and neural spines in the pelvic fin ray at juvenile stages indicates that the dorsally segmented fin spines are derived from the fin ray located at the ninth vertebral level (white asterisks in Fig. 24B,D).

Anal Fin Skeletons

Throughout postembryonic development, the anal fin contains relatively few rays, as compared with the other median fins (Figs. 6, 32) (Koh, 1931). At the Pb stage, four anal fin rays can be observed (Fig. 32A), and six mineralized fin rays are visible at the Pr stage (Fig. 32B). At these stages, the postanal fin fold is still visible (Fig. 32A,B). At the IsJ sub-stage, eight fin rays are visible, of which five are bifurcated at their distal side (Fig. 32C). In an early Pr stage specimen, calcification of the anal fin radials can be observed (Fig. 24A). Akin to the dorsal fin, the anal fin also has a fin ray with posterior serrations (Figs. 24A, 23C,D). The first and second radials tend to elongate toward the hemal arch (Fig. 24A). The second radial, which is attached to the segmented fin spines, tends to exhibit strong calcification patterns (Fig. 24C). Comparison of transparent Pr and juvenile stage individuals at the anal fin level suggests that the anal segmented fin spines are differentiated from the fin ray located at the 19th to 20th vertebral levels (afr and asfs in Fig. 24C).

Caudal Fin Skeleton

The caudal fin skeleton consists of the fin rays and the attached internal skeletal systems (notochord and caudal vertebrae) (Figs. 33–35). Two calcified fin rays were observed in a calcein-stained Psb stage individual under fluorescent microscopy; these fin rays are hard to detect under light field stereomicroscopy (Figs. 8, 33A). During the subsequent stages, the number of caudal fin rays is increased (Fig. 33B–D). In particular, a dramatic increase

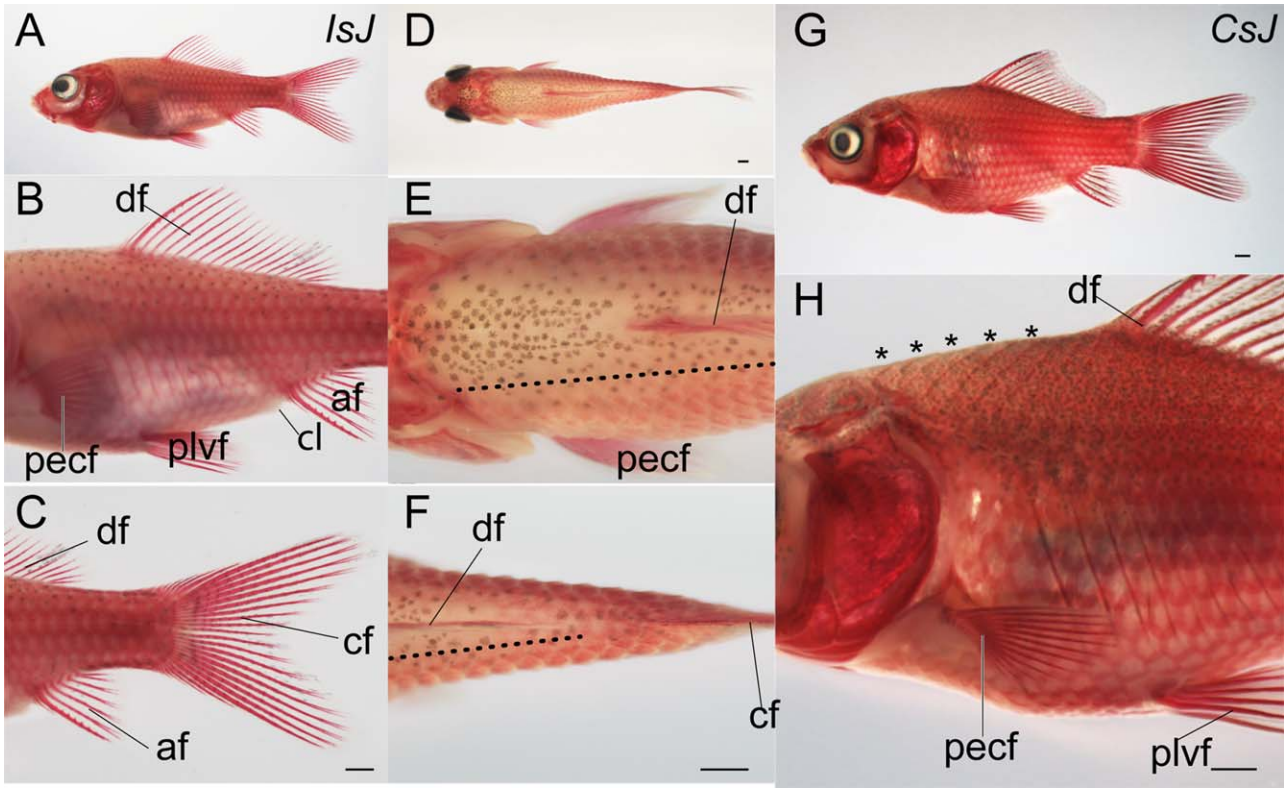

Fig. 21. Scale distribution patterns of juveniles. **A–F**: IsJ sub-stage juvenile (18.1 mm). Lateral view of the whole body (A), and magnified views of the trunk (B) and caudal region (C). Dorsal view of the whole body (D), and magnified dorsal views at the pectoral fin level (E) and caudal level (F). The lateral side is almost completely covered by calcified scales (A–C), while a large region of the anterior side of the dorsal fin lacks scales (D–F). **G,H**: Completely scaled juvenile (21.5 mm). Lateral view of the whole body (G), and magnified view of the trunk (H). The anterior dorsal trunk region is completely covered by scales (H). Asterisks indicate scales of the anterior dorsal trunk region. Dotted lines indicate the approximate boundary between scaled and scale-less areas on the left side of the body (E). Sub-stages are labeled in the upper right-hand corner of panels A and G in italics. af, anal fin, cf, caudal fin; cl, cloaca; df, dorsal fin; pecf, pectoral fin; plvf, pelvic fin. Scale bars = 1 mm.

in number is observed as standard length increases from 6 to 7 mm (Fig. 6).

At the Asb and Pb stages, the posterior end of the lepidotrichia remains un-calcified (Fig. 34A,B). All of the fin rays are calcified in our observed juvenile specimens (Fig. 34C,D). At the IsJ sub-stage, 30 caudal fin rays are visible, and half of them are bifurcated (Fig. 34C). The total numbers of visible caudal fin rays and bifurcated fin rays are almost the same between the IsJ and CsJ sub-stages (Fig. 34C,D); however, the depth of the bifurcations are obviously different between these stages (Fig. 34C,D). The process of caudal fin ray development is similar between goldfish and zebrafish (Parichy et al., 2009; Bensimon-Brito et al., 2012).

The caudal skeleton complex is also similar between goldfish and zebrafish; however, there is a clear difference in the number of the hypurals between these two teleosts (Fig. 29): the zebrafish has five hypurals, while goldfish have six (Fujita, 1990; Parichy et al., 2009). Most of the caudal skeletons located at the posterior caudal region are derived from the ventral region (Fig. 29), as has been reported for several teleost species (Bensimom-Brito et al., 2012).

There appears to be a drastic and consistent increase of calcified caudal fin rays and calcification of the caudal skeletal complex (Figs. 6, 33). We observed mineralization of the first to third hypural at the Cr9 sub-stage (Fig. 33C), and subsequent appearance of the parhypural and fourth hypural (Fig. 33D). At the Fcf stage, almost all of the ventral caudal skeletal elements (parhypural, hypurals, and hemal spines) were present (Fig. 34E). From this stage onward, the ventral caudal vertebral elements exhibit similar morphology to that of juvenile goldfish (Figs. 34E,F, 35A–D). On the other hand, calcification of dorsal vertebral elements (neural spines) does not proceed at this stage (Fig. 33E). At the Asb stage, neural spines are relatively highly calcified (Fig. 33F), and these neural spines are elongated in Pb stage and CsJ sub-stage individuals (Fig. 35A–D). Each skeletal element in the caudal fin complex tends to be closer in CsJ sub-stage individuals (Fig. 35C,D) than in individuals of earlier stages (Fig. 35A,B).

Condensation of Mesenchymal Cells in Fin Folds

Although the dorsal and anal condensation processes are considered as indices in the zebrafish postembryonic staging table (Parichy et al., 2009), they were not used as indices in our goldfish staging table because of the difficulty of identifying the timing of their appearance under stereomicroscopy in live goldfish juveniles (Table 2; Figs. 6–9). It is particularly difficult to identify the time at which anal fin condensation begins, because the blood and blood vessels located at the postanal region tend to be misidentified as anal fin primordia during early stages (Figs. 8–10; Tsai et al., 2013). However, studying the process of fin mesenchyme condensation may allow us to determine whether goldfish and zebrafish differ in anal and dorsal fin development at early postembryonic stages. Thus, we performed histological analysis, focusing on anal and dorsal fin condensation (Fig. 36).

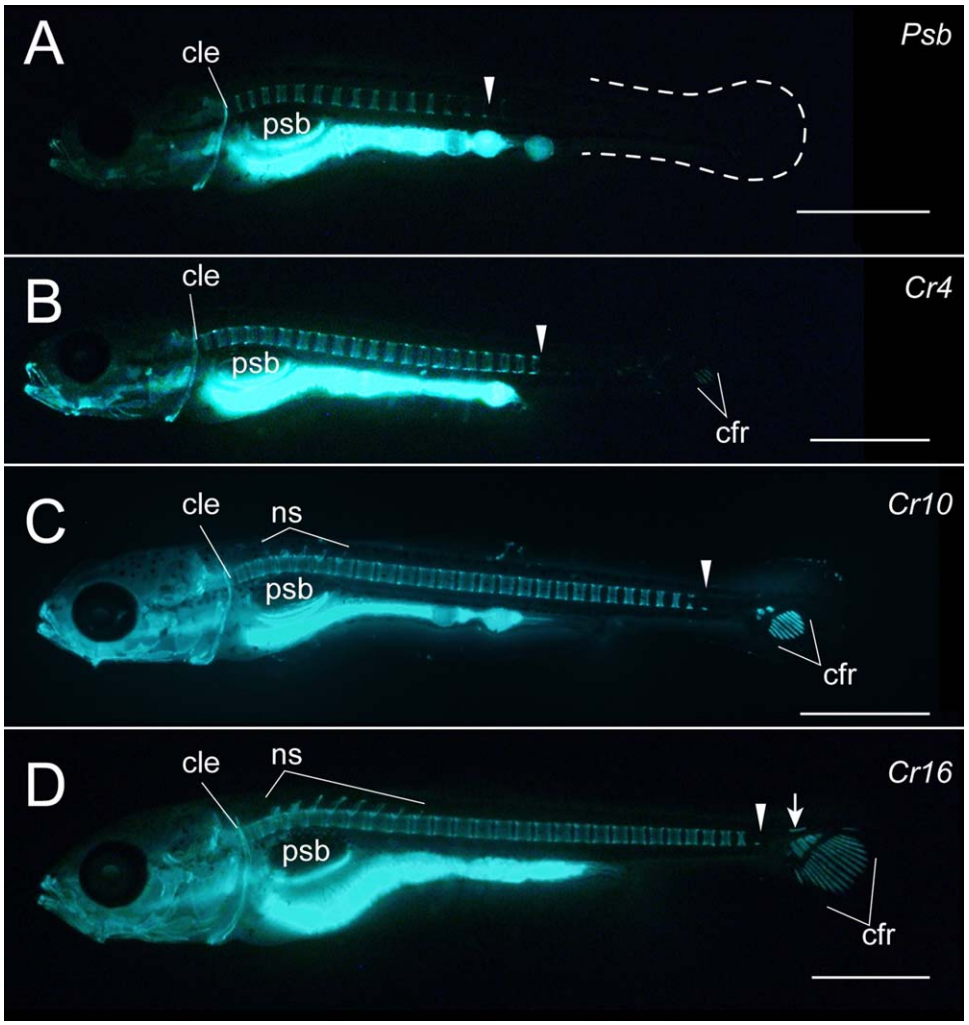

Fig. 22. Calcein-stained specimens from the Psb to the Cr stage. **A–D**: Psb stage (5.6 mm) (A), Cr4 (5.8 mm) (B), Cr10 (6.2 mm) (C), and Cr16 (7.1 mm) (D) sub-stage specimens were photographed under fluorescence microscopy. Hatched lines indicate the larval caudal region in A. White arrowheads indicate the most posterior end vertebra. The white arrow indicates the calcified position of the dorsal side of the notochord. The stages and sub-stages are labeled in italics in the upper right-hand corner of each panel. The strong fluorescence is derived from undigested brine shrimps in the intestines. cfr, caudal fin ray; cle, cleithrum; psb, posterior swim bladder; ns, neural spine. Scale bars = 1 mm.

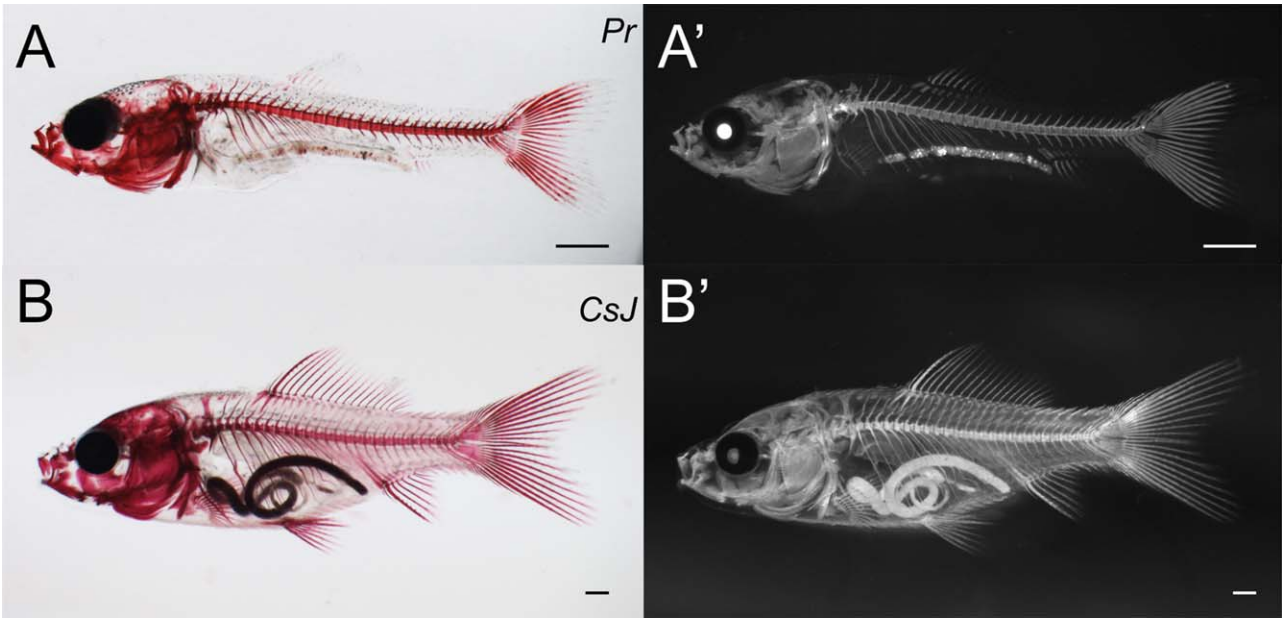

Fig. 23. Alizarin red-stained specimens from the early Pr stage to CsJ sub-stage. **A–B′**: Lateral views of early pelvic fin ray stage larva (9.2 mm) (A,A′), and completely scaled juvenile (18.6 mm) (B,B′) were photographed under white light (A, B) or under fluorescent light as gray scale images (A′,B′). The stage and sub-stage are labeled in italics in the upper right-hand corner of the panels on the left. The intestines are still present in the samples (see the Experimental Procedures section). Scale bars = 1 mm.

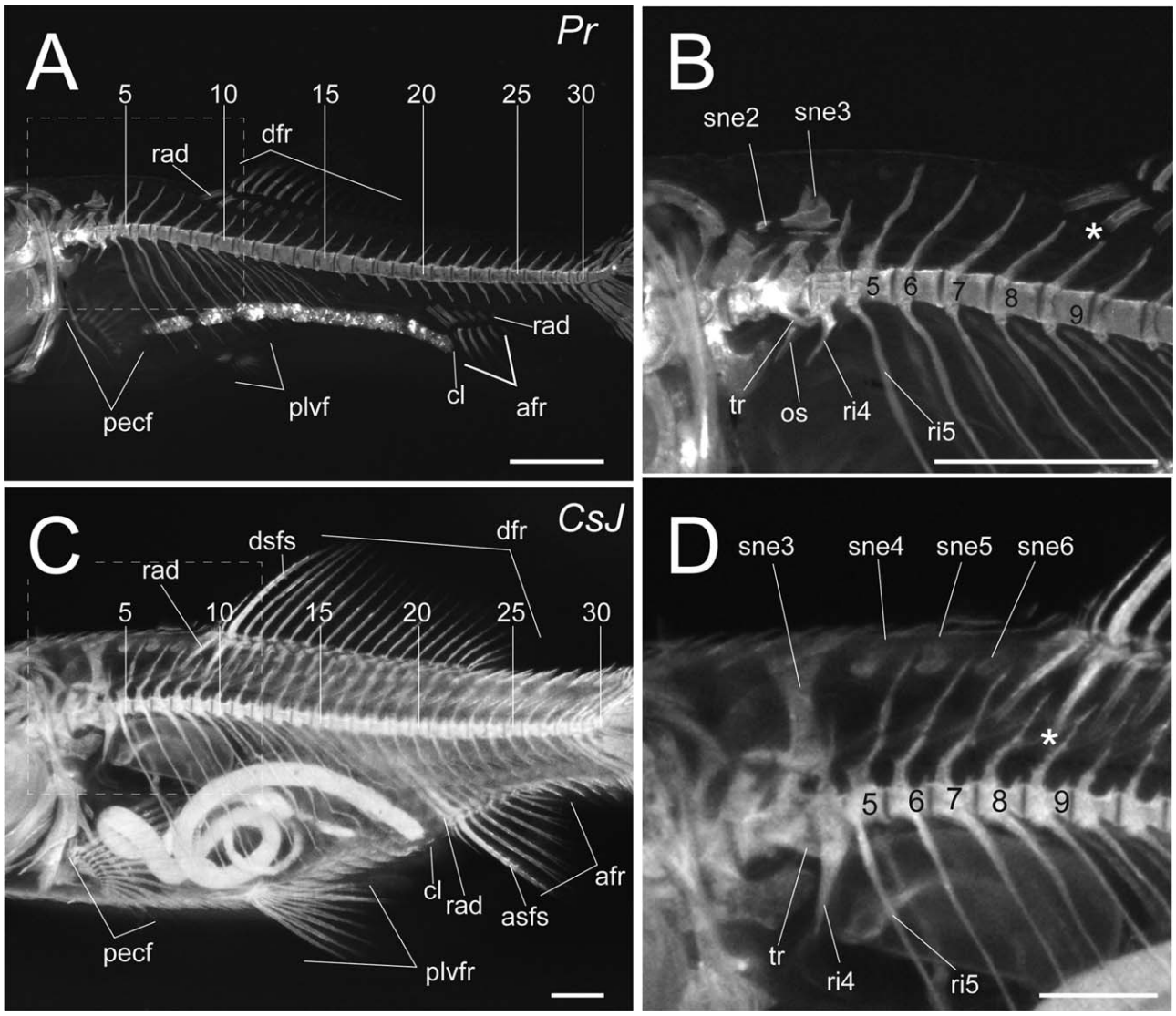

Fig. 24. Mid-trunk regions of alizarin red-stained skeletons. **A–D**: Lateral views of Pr stage (9.2 mm) (A,B) and CsJ (18.6 mm) (C,D) sub-stage specimens were photographed at the mid-trunk level (A,C) and at the level of the Weberian apparatus (B,D). These individuals are the same individuals as in Figure 23A,B. The stage and sub-stage are labeled in italics in the upper right-hand corner of the panels on the left. The numbers indicate the vertebral number. White asterisks in B and D indicate the radials located at the ninth vertebral level. afr, anal fin ray; asfs, anal segmented fin spine; cl, cloaca; dfr, dorsal fin ray; dsfs, dorsal segmented fin spine; os, os suspensorium; pecf, pectoral fin; plvf, pelvic fin; plvfr, pelvic fin ray; rad, radial; ri, rib; sne, supraneurals; tr, tripus. Scale bars = 1 mm.

Anal and dorsal fin condensation can be observed relatively easily in Bouin's fixed larvae (posterior swim bladder and Cr20 sub-stage; Fig. 36A,D). Migrated cells are visible only in the postanal fin fold at the anal fin level of Psb stage larvae (Fig. 36A–C). Moreover, dorsal and anal fin condensation can be clearly detected at Cr20 sub-stage (Fig. 36D–J). From these results, it is apparent that the ontogenetic sequence of early anal and dorsal fin formation is conserved between these two teleost species, despite the differences in fin ray appearance (Figs. 14, 15).

Discussion

Here, we describe the postembryonic developmental process of goldfish (Figs. 2–19), which we categorized into 11 stages based on visible indices (Table 2). Because our descriptions were derived using wild-type goldfish, it is expected to serve as a suitable standard for comparative ontogenetic analysis between morphologically divergent goldfish strains (for example, bifurcated caudal fin, dorsal fin less, pop eye, and peal scale strains) (Smartt, 2001). Moreover, we revealed several dissimilarities between goldfish and zebrafish in their postembryonic development, in contrast to the embryonic similarities between these two teleost species (Tsai et al., 2013). For example, the processes of squamation and reduction of the fin fold are evidently different between these species (Figs. 18–21). Anterior squamation (SA) stage zebrafish larvae possess scales at the anterior side of the trunk, and retain the residual of the preanal fin fold (Parichy et al., 2009). However, no goldfish larval or juvenile individuals with scales at the anterior side of trunk and residual fin folds were observed (Figs. 20, 21).

In addition, the zebrafish anal fin condensation (AC) and dorsal fin condensation (DC) stages seem to be equivalent with the

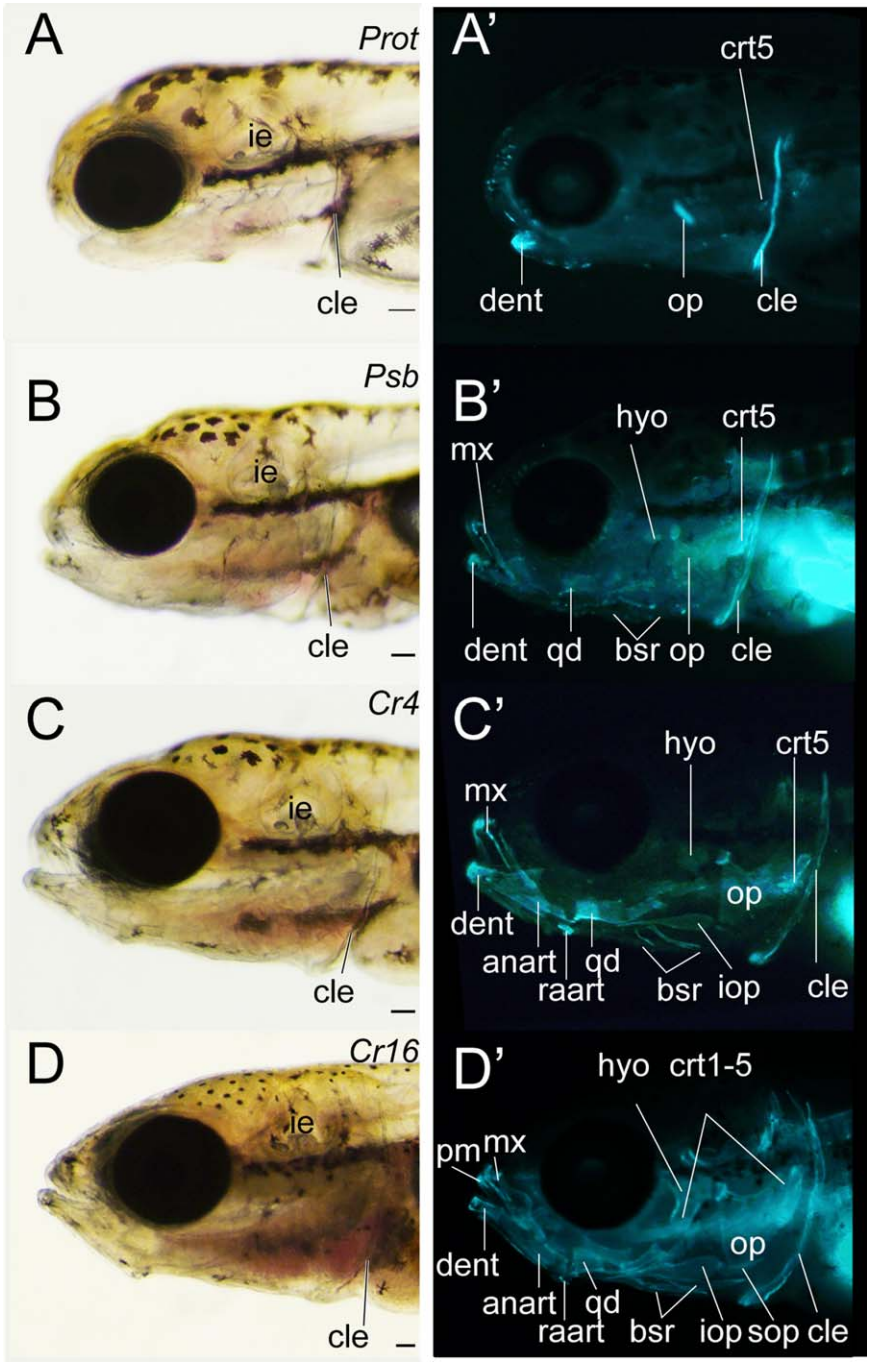

Fig. 25. Calcein-stained cranial skeletons. **A–D′**: Prot stage (5.6 mm) (A,A′) and Psb (5.5 mm) stage (B,B′) larvae, Cr4 (5.8 mm) stage (C,C′), and Cr16 (7.1 mm) (D,D′) sub-stage specimens were photographed under a light field (A, B, C, D) and fluorescence microscopy (A′,B′,C′,D′). The stages and sub-stages are labeled in italics in the upper right-hand corner of the panels on the left. aart, anguloarticular; bsr, branchiostegal rays; cle, cleithrum; crt, ceratobranchial; dent, dentary; hyo, hyoid; iop, interopercular; mx, maxilla; op, opercular; par, parietal; pm, premaxilla; qd, quadrate; rart, retroarticular; sop, subopercular. Scale bars = 0.1 mm in A–D. A, B, C, and D, and A′, B′, C′, and D′, are identical individuals at the same magnification.

goldfish late Cr and Fcf stages (Figs. 11, 12), respectively; however, the presence or absence of mesenchymal cells in the anal and dorsal fin folds is not as clear in goldfish as in zebrafish larvae at these equivalent stages (Parichy et al., 2009). This lack of clarity may be due to the opacity of anal and dorsal fin development. While the dorsal fin ray appears earlier than the anal fin ray during zebrafish postembryonic development (Parichy et al., 2009), this pattern is reversed in the goldfish (Table 2; Figs. 14, 15).

Furthermore, segmented fin spines are absent in zebrafish (Mabee et al., 2002). Thus, we first consider the ontogenetic appearance of the scales, anal and dorsal fins, and the segmented fin spines, to highlight the dissimilarities between zebrafish and goldfish at postembryonic stages. And finally, we offer our perspective on the role

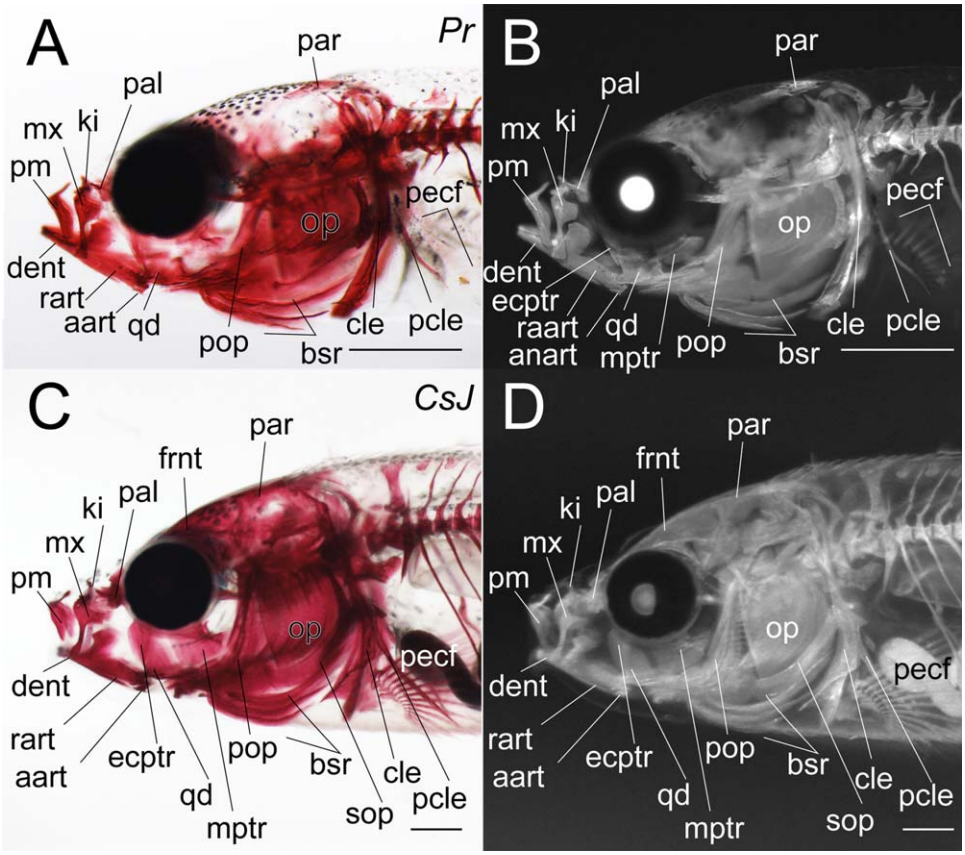

Fig. 26. Alizarin-stained cranial skeletons. **A–D**: Pr stage (9.2 mm) (A,B), and CsJ sub-stage (18.6 mm) (C,D) specimens were photographed under a light field (A,C) and fluorescence microscopy as gray scale images (B,D). The individuals in E and F are the same as those in Figure 22A and B, respectively. The stage and sub-stage are labeled in italics in the upper right-hand corner of panels on the left. aart, anguloarticular; bsr, branchiostegal rays; cle, cleithrum; dent, dentary; ecptr, ectopterygoid; frnt, frontal; iop, interopercular; ki, kinethmoid; mptr, metapterygoid; mx, maxilla; op, opercular; pal, palatine; par, parietal; pcle, postcleithrum; pecf, pectoral fin; pm, premaxilla; pop, preopercular; qd, quadrate; rart, retroarticular; sop, subopercular. Scale bars = 1 mm.

of wild-type and mutant goldfish embryonic and postembryonic studies in enhancing our understanding of the evolution of developmental processes.

Altered Timing of Scale Formation and Reduction of the Fin Fold

The squamation process has been studied in several teleost species (Sire and Huysseune, 2003; Sire and Arnulf, 2000, 1990; Sire et al., 1997; Koumoundouros et al., 2001), revealing variation in the squamation patterns between species; for example, the squamation processes of zebrafish, sea bream, and *Rivulus marmoratus* start from the lateral caudal (Sire et al., 1997), mid lateral, (Koumoundouros et al., 2001), and anterior dorsal areas (Park and Lee, 1988), respectively. Because our observations suggest that scales first emerge at the lateral caudal level (Fig. 20), the squamation process may be conserved between goldfish and zebrafish, reflecting their phylogenetic relationship (Saitoh et al., 2003, 2006). However, it appears that the ontogenetic sequence of fin fold reduction and squamation are different in the goldfish and zebrafish lineages (Fig. 20). Although the details of the divergence of their ontogenetic sequence remain unknown, it is assumed that the ontogenetic sequences may reflect the differences in morphology and relative size of the median fins between goldfish and zebrafish (Fig. 2; Mabee et al., 2002; Parichy et al., 2009).

Ontogenetic Sequence of the Anal and Dorsal Fins

Our histological observations of Psb and Cr stage specimens indicate that the fin condensation sequence is similar in goldfish and zebrafish larvae (Fig. 36), in contrast with the timing of dorsal and anal fin ray appearance (Figs. 14, 15) (Parichy et al., 2009). As noted above, the divergence in the ontogenetic sequence of these fins reflects differences in their adult fin morphologies (Fig. 2; Koh, 1931; Mabee et al., 2002; Parichy et al., 2009).

In adult goldfish, the dorsal fin is larger than the anal fin in terms of both size and fin ray number (Koh, 1931); the opposite is true in zebrafish (Mabee et al., 2002). On the basis that goldfish dorsal and anal fin development proceeds bidirectionally (Figs. 31, 32), it was hypothesized that these fins share a common positional value and patterning mechanism (the so-called Dorsal + Anal fin patterning module, proposed by Mabee et al., 2002). It is known that the median fin rays and their primordial cells are derived from the somite in medaka (Shimada et al., 2013), suggesting that the anal and dorsal fins of zebrafish and goldfish are also derived from somite derivatives. In summary, it is expected that the anal and dorsal fin rays may be derived from somite-derived cells in both zebrafish and goldfish, but the timing of mesenchymal cell differentiation has altered between these two lineages.

Why is it that the condensation of mesenchymal cells in the anal and dorsal fin folds seems to be conserved during early

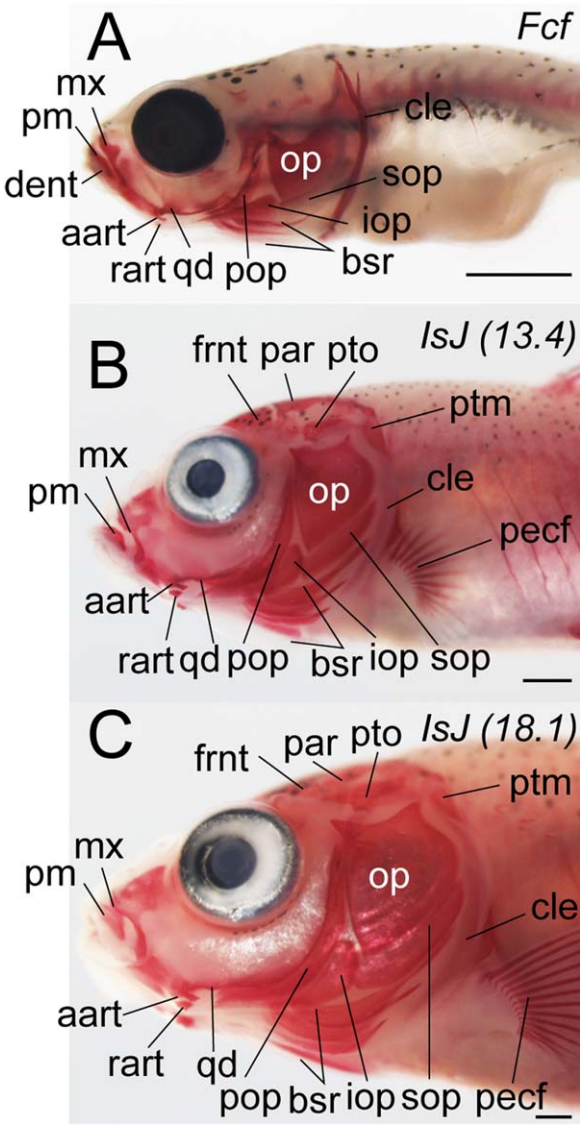

Fig. 27. Lateral external surface of the cranial skeleton. **A–C**: Fcf stage (7.7 mm) (A), early lsJ (13.4 mm) (B), and late lsJ (18.1 mm) (C) sub-stage specimens were photographed under a light field. Iridophores in eye are dropped during the fixation process (A). The stage and sub-stage (standard length) are labelled in italics in the upper right-hand corner of each panel. aart, anguloarticular; bsr, branchiostegal rays; cle, cleithrum; dent, dentary; frnt, frontal; iop, interopercular; mx, maxilla; op, opercular; par, parietal; pecf, pectoral fin; pm, premaxilla; pop, preopercular; ptm, posttemporal; pto, pterotic; qd, quadrate; rart, retroarticular; sop, subopercular. Scale bars = 1 mm.

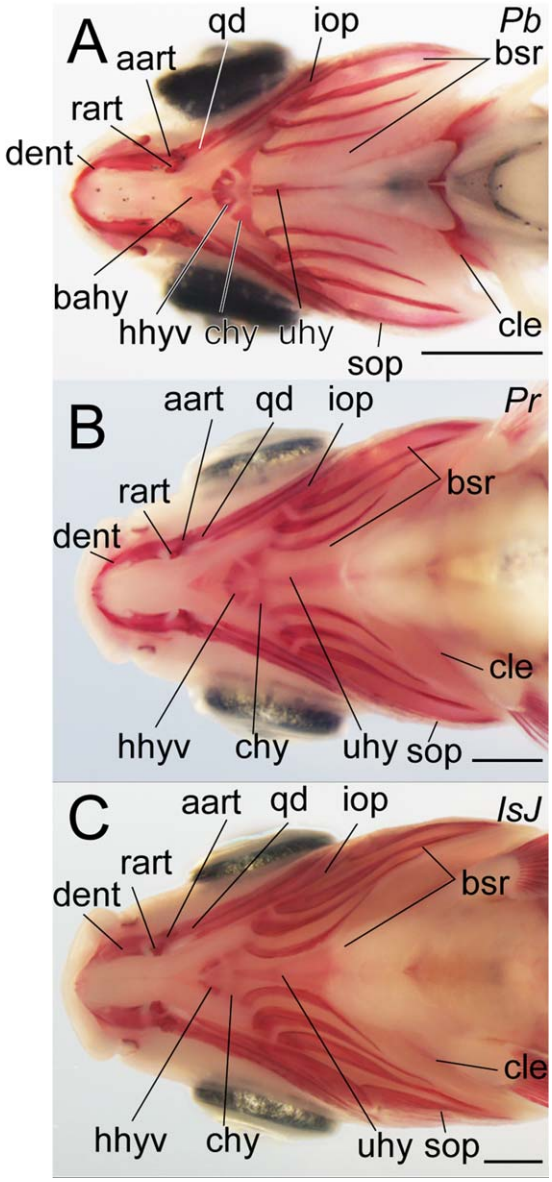

Fig. 28. Ventral external surface of the cranial skeleton. **A–C**: Pb stage (8.5 mm) (A), early Pr stage (10.2 mm) (B), and lsJ sub-stage (18.1 mm) (C) specimens were photographed under a light field. The stage and sub-stage are labelled in italics in the upper right-hand corner of each panel. aart, anguloarticular; bsr, branchiostegal rays; chy, ceratohyal; cle, cleithrum; bahy, basihyal; dent, dentary; hhyv, hyophyal ventral; iop, interopercular; qd, quadrate; rart, retroarticular; sop, subopercular; uhy, urohyal. Scale bars = 1 mm.

stages of development in goldfish and zebrafish, while their dorsal and anal fin developmental sequences diverged at late stages? Similar questions related to the conservation of developmental processes in the face of evolutionary morphological changes were previously asked in the context of modern and classic Evodevo (Haeckel and McCabe, 1912; von Baer, 1828; Gould, 1977; Riedl, 1978; Irie and Kuratani, 2011; Koyabu et al., 2011).

Given that exoskeletons of different teleost groups have undergone evolutionary changes through selective pressure from environmental factors (Mabee et al., 2002; Nelson, 2006), it is expected that the differences observed between goldfish and zebrafish may be reflected by different teleost lineages. For example, observations of embryos of Victoria Cichlid (*Haplochromis piceatus*) revealed that anal fin condensation occurs first, followed by dorsal fin condensation (de Jong et al., 2009); however, the dorsal fin rays appear first in larvae of Nile tilapia, which has similar anal and dorsal fin ray morphology with *H. piceatus* (Fujimura and Okada, 2007). Thus, the order of appearance of mesenchymal condensation and fin rays in dorsal and anal fins are inconsistent in these species.

It is expected that intensive and extensive genomic, transcriptomic, and molecular developmental studies, using not only goldfish and zebrafish, but also several more divergent teleost species, will contribute to revealing how the ontogenetic sequence of

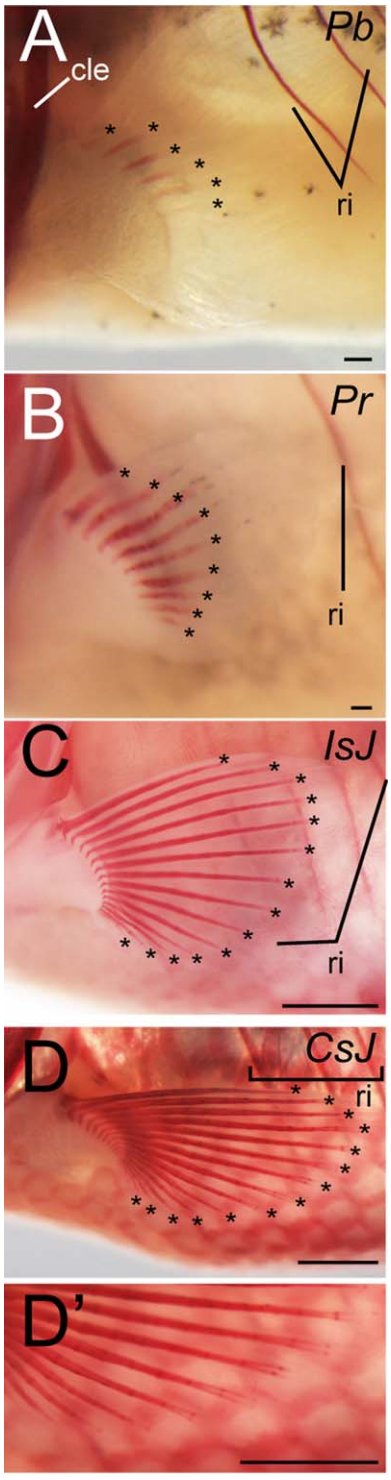

Fig. 29. Pectoral fin rays. **A–D**: Lateral views of Pb stage (8.5 mm) (A), Pr stage (13.6 mm) (B), IsJ (18.1 mm) sub-stage (C), and CsJ (21.5 mm) sub-stage (D) specimens were photographed under a light field. **D′**: Magnified view of panel D. The stage and sub-stage are labelled in italics in the upper right-hand corner of each panel. Black asterisks indicate the most distal tip of calcified fin rays. cle, cleithrum; ri, rib. Scale bars = 0.1 mm in A,B; 1 mm in C,D,D′.

morphologically divergent skeletons and primordia are conserved (or diverged) in each lineage, and consequently provide clues to answering the above question.

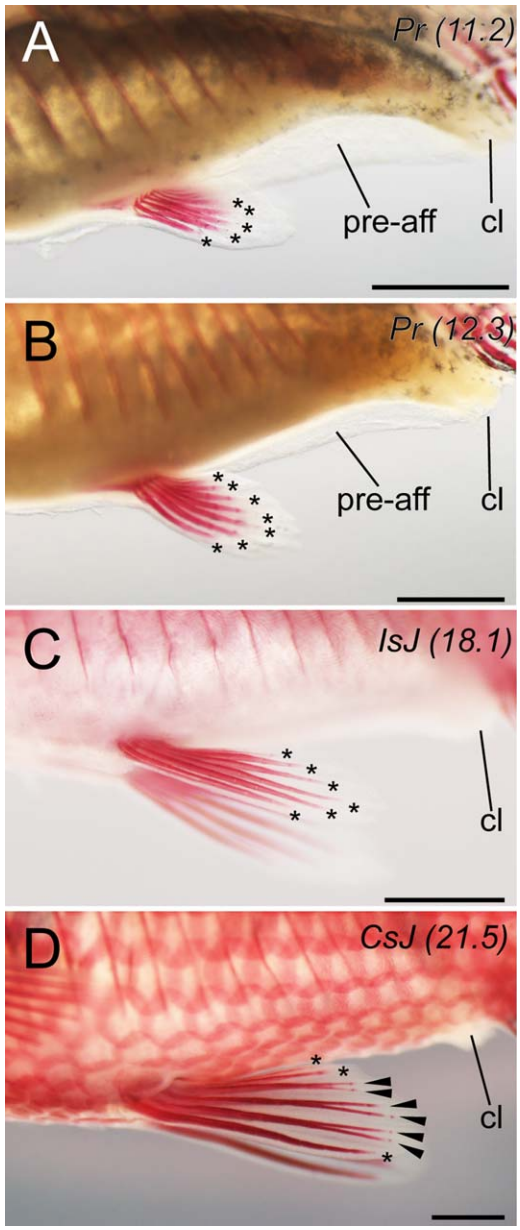

Fig. 30. Pelvic fin rays. **A–D**: Lateral views of early Pr stage (11.2 mm) (A), late Pr stage (12.3 mm) (B), IsJ (18.1 mm) sub-stage (C), and CsJ sub-stage (D) (21.5 mm) specimens were photographed under a light field. The stage and sub-stage (standard length) are labelled in italics in the upper right-hand corner of each panel. Black asterisks indicate unbranched calcified fin rays. Black arrowheads indicate the branched fin rays. cl, cloaca; preaff, preanal fin fold. Scale bars = 1 mm.

Segmented Fin Spine

Segmented fin spines may have independently evolved in different Ostariophysan fish lineages (Fink and Fink, 1981; Saitoh et al., 2003; Nelson, 2006); for example, goldfish and carp have segmented fin spines in the dorsal and anal fins, while several catfish have segmented spines in the pectoral fin (Alexander, 1966; Fink and Fink, 1981; Reis, 1998; Huysentruyt and Adriaens, 2005; Huang et al., 2014). Because the spines in some of these Ostariophysan fish equip the venom glands (Wright, 2009), it may be presumed that the segmented fin spines have a protective function against predators;

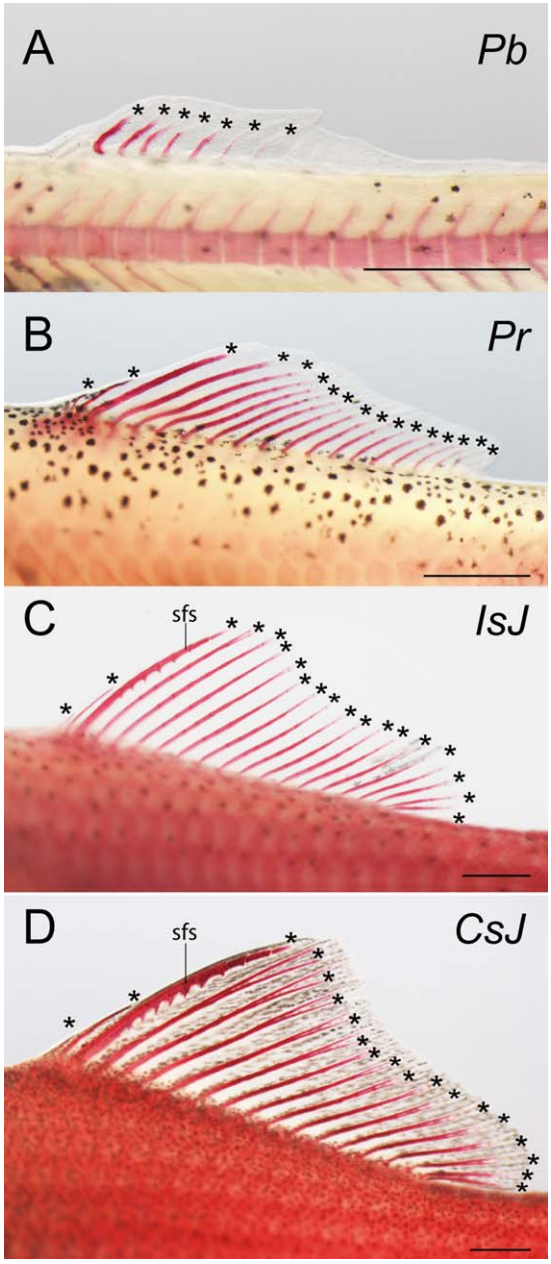

Fig. 31. Dorsal fin rays. **A–D**: Lateral views of Pb stage (9.24 mm) (A), Pr stage (13.75 mm) (B), IsJ sub-stage (18.09 mm) (C), and CsJ sub-stage (21.46 mm) (D) specimens were photographed under a light field. The stage and sub-stage are labelled in italics in the upper right-hand corner of each panel. Black asterisks indicate calcified fin rays. sfs, segmented fin spine. Scale bars = 1 mm.

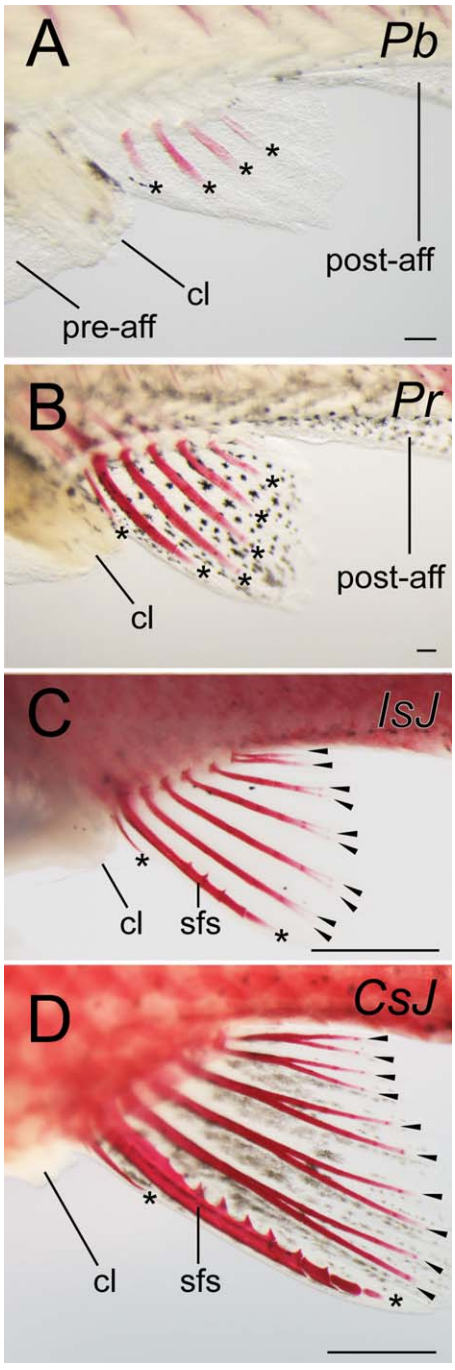

Fig. 32. Anal fin rays. **A–D**: Lateral views of Pb stage (9.2 mm) (A), Pr stage (11.2 mm) (B), IsJ (13.4 mm) sub-stage (C), and CsJ (21.5 mm) sub-stage (D) specimens were photographed under a light field. Black asterisks and arrowheads indicate the un-bifurcated and bifurcated fin rays, respectively. The stage and sub-stage are labelled in italics in the upper right-hand corner of each panel. cl, cloacal; preaff, preanal fin fold; postaff, postanal fin fold; sfs, segmented fin spine. Scale bars = 0.1 mm in A,B; 1 mm in C,D.

furthermore, its evolution may be related to other environmental factors, akin to the pelvic spines of sticklebacks (Hoogland et al., 1956; Bell, 1987; Bell et al., 1993; Shapiro et al., 2004; Chan et al., 2010).

Although the evolution and development of the stickleback spine has been well investigated at the molecular level (Shapiro et al., 2004; Chan et al., 2010), little is known of that of Ostariophysan fish; this may be due to the absence of the segmented fin spine in zebrafish (Mabee et al., 2002). At present, the gene(s) responsible for segmented fin spine formation and its divergence in the Ostariophysan fish lineage is (are) unknown. It is expected that developmental studies of goldfish postembryonic stages may further elucidate the molecular developmental mechanism of these spines and the divergent processes. Moreover, comparison between the evolutionary developmental processes of the spines between Ostariophysan fish and sticklebacks may help identify

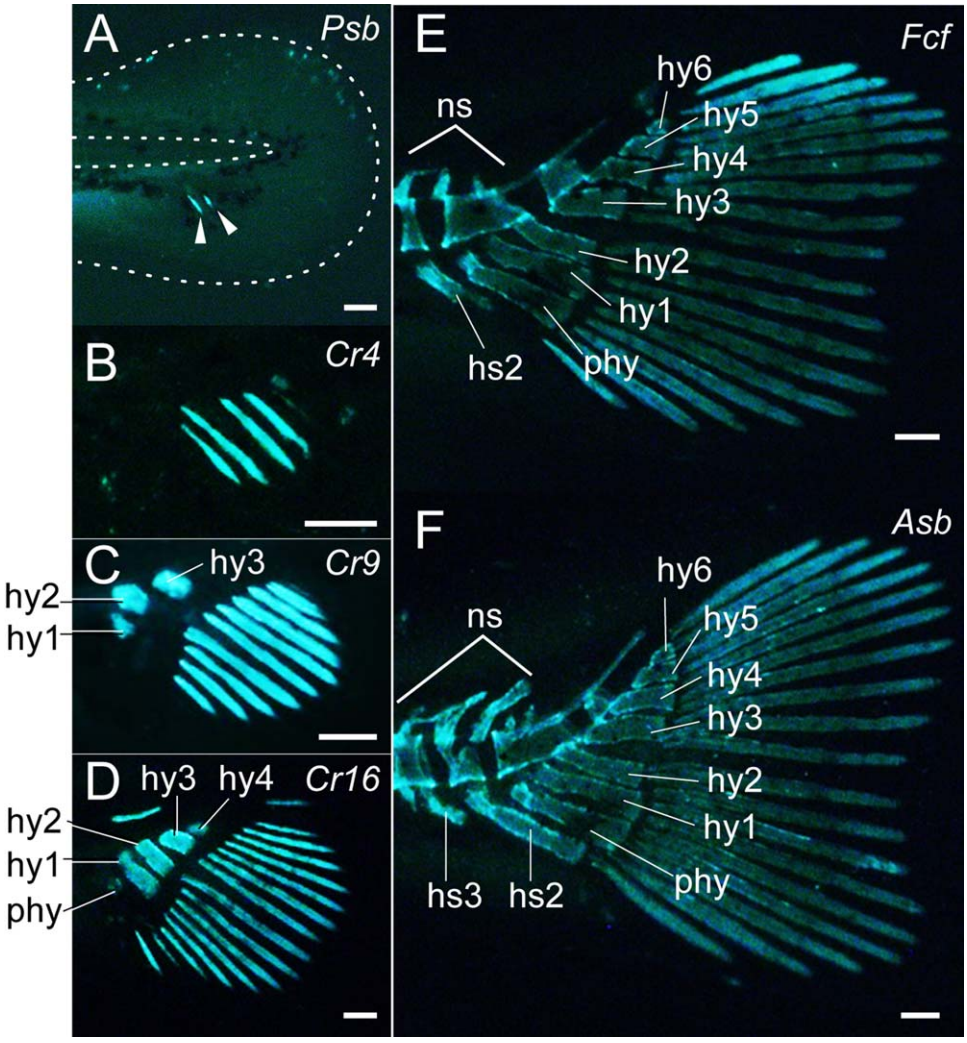

Fig. 33. Caudal fin skeletons in calcein-stained larvae. **A–F**: Lateral views of Psb (5.6 mm) (A), Cr4 (5.8 mm) (B), Cr9 (6.2 mm) (C), Cr16 (7.1 mm) (D), Fcf (7.8 mm) (E), and Asb (7.8 mm) (F) stage (and sub-stage) specimens were photographed under fluorescent microscopy. The stage and sub-stage are labelled in italics in the upper right-hand corner of each panel. hy, hypural; hs, hemal spine; ns, neural spine; phy, parhypural. Scale bars = 0.1 mm in A–G; 1 mm in H.

general principles for how developmental mechanisms react to selective pressures from predators.

Artificial Selection and Development

The crucial difference between goldfish strains and zebrafish mutants is the process of selection. Researchers have used large-scale mutant screening to identify mutated loci and alleles (Mullins et al., 1994; Haffter et al., 1996; Driever et al., 1996; Amsterdam et al., 1999, 2004; Golling et al., 2002; Wienholds et al., 2003; Sivasubbu et al., 2006; Nagayoshi et al., 2008). The established zebrafish mutant strains tend to be maintained for detailed investigation of the molecular function of the responsible locus and allele (Mullins et al., 1994; Gaiano et al., 1996; vanEeden et al., 1996; Amsterdam et al., 1999). During this maintenance process, intensive directional selection to a certain morphological feature rarely occurs (and may, in fact, be discouraged). On the other hand, traditional and legacy breeding of goldfish tends to involve targeting of a certain postembryonic morphological feature (for example, popped eyes or twin-tail), and consequently these features were placed under intensive directional selection (Matsui et al., 1981; Smartt, 2001). This difference between zebrafish and goldfish allow us to use these teleost species for different purposes. The former facilitates identification of the alleles and loci responsible for the mutated phenotype, while the latter provides an opportunity to investigate the evolutionary consequences of continuous and directional artificial selection of postembryonic morphological features, and its influence on embryonic and postembryonic development.

As an example, we can compare twin-tail goldfish and the zebrafish *chordin* mutant (Abe et al., 2014). Our previous data suggest that, in addition to *chordin*, other mutated alleles may have been fixed in twin-tail goldfish strains during artificial selection (Abe et al., 2014). Moreover, it has also been reported that the zebrafish *dino/chordin* mutant shows high mortality, and a large number of individuals exhibited malformed swim bladders (Fisher and Halpern, 1991). In contrast, the twin-tail goldfish larvae have a high survival rate, equivalent to that of wild-type goldfish (Abe et al., 2014). This high survival rate may be due to the recently duplicated *chordin* genes. To further investigate how the duplicated *chordin* genes coordinate spatial and temporal

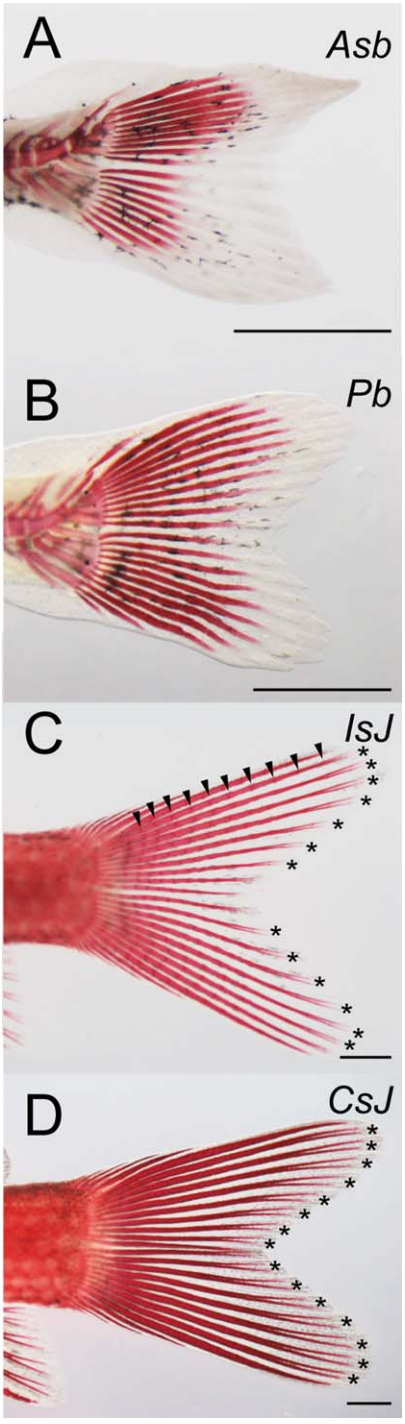

Fig. 34. Caudal fin rays. **A–D**: Lateral views of Asb (7.73 mm) (A), Pb (9.24 mm) (B), lsJ (18.09 mm) (C), and CsJ (21.46 mm) (D) stage (and sub-stage) specimens were photographed under a light field. Black asterisks and arrowheads indicate branched fin rays and segmentations, respectively (C,D). The stage and sub-stage are labelled in italics in the upper right-hand corner of each panel. Scale bars = 1 mm.

patterning of their gene expression patterns to establish a twin-tail phenotype and high survival rate requires not only comparative genomics, but also comparison of the embryonic and post-embryonic features between wild-type and twin tail goldfish.

Other morphologically divergent goldfish strains may be investigated in the contexts outlined above: how is it that a strain exhibits both an ornamental mutated phenotype and a high survival rate? Based on the observation that the common carp (*Cyprinus carpio*), one of the closest relatives of the goldfish, is derived from allotetraploidization (species hybridization), rather than autotetraploidization (genome doubling) (Saitoh et al., 2003, 2006; Xu et al., 2014), it is believed that the goldfish genome also originated from allotetraploidization. If so, appropriate comparison between wild-type and mutant goldfish strains may provide further opportunities to investigate the relationship between selective pressures at postembryonic stages, early developmental processes, and allotetraploidization-derived duplicated genes that exhibit slight divergence.

Conclusions

Here, we have provided the first comprehensive postembryonic staging table for goldfish, in which goldfish larvae and juveniles are categorized into 11 stages. In contrast to the embryonic and early larval stages, the late postembryonic stages differ substantially between zebrafish and goldfish, especially in terms of the ontogenetic sequence of squamation, and fin fold and median fin formation. These differences may reflect their adult morphology and evolutionary course. It is expected that further comparative analysis between wild-type goldfish, zebrafish, and their morphologically divergent mutant strains will provide insights into how selection and development are related to each other.

Experimental Procedures

Goldfish Breeding

Two different types of common goldfish strains were purchased from an aquarium fish agency and breeder in Taiwan. One is imported from Japan, and the other is bred in Taiwan; they are designated as the Japanese single tail *Wakin* strain and the common goldfish strain of Taiwan, respectively (Fig. 1). During the spring season (April to June), sperm was extracted from multiple male goldfish and separately preserved in Modified Kurokawa's extender 2 solution at 4°C (Magyary et al., 1996). Eggs were squeezed from mature female goldfish onto Teflon-coated dishes, and fertilized with sperm using dry methods. Fertilized eggs were placed in 9-cm plastic dishes containing tap water (24°C). Plastic dishes containing approximately 50 to 100 fertilized eggs were maintained at 24°C until hatching. The hatched goldfish specimens were used for the analysis of growth rate, skeletal observation, histological analysis, and image acquisition. The research was performed in accordance with internationally recognized guidelines. We received ethical approval from the Institutional Animal Care & Utilization Committee of Academia Sinica, Taiwan.

Analysis of Growth Rate

Goldfish specimens derived from the same clutch were divided into two groups ("individually maintained" and "collectively maintained" groups). Measurements of standard length and observation of staging index were conducted on three different clutches: #20140313, #20140331, and #20140419 (these experiment ID numbers represent the date of fertilization). Individuals of #20140313 and others are derived from Japanese single tail

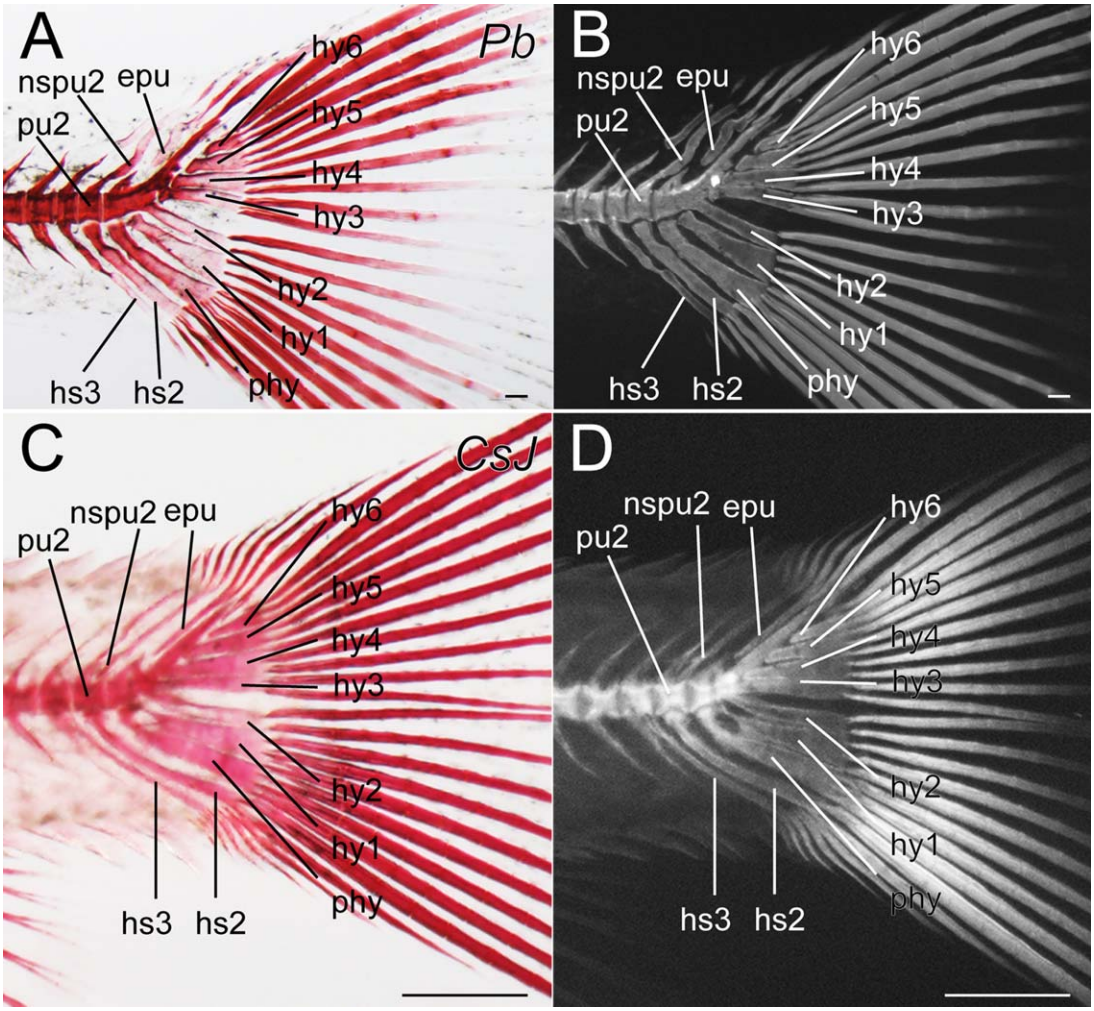

Fig. 35. Caudal fin skeletons in alizarin red-stained samples. **A–D**: Lateral views of Pb stage (9.2 mm) (A,B) and CsJ sub-stage (18.6 mm) (C,D) specimens were photographed under fluorescent microscopy. Panels B and D are gray scale images. The stage and sub-stage are labelled in italics in the upper right-hand corner of left column panels. epu, epural; hy, hypural; hs, hemal spine; nspu, neural spine of preural; phy, parhypural, pu, preural. Scale bars = 0.1 mm in A,B; 1 mm in C,D.

Wakin strain and the common goldfish strain of Taiwan, respectively. For the individually maintained group, we randomly selected 33, 24, and 22 hatched larvae from clutches #20140313, #20140331, and #20140419, respectively. Larvae at 6–8 dpf from the individually maintained group were initially kept separately in a 9-cm dish; these specimens were subsequently moved into a 500-ml tank at 18–28 dpf, and maintained separately. For the collectively maintained group, 30 hatched larvae from clutches #20140313, #20140331, and #20140419 were randomly selected and moved into 500-ml tanks at 28 dpf, 22 dpf, and 7 dpf, respectively. Subsequently, these larval specimens were moved into 5,000-ml tanks, on the following dpf: #20140313 – 43 dpf; #20140331 – 24 dpf; and #20140419 – 23 dpf. The bottom area of the 500- and 5,000-ml tanks had dimensions of 16 × 8.5 cm and 26.5 × 15.5 cm, respectively. These two groups were maintained under identical temperature conditions (water temperature: approximately 24°C) until reaching the juvenile stage. To avoid water pollution, dead individuals were removed. Brine shrimp was fed to larval individuals and early juveniles, and pellets were given to late juvenile larvae (over approximately 2 cm in length).

The standard length of onset for each larval stage was estimated from 25 to 50% probability of appearance of the staging indices in 76 individually maintained goldfish specimens (Table 2; Fig. 5). Furthermore, 10 adult goldfish specimens were used for the approximation of the onset of the standard length of the adult stage (Table 2).

Skeletal Observation

Early goldfish larvae specimens were maintained in 0.1% calcein solution (Sigma C0875) and mounted in 0.5–1.0% low-melting agarose (LE Agarose, SeaKem®); mounted and stained specimens were observed under a fluorescence microscope system. Late larval and juvenile specimens were anesthetized with MS222 (Sigma A5040), and then fixed with 4% paraformaldehyde or 5% formalin, washed in 70% ethanol, and stained with alizarin red solution (0.1% alizarin red in 95% ethanol). Alizarin red-stained specimens were washed with 70% ethanol to reduce background. Stained specimens (opaque samples) were photographed to observe external skeletal systems (scales, fin rays, and facial

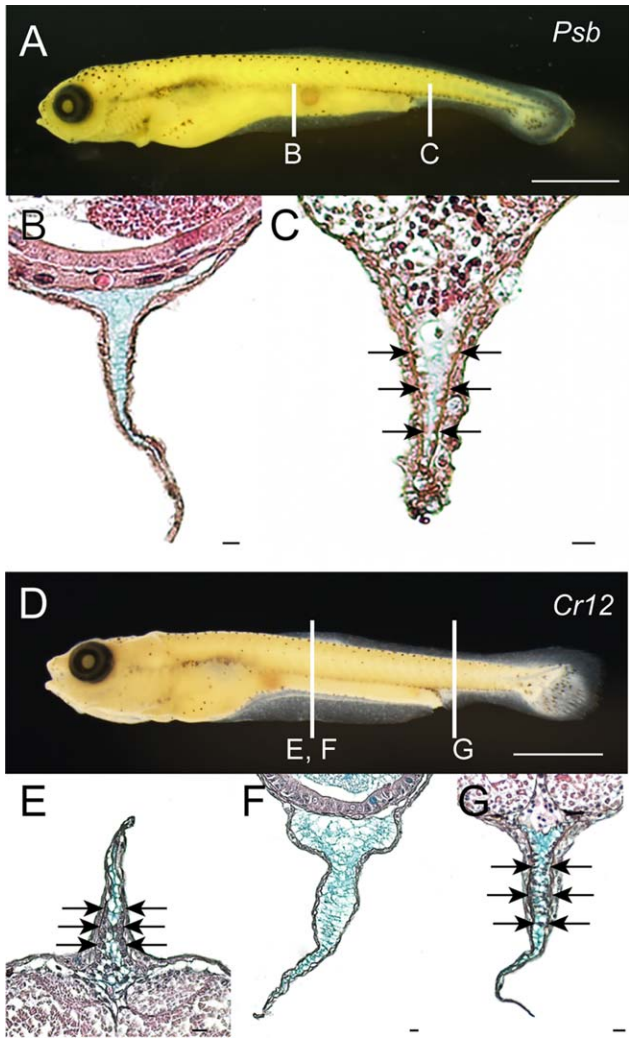

Fig. 36. **A–G**: Histological analysis of Psb stage (A–C) and Cr12 substage (D–G) specimens. The fixed specimens (A,D) were sectioned at the anal (C,G) and dorsal fin (B,E,F) primordial levels. Black arrows indicate the boundary of epithelial and mesenchymal cells in the fin folds. Mesenchymal cells are observed at the side of the epithelial tissues of the fin fold (C,E,G). No mesenchymal cells are observed in preanal fin fold in either larval specimen at the sectioned levels (B,F). White lines in A and D indicate the sectioned levels. Scale bars = 1 mm in A,D; 0.01 mm in B,C,E–G.

bones). To avoid damage or demineralization, gut and skin were not removed or breached.

For image acquisition of deeper parts of the skeletal systems, stained specimens were cleared using Sca*l*eA2 (Hama et al., 2011), and then immersed in 30–60% glycerol solution. To visualize autofluorescence, transparent samples (cleared larvae and juveniles) were photographed under a fluorescence microscope in two different modes (colored for calcein-stained samples and grey scale for fixed and alizarin red-stained samples), through a modification of previously reported methods (Kimmel et al., 2010). Moreover, light-field images of alizarin red-stained samples were acquired. Image acquisition was performed using IX71 and Szx16 with DP80 (Olympus). We identified skeletal elements based on nomenclature used in previous studies (Gregory, 1933; Fink and Fink, 1981; Fujita, 1990; Cubbage and Mabee, 1996; Bird and Mabee, 2003; Mabee et al., 2007; Parichy et al., 2009; Bensimon-Brito et al., 2012).

Histological Analysis

Goldfish larvae and juvenile specimens were anesthetized and fixed using Bouin's fixative. After dehydration, specimens were embedded in paraffin, sectioned to 5 μm using a slicer (RM2245, Leica), and stained with Alcian blue (Sigma A5268), hematoxylin (Sigma MHS32), and eosin (Sigma AL-318906). The stained samples were observed and photographed under standard microscopes (BX43, Olympus).

Image processing, data acquisition, and measurement of standard length

Adobe Photoshop CS5 was used to process images for color balance. Image analysis software (ImageJ 1.48v; Schneider et al., 2012) was used to generate fully focused images and to measure the standard length of goldfish larvae and juvenile specimens.

Statistical Analyses

All statistical analyses and plots were made using the R statistical computing package of RStudio v0.98.1049 (Figs. 3–6). The relationship between standard length and days post fertilization was examined using a standard linear model, whereas presence/absence of the indices was analyzed with a binomial generalized linear model.

Acknowledgments

We are grateful to Wen-Hui Su (SHUEN-SHIN Breeding Farm) and You Syu Huang, of the Aquaculture Breeding Institute, Hualien, for technical advice on goldfish breeding in Taiwan. We also thank the following members of the Marine Research Station, Institute of Cellular and Organismic Biology: Hung-Tsai Lee, Jhih-Hao Wei, Chia-Chun Lee, and Chih-Chiang Lee for goldfish maintenance; and Shu-Hua Lee, Chi-Fu Hung, and Fei-Chu Chen for administrative support. Finally, we thank Duncan Wright for critical reading of our manuscript. This research was supported by MST grant 102-2313-B-001-005-MY3 from the Ministry of Science and Technology, and Career Development Award (CDA-103-L05) from Academia Sinica, Taiwan.

References

Abe G, Lee S-H, Chang M, Liu S-C, Tsai H-Y, Ota KG. 2014. The origin of the bifurcated axial skeletal system in the twin-tail goldfish. Nat Commun 5:3360.

Akey JM, Ruhe AL, Akey DT, Wong AK, Connelly CF, Madeoy J, Nicholas TJ, Neff MW. 2010. Tracking footprints of artificial selection in the dog genome. Proc Natl Acad Sci U S A 107: 1160–1165.

Alexander RM. 1966. Structure and function in the catfish. J Zool 148:88–152.

Amsterdam A, Nissen RM, Sun Z, Swindell EC, Farrington S, Hopkins N. 2004. Identification of 315 genes essential for early zebrafish development. Proc Natl Acad Sci U S A 101:12792–12797.

Amsterdam A, Burgess S, Golling G, Chen W, Sun Z, Townsend K, Farrington S, Haldi M, Hopkins N. 1999. A large-scale insertional mutagenesis screen in zebrafish. Gene Dev 13:2713–2724.

Armstrong PB, Child JS. 1965. Stages in the normal development of Fundulus heteroclitus. Biol Bull 128:143–168.

Arratia G, Schultze H-P. 1990. The urohyal: development and homology within osteichthyans. J Morphol 203:247–282.

Arratia G, Schultze H-P. 1991. Palatoquadrate and its ossifications: development and homology within osteichthyans. J Morphol 208:1–81.
Asano H, Kubo Y. 1972. Variation of spinal curvature and vertebral number in goldfish. Jpn J Ichthyol 19:233–231.
Ballard WW. 1973. Normal embryonic stages for salmonid fishes, based on Salmo gairdneri Richardson and Salvelinus fontinalis (Mitchill). J Exp Zool 184:7–25.
Bateson W. 1894. Materials for the study of variation: treated with special regard to discontinuity in the origin of species. London: Macmillan.
Battle HI. 1940. The embryology and larval development of the goldfish (Carassius auratus L.) from Lake Erie. Ohio J Sci 40:82–93.
Bell MA. 1987. Interacting evolutionary constraints in pelvic reduction of threespine sticklebacks, Gasterosteus aculeatus (Pisces, Gasterosteidae). Biol J Linn Soc 31:347–382.
Bell MA, Orti G, Walker JA, Koenings JP. 1993. Evolution of pelvic reduction in threespine stickleback fish: a test of competing hypotheses. Evolution 47:906–914.
Bensimon-Brito A, Cancela ML, Huysseune A, Witten PE. 2012. Vestiges, rudiments and fusion events: the zebrafish caudal fin endoskeleton in an evo-devo perspective. Evol Dev 14:116–127.
Berndt W. 1925. Vererbungsstudien an Goldfischrassen. Zeit F Indukt Abst U Vererb Bd 36:161–349.
Bird NC, Mabee PM. 2003. Developmental morphology of the axial skeleton of the zebrafish, Danio rerio (Ostariophysi: Cyprinidae). Dev Dyn 228:337–357.
Bradford Y, Conlin T, Dunn N, Fashena D, Frazer K, Howe DG, Knight J, Mani P, Martin R, Moxon SA, Paddock H, Pich C, Ramachandran S, Ruef BJ, Ruzicka L, Bauer Schaper H, Schaper K, Shao X, Singer A, Sprague J, Sprunger B, Van Slyke C, Westerfield M. 2011. ZFIN: enhancements and updates to the Zebrafish Model Organism Database. Nucleic Acids Res 39: D822–D829.
Budi EH, Patterson LB, Parichy DM. 2011. Post-Embryonic Nerve-Associated Precursors to Adult Pigment Cells: Genetic Requirements and Dynamics of Morphogenesis and Differentiation. PLoS Genet 7:e1002044.
Chan YF, Marks ME, Jones FC, Villarreal G, Shapiro MD, Brady SD, Southwick AM, Absher DM, Grimwood J, Schmutz J, Myers RM, Petrov D, Jónsson B, Schluter D, Bell MA, Kingsley DM. 2010. Adaptive evolution of pelvic reduction in sticklebacks by recurrent deletion of a Pitx1 enhancer. Science 327:302–305.
Chen SC. 1925. Variation in external characteristics of goldfish Carassius auratus. In: contributions from the Biological Laboratory of the Science Society of China. p 1–64.
Chen SC. 1956. A history of the domestication and the factors of the varietal formation of the common goldfish, Carassius auratus. Sci Sinica 6:89–116.
Coburn MM, Futey LM. 1996. The ontogeny of supraneurals and neural arches in the cypriniform Weberian Apparatus (Teleostei: Ostariophysi). Zool J Linn Soc Lond 116:333–346.
Cresko W, McGuigan K, Phillips P, Postlethwait J. 2007. Studies of threespine stickleback developmental evolution: progress and promise. Genetica 129:105–126.
Cubbage CC, Mabee PM. 1996. Development of the cranium and paired fins in the zebrafish Danio rerio (Ostariophysi, Cyprinidae). J Morphol 229:121–160.
Darwin C. 1868. The variation of animals and plants under domestication. London: John Murray.
de Jong IML, Witte F, Richardson MK. 2009. Developmental stages until hatching of the Lake Victoria cichlid Haplochromis piceatus (Teleostei: Cichlidae). J Morphol 270:519–535.
Dranow DB, Tucker RP, Draper BW. 2013. Germ cells are required to maintain a stable sexual phenotype in adult zebrafish. Dev Biol 376:43–50.
Driever W, Solnica-Krezel L, Schier AF, Neuhauss SC, Malicki J, Stemple DL, Stainier DY, Zwartkruis F, Abdelilah S, Rangini Z, Belak J, Boggs C. 1996. A genetic screen for mutations affecting embryogenesis in zebrafish. Development 123:37–46.
Du SJ, Frenkel V, Kindschi G, Zohar Y. 2001. Visualizing normal and defective bone development in zebrafish embryos using the fluorescent chromophore calcein. Dev Biol 238:239–246.
Eaton TH. 1945. Skeletal Supports of the Median Fins of Fishes. J Morphol 76:193–212.
Elizondo MR, Arduini BL, Paulsen J, MacDonald EL, Sabel JL, Henion PD, Cornell RA, Parichy DM. 2005. Defective skeletogenesis with kidney stone formation in dwarf zebrafish mutant for trpm7. Curr Biol 15:667–671.
Feldlite M, Milstein A. 2000. Effect of density on survival and growth of cyprinid fish fry. Aquacult Int 7:399–411.
Fink SV, Fink WL. 1981. Interrelationships of the ostariophysan fishes (Teleostei). Zool J Linn Soc Lond 72:297–353.
Fisher S, Halpern ME. 1999. Patterning the zebrafish axial skeleton requires early chordin function. Nat Genet 23:442–446.
Fujimura K, Okada N. 2007. Development of the embryo, larva and early juvenile of Nile tilapia Oreochromis niloticus (Pisces: Cichlidae). Developmental staging system. Dev Growth Differ 49:301–324.
Fujita K. 1990. The caudal skeleton of teleostean fishes. Tokyo, Japan: Tokai University Press.
Gaiano N, Amsterdam A, Kawakami K, Allende M, Becker T, Hopkins N. 1996. Insertional mutagenesis and rapid cloning of essential genes in zebrafish. Nature 383:829–832.
Golling G, Amsterdam A, Sun Z, Antonelli M, Maldonado E, Chen W, Burgess S, Haldi M, Artzt K, Farrington S, Lin SY, Nissen RM, Hopkins N. 2002. Insertional mutagenesis in zebrafish rapidly identifies genes essential for early vertebrate development. Nat Genet 31:135–140.
Goodrich HB, Anderson PL. 1939. Variations of color patterns in hybrids of the goldfish, Carassius auratus. Biol Bull 77:184–191.
Goodrich HB, Hansen IB. 1931. The postembryonic development of mendelian characters in the goldfish, carassius auratus. J Exp Zool 59:337–358.
Gould SJ. 1977. Ontogeny and phylogeny. Cambridge, MA: Belknap Press of Harvard University Press.
Grande T, Young B. 2004. The ontogeny and homology of the Weberian apparatus in the zebrafish Danio rerio (Ostariophysi: Cypriniformes). Zool J Linn Soc Lond 140:241–254.
Grandel H, Schulte-Merker S. 1998. The development of the paired fins in the zebrafish (Danio rerio). Mech Dev 79:99–120.
Gregory WK. 1933. Fish skulls: a study of the evolution of natural mechanisms. Philadelphia: American Philosophical Society.
Haeckel E, McCabe J. 1912. The evolution of man. London: Watts & Co.
Haffter P, Granato M, Brand M, Mullins MC, Hammerschmidt M, Kane DA, Odenthal J, van Eeden FJ, Jiang YJ, Heisenberg CP, Kelsh RN, Furutani-Seiki M, Vogelsang E, Beuchle D, Schach U, Fabian C, Nusslein-Volhard C. 1996. The identification of genes with unique and essential functions in the development of the zebrafish, Danio rerio. Development 123:1–36.
Hama H, Kurokawa H, Kawano H, Ando R, Shimogori T, Noda H, Fukami K, Sakaue-Sawano A, Miyawaki A. 2011. Scale: a chemical approach for fluorescence imaging and reconstruction of transparent mouse brain. Nat Neurosci 14:1481–1488.
Hervey GF, Billardon-Sauvigny E, Muséum national d'histoire naturelle (France). 1950. The goldfish of China in the XVIII century. London: China Society.
Hervey GF, Hems J. 1948. The goldfish. London: Batchworth Press.
Hoogland R, Morris D, Tinbergen N. 1956. The Spines of Sticklebacks (Gasterosteus and Pygosteus) as Means of Defence against Predators (Perca and Esox). Behaviour 10:205–236.
Huang C, Tan X-Y, Wu K, Chen Q-L, Zhuo M-Q, Pan Y-X, Song Y-F. 2014. Osteological development and anomalies in larval stage of hatchery-reared yellow catfish Pelteobagrus fulvidraco. Aquac Res (in press).
Huysentruyt F, Adriaens D. 2005. Descriptive osteology of Corydoras aeneus (Siluriformes: Callichthyidae). Cybium 23:261–273.
Irie N, Kuratani S. 2011. Comparative transcriptome analysis reveals vertebrate phylotypic period during organogenesis. Nat Commun 2:248.
Iwamatsu T. 2004. Stages of normal development in the medaka Oryzias latipes. Mech Dev 121:605–618.
Kajishima T. 1960. The normal developmental stages of the goldfish Carassius auratus. Jpn J Ichthyol 8:20–28.
Kajishima T. 1977. Genetic and developmental analysis of some new color mutants in the goldfish, Carassius auratus. Genetics 86:161–174.

Kardong KV. 2012. Vertebrates: comparative anatomy, function, evolution. London: McGraw-Hill Higher Education.
Khan MH. 1929. Early stages in the development of the goldfish (Carassius auratus). J Bombay Nat Hist Soc 33:614–617.
Kilambi RV, Robinson WR. 1979. Effects of temperature and stocking density on food consumption and growth of grass carp Ctenopharyngodon idella, Val. J Fish Biol 15:337–342.
Kimmel CB, Ballard WW, Kimmel SR, Ullmann B, Schilling TF. 1995. Stages of embryonic development of the zebrafish. Dev Dyn 203:253–310.
Kimmel CB, DeLaurier A, Ullmann B, Dowd J, McFadden M. 2010. Modes of Developmental Outgrowth and Shaping of a Craniofacial Bone in Zebrafish. PLoS One 5:e9475.
Kimmel CB, Walker MB, Miller CT. 2007. Morphing the hyomandibular skeleton in development and evolution. J Exp Zool Part B 308B:609–624.
Koh T-P. 1931. Osteology of Carassius auratus. Science report national Ts'ing Hua University 1:61–81.
Koh T-P. 1932. Osteological variations in the axial skeleton of goldfish (Carassius auratus). Science report national Ts'ing Hua University 2:109–121.
Komiyama T, Kobayashi H, Tateno Y, Inoko H, Gojobori T, Ikeo K. 2009. An evolutionary origin and selection process of goldfish. Gene 430:5–11.
Koumoundouros G, Divanach P, Kentouri M. 2001. Osteological development of Dentex (Osteichthyes: Sparidae): dorsal, anal, paired fins and squamation. Mar Biol 138:399–406.
Koyabu D, Endo H, Mitgutsch C, Suwa G, Catania KC, Zollikofer CP, Oda S, Koyasu K, Ando M, Sanchez-Villagra MR. 2011. Heterochrony and developmental modularity of cranial osteogenesis in lipotyphlan mammals. Evol Dev 2:21.
Li P, Wang AQ, Cui DF, Mou GY, Wang CY, Zhang RQ, Ning YH, Zhang NC. 1959. Normal stages in the development of wild and domesticated goldfish. Carassius auratus. Acta Zool Sinica 11: 145–154.
Li X-Y, Zeng S-H, Dong X-Y, Ma J-G, Wang J-J. 2012. Acute toxicity and responses of antioxidant systems to 1-methyl-3-octylimidazolium bromide at different developmental stages of goldfish. Ecotoxicology 21:253–259.
Liem KF, Bemis WE, Walker WF, Kabce G. 2001. Functional anatomy of the vertebrates: an evolutionary perspective. Belmont: Brooks Cole.
Lindsey CC. 1955. Evolution of meristic relation in the dorsal and anal fins of teleost fishes. Trans R Soc Can 49:35–49.
Lindblad-Toh K, Wade CM, Mikkelsen TS, Karlsson EK, Jaffe DB, Kamal M, Clamp M, Chang JL, Kulbokas EJ III, Zody MC, Mauceli E, Xie X, Breen M, Wayne RK, Ostrander EA, Ponting CP, Galibert F, Smith DR, DeJong PJ, Kirkness E, Alvarez P, Biagi T, Brockman W, Butler J, Chin CW, Cook A, Cuff J, Daly MJ, DeCaprio D, Gnerre S, Grabherr M, Kellis M, Kleber M, Bardeleben C, Goodstadt L, Heger A, Hitte C, Kim L, Koepfli KP, Parker HG, Pollinger JP, Searle SM, Sutter NB, Thomas R, Webber C, Baldwin J, Abebe A, Abouelleil A, Aftuck L, Ait-Zahra M, Aldredge T, Allen N, An P, Anderson S, Antoine C, Arachchi H, Aslam A, Ayotte L, Bachantsang P, Barry A, Bayul T, Benamara M, Berlin A, Bessette D, Blitshteyn B, Bloom T, Blye J, Boguslavskiy L, Bonnet C, Boukhgalter B, Brown A, Cahill P, Calixte N, Camarata J, Cheshatsang Y, Chu J, Citroen M, Collymore A, Cooke P, Dawoe T, Daza R, Decktor K, DeGray S, Dhargay N, Dooley K, Dorje P, Dorjee K, Dorris L, Duffey N, Dupes A, Egbiremolen O, Elong R, Falk J, Farina A, Faro S, Ferguson D, Ferreira P, Fisher S, FitzGerald M, Foley K, Foley C, Franke A, Friedrich D, Gage D, Garber M, Gearin G, Giannoukos G, Goode T, Goyette A, Graham J, Grandbois E, Gyaltsen K, Hafez N, Hagopian D, Hagos B, Hall J, Healy C, Hegarty R, Honan T, Horn A, Houde N, Hughes L, Hunnicutt L, Husby M, Jester B, Jones C, Kamat A, Kanga B, Kells C, Khazanovich D, Kieu AC, Kisner P, Kumar M, Lance K, Landers T, Lara M, Lee W, Leger JP, Lennon N, Leuper L, LeVine S, Liu J, Liu X, Lokyitsang Y, Lokyitsang T, Lui A, Macdonald J, Major J, Marabella R, Maru K, Matthews C, McDonough S, Mehta T, Meldrim J, Melnikov A, Meneus L, Mihalev A, Mihova T, Miller K, Mittelman R, Mlenga V, Mulrain L, Munson G, Navidi A, Naylor J, Nguyen T, Nguyen N, Nguyen C, Nicol R, Norbu N, Norbu C, Novod N, Nyima T, Olandt P, O'Neill B, O'Neill K, Osman S, Oyono L, Patti C, Perrin D, Phunkhang P, Pierre F, Priest M, Rachupka A, Raghuraman S, Rameau R, Ray V, Raymond C, Rege F, Rise C, Rogers J, Rogov P, Sahalie J, Settipalli S, Sharpe T, Shea T, Sheehan M, Sherpa N, Shi J, Shih D, Sloan J, Smith C, Sparrow T, Stalker J, Stange-Thomann N, Stavropoulos S, Stone C, Stone S, Sykes S, Tchuinga P, Tenzing P, Tesfaye S, Thoulutsang D, Thoulutsang Y, Topham K, Topping I, Tsamla T, Vassiliev H, Venkataraman V, Vo A, Wangchuk T, Wangdi T, Weiand M, Wilkinson J, Wilson A, Yadav S, Yang S, Yang X, Young G, Yu Q, Zainoun J, Zembek L, Zimmer A, Lander ES. 2005. Genome sequence, comparative analysis and haplotype structure of the domestic dog. Nature 438:803–819.
Ma J, Liu Y, Niu D, Li X. 2015. Effects of chlorpyrifos on the transcription of CYP3A cDNA, activity of acetylcholinesterase, and oxidative stress response of goldfish (Carassius auratus). Environ Toxicol 30:422–429.
Mabee PM, Arratia G, Coburn M, Haendel M, Hilton EJ, Lundberg JG, Mayden RL, Rios N, Westerfield M. 2007. Connecting evolutionary morphology to genomics using ontologies: a case study from Cypriniformes including zebrafish. J Exp Zool Part B 308: 655–668.
Mabee PM, Crotwell PL, Bird NC, Burke AC. 2002. Evolution of median fin modules in the axial skeleton of fishes. J Exp Zool 294:77–90.
Magyary I, Urbányi B, Horváth L. 1996. Cryopreservation of common carp (Cyprinus carpio L.) sperm II. Optimal conditions for fertilization. J Appl Ichthyol 12:117–119.
Martinez GM, Bolker JA. 2003. Embryonic and larval staging of summer flounder (Paralichthys dentatus). J Morphol 255:162–176.
Matsui Y. 1933. Preliminary note on the inheritance of caudal and anal fins in goldfish of Japan Proc Imp Acad 655–658.
Matsui Y. 1934. Genetical studies on gold-fish of Japan. J Imp Fish Inst 30:1–96.
Matsui Y. 1972. Pet Library goldfish guide: with a section on Koi. New York: Pet Library.
Matsui Y, Kumagai T, Betts LC. 1981. Goldfish guide. Neptune, NJ: T.F.H. Publications.
Merino GE, Piedrahita RH, Conklin DE. 2007. The effect of fish stocking density on the growth of California halibut (Paralichthys californicus) juveniles. Aquaculture 265:176–186.
Morrison CM, Miyake T, Wright JR. 2001. Histological study of the development of the embryo and early larva of Oreochromis niloticus (Pisces: Cichlidae). J Morphol 247:172–195.
Mullins MC, Hammerschmidt M, Haffter P, Nüsslein-Volhard C. 1994. Large-scale mutagenesis in the zebrafish: in search of genes controlling development in a vertebrate. Curr Biol 4:189–202.
Nagayoshi S, Hayashi E, Abe G, Osato N, Asakawa K, Urasaki A, Horikawa K, Ikeo K, Takeda H, Kawakami K. 2008. Insertional mutagenesis by the Tol2 transposon-mediated enhancer trap approach generated mutations in two developmental genes: tcf7 and synembryn-like. Development 135:159–169.
Nelson JS. 2006. Fishes of the world. Hoboken, NJ: Wiley. p 19.
Parichy DM, Elizondo MR, Mills MG, Gordon TN, Engeszer RE. 2009. Normal table of postembryonic zebrafish development: staging by externally visible anatomy of the living fish. Dev Dyn 238:2975–3015.
Park E-H, Lee S-H. 1988. Scale Growth and Squamation Chronology for the Laboratory-Reared Hermaphroditic Fish Rivulus marmoratus (Cyprinodontidae). Jpn J Ichthyol 34:476–482.
Patricia Hernandez L, Bird NC, Staab KL. 2007. Using zebrafish to investigate cypriniform evolutionary novelties: functional development and evolutionary diversification of the kinethmoid. J Exp Zool Part B 308B:625–641.
Patterson C. 1992. Supernumerary median fin-rays in teleostean fishes. Zool J Linn Soc Lond 106:147–161.
Patterson SE, Mook LB, Devoto SH. 2008. Growth in the larval zebrafish pectoral fin and trunk musculature. Dev Dyn 237:307–315.
Razani H, Hanyu I. 1986. Annual reproductive cycle of 2-3 years old female goldfish and its artificial modification by manipulations of water temperature and photoperiod. Nippon Suisan Gakkaishi 52:965–969.

Reis RE. 1998. Anatomy and phylogenetic analysis of the neotropical callichthyid catfishes (Ostariophysi, Siluriformes). Zool J Linn Soc Lond 124:105–168.
Riedl R. 1978. Order in living organisms: a systems analysis of evolution. New York: Wiley.
Saitoh K, Miya M, Inoue JG, Ishiguro NB, Nishida M. 2003. Mitochondrial genomics of ostariophysan fishes: perspectives on phylogeny and biogeography. J Mol Evol 56:464–472.
Saitoh K, Sado T, Mayden RL, Hanzawa N, Nakamura K, Nishida M, Miya M. 2006. Mitogenomic evolution and interrelationships of the cypriniformes (Actinopterygii: Ostariophysi): the first evidence toward resolution of higher-level relationships of the world's largest freshwater fish clade based on 59 whole mitogenome sequences. J Mol Evol 63:826–841.
Schilling TF, Kimmel CB. 1997. Musculoskeletal patterning in the pharyngeal segments of the zebrafish embryo. Development 124:2945–2960.
Schilling TF, Webb J. 2007. Considering the zebrafish in a comparative context. J Exp Zool Part B 308B:515–522.
Schneider CA, Rasband WS, Eliceiri KW. 2012. NIH Image to ImageJ: 25 years of image analysis. Nat Methods 9:671–675.
Schram E, Van der Heul JW, Kamstra A, Verdegem MCJ. 2006. Stocking density-dependent growth of Dover sole (Solea solea). Aquaculture 252:339–347.
Shapiro MD, Kronenberg Z, Li C, Domyan ET, Pan H, Campbell M, Tan H, Huff CD, Hu H, Vickrey AI, Nielsen SC, Stringham SA, Willerslev E, Gilbert MT, Yandell M, Zhang G, Wang J. 2013. Genomic diversity and evolution of the head crest in the rock pigeon. Science 339:1063–1067.
Shapiro MD, Marks ME, Peichel CL, Blackman BK, Nereng KS, Jonsson B, Schluter D, Kingsley DM. 2004. Genetic and developmental basis of evolutionary pelvic reduction in threespine sticklebacks. Nature 428:717–723.
Shelton WL, Smitherman RO, Jensen GL. 1981. Density related growth of grass carp, Ctenopharyngodon idella (Val.) in managed small impoundments in Alabama. J Fish Biol 18:45–51.
Shimada A, Kawanishi T, Kaneko T, Yoshihara H, Yano T, Inohaya K, Kinoshita M, Kamei Y, Tamura K, Takeda H. 2013. Trunk exoskeleton in teleosts is mesodermal in origin. Nature Commun 4: 1639.
Sire JY, Akimenko MA. 2004. Scale development in fish: a review, with description of sonic hedgehog (shh) expression in the zebrafish (Danio rerio). Int J Dev Biol 48:233–247.
Sire JY, Allizard F, Babiar O, Bourguignon J, Quilhac A. 1997. Scale development in zebrafish (Danio rerio). J Anat 190(pt 4):545–561.
Sire J-Y, Arnulf I. 1990. The development of squamation in four teleostean fishes with a survey of the literature. Jpn J Ichthyol 37: 133–143.
Sire J-Y, Arnulf I. 2000. Structure and development of the ctenial spines on the scales of a teleost fish, the cichlid Cichlasoma nigrofasciatum. Acta Zool 81:139–158.
Sire J-Y, Huysseune ANN. 2003. Formation of dermal skeletal and dental tissues in fish: a comparative and evolutionary approach. Biol Rev 78:219–249.
Sivasubbu S, Balciunas D, Davidson AE, Pickart MA, Hermanson SB, Wangensteen KJ, Wolbrink DC, Ekker SC. 2006. Gene-breaking transposon mutagenesis reveals an essential role for histone H2afza in zebrafish larval development. Mech Dev 123: 513–529.
Smartt J. 2001. Goldfish varieties and genetics: a handbook for breeders. Oxford: Blackwell Science.
Swarup H. 1958. Stages in the development of the stickleback Gasterosteus aculeatus (L.). J Embryol Exp Morphol 6:373–383.
Thorsen DH, Hale ME. 2005. Development of zebrafish (Danio rerio) pectoral fin musculature. J Morphol 266:241–255.
Tsai HY, Chang M, Liu SC, Abe G, Ota KG. 2013. Embryonic development of goldfish (Carassius auratus): a model for the study of evolutionary change in developmental mechanisms by artificial selection. Dev Dyn 242:1262–1283.
Van der heyden C, Huysseune A. 2000. Dynamics of tooth formation and replacement in the zebrafish (Danio rerio) (Teleostei, Cyprinidae). Dev Dyn 219:486–496.
Van der heyden C, Huysseune A, Sire JY. 2000. Development and fine structure of pharyngeal replacement teeth in juvenile zebrafish (Danio rerio) (Teleostei, Cyprinidae). Cell Tissue Res 302: 205–219.
vanEeden FJM, Granato M, Schach U, Brand M, FurutaniSeiki M, Haffter P, Hammerschmidt M, Heisenberg CP, Jiang YJ, Kane DA, Kelsh RN, Mullins MC, Odenthal J, Warga RM, NussleinVolhard C. 1996. Genetic analysis of fin formation in the zebrafish, Danio rerio. Development 123:255–262.
von Baer KE. 1828. Über Entwickelungsgeschichte der Thiere: Beobachtung und Reflexion. Königsberg: Bornträger.
Vonholdt BM, Pollinger JP, Lohmueller KE, Han E, Parker HG, Quignon P, Degenhardt JD, Boyko AR, Earl DA, Auton A, Reynolds A, Bryc K, Brisbin A, Knowles JC, Mosher DS, Spady TC, Elkahloun A, Geffen E, Pilot M, Jedrzejewski W, Greco C, Randi E, Bannasch D, Wilton A, Shearman J, Musiani M, Cargill M, Jones PG, Qian Z, Huang W, Ding ZL, Zhang YP, Bustamante CD, Ostrander EA, Novembre J, Wayne RK. 2010. Genome-wide SNP and haplotype analyses reveal a rich history underlying dog domestication. Nature 464:898–902.
Wang J, Liu S, Xiao J, Tao M, Zhang C, Luo K, Liu Y. 2014. Evidence for the evolutionary origin of goldfish derived from the distant crossing of red crucian carp x common carp. BMC Genet 15:33.
Wang S-H, Huang P-P, Li X-Y, Wang C-Y, Zhang W-H, Wang J-J. 2010. Embryonic and developmental toxicity of the ionic liquid 1-methyl-3-octylimidazolium bromide on goldfish. Environ Toxicol 25:243–250.
Wang SY, Luo J, Murphy RW, Wu SF, Zhu CL, Gao Y, Zhang YP. 2013. Origin of Chinese goldfish and sequential loss of genetic diversity accompanies new breeds. PLoS One 8:e59571.
Watase S. 1887. On the caudal and anal fins of goldfishes. J Sci Coll Imp Univ Tokyo, Japan 1:247–267.
Watson JM. 1939. The Development of the Weberian ossicles and anterior vertebrae in the goldfish. Proc R Soc Lond Ser B 127: 452–472.
Wayne RK, Ostrander EA. 2007. Lessons learned from the dog genome. Trends Genet 23:557–567.
Webb JF, Shirey JE. 2003. Postembryonic development of the cranial lateral line canals and neuromasts in zebrafish. Dev Dyn 228:370–385.
Wienholds E, van Eeden F, Kosters M, Mudde J, Plasterk RH, Cuppen E. 2003. Efficient target-selected mutagenesis in zebrafish. Genome Res 13:2700–2707.
Witten PE, Hansen A, Hall BK. 2001. Features of mono- and multinucleated bone resorbing cells of the zebrafish Danio rerio and their contribution to skeletal development, remodeling, and growth. J Morphol 250:197–207.
Wright JJ. 2009. Diversity, phylogenetic distribution, and origins of venomous catfishes. BMCEvol Biol 9:282.
Xu P, Zhang X, Wang X, Li J, Liu G, Kuang Y, Xu J, Zheng X, Ren L, Wang G, Zhang Y, Huo L, Zhao Z, Cao D, Lu C, Li C, Zhou Y, Liu Z, Fan Z, Shan G, Li X, Wu S, Song L, Hou G, Jiang Y, Jeney Z, Yu D, Wang L, Shao C, Song L, Sun J, Ji P, Wang J, Li Q, Xu L, Sun F, Feng J, Wang C, Wang S, Wang B, Li Y, Zhu Y, Xue W, Zhao L, Wang J, Gu Y, Lv W, Wu K, Xiao J, Wu J, Zhang Z, Yu J, Sun X. 2014. Genome sequence and genetic diversity of the common carp, Cyprinus carpio. Nat Genet 46:1212–1219.
Yelick PC, Schilling TF. 2002. Molecular dissection of craniofacial development using zebrafish. Crit Rev Oral Biol Med 13:308–322.